2019

Toward a better understanding of changes in Northern vegetation using long-term remote sensing data

https://hdl.handle.net/2144/39591

Boston University

BOSTON UNIVERSITY

GRADUATE SCHOOL OF ARTS AND SCIENCES

Dissertation

TOWARD A BETTER UNDERSTANDING OF CHANGES IN NORTHERN VEGETATION USING LONG-TERM REMOTE SENSING DATA

by

TAEJIN PARK

B.S., Korea University, 2010
M.S., Korea University, 2012

Submitted in partial fulfillment of the
requirements for the degree of
Doctor of Philosophy

2019

Approved by

First Reader ______________________________

Ranga B. Myneni, Ph.D.
Professor of Earth and Environment

Second Reader ______________________________

Yuri Knyazikhin, Ph.D.
Research Professor of Earth and Environment

Third Reader ______________________________

Curtis E. Woodcock, Ph.D.
Professor of Earth and Environment

DEDICATION

사랑하고 존경하는 나의 아버지 그리고 어머니 앞에…

ACKNOWLEDGMENTS

NASA Earth and Space Science Fellowship Program (grant NNX16AO34H) and Earth Science Research Program (grants NNX14AP80A and NNX14AI71G) supported this research.

First and foremost I would like to express my sincere gratitude to my advisors, Ranga Myneni and Yuri Knyazikhin, for their patient guidance and continuous encouragement throughout my Ph.D. program. They gave me freedom to develop my research interests, set a high standard for me just as for themselves, taught me how to cope with difficult encounters not only in research but also in personal life, and provided me generous help in uncountable occasions. I also want to express my appreciation to my committee members at Boston University, Curtis Woodcock and Nathan Phillips, for their generous and constructive advice and feedbacks. Special gratitude should go to Scott Goetz, Hans Tømmervik, Ramakrishna Nemani and *ArcticBiomass* working group members who always enlightened me with their expertise on vegetation remote sensing and northern vegetation dynamics.

I must thank to Sungho Choi for his valuable guidance and warm support during our long journey from undergrad to graduate school. I am also thankful to the former and current Climate and Vegetation Research Group members: Chi Chen, Sangram Ganguly, Weile Wang, Jian Bi, Kai Yan, Baodong Xu, Bin Yang, Wanjuan Song, Ling Chen, Yepei Chen, Xiaojun She, for numerous scientific interactions and invaluable assistance during my stay at Boston University. I appreciate the memorable time with the current and former E&E colleagues including Xiaojing Tang, Eli Melaas, Shixiong Wang, Daniel Gianotti, Zhan Li, Larissa Hallack, Érica Nakai, Yaxiong Ma and Jessica Wright. Special thanks go to Jihyun Kim, Ilyun Koh, Minkyu Moon and Daekoo Kim for their unforgettable friendship. My deepest gratitude goes to Alissa Beideck, William Edwards, Matthew Dicintio, Frederick George III, Sayaka Yamaki and all the staff of the Earth and Environment Department for their kind administrative help that makes my life at Boston University easy and enjoyable.

I'm extremely grateful to my parents, parents in law and family in Korea for their sustained encouragement and support. I can always feel their love over the years, thus I could firmly stand on my own feet. Chloe, my daughter, offered me a full of joy in my life. I hope she grow up with creative, positive and generous mind. Last but not least, I am greatly indebted to my lovely wife, Hanna, for the endless and unconditional love she gives to me. My work, my life, and every bit of success of mine, if any, are deeply rooted in her support. I could never complete my Ph.D. without her.

TOWARD A BETTER UNDERSTANDING OF CHANGES IN NORTHERN VEGETATION USING LONG-TERM REMOTE SENSING DATA

TAEJIN PARK

Boston University Graduate School of Arts and Sciences, 2019

Major Professor: Ranga B. Myneni, Professor of Earth and Environment

ABSTRACT

Cascading consequences of recent changes in the physical environment of northern lands associated with rapid warming have affected a broad range of ecosystem processes, particularly, changes in structure, composition, and functioning of vegetation. Incomplete understanding of underlying processes driving such changes is the primary motivation for this research. We report here the results of three studies that use long-term remote sensing data to advance our knowledge of spatiotemporal changes in growing season, greenness and productivity of northern vegetation. First, we improve the remote sensing-based detection of growing season by fusing vegetation greenness, snow and soil freeze/thaw condition. The satellite record reveals extensive lengthening trends of growing season and enhanced annual total greenness during the last three decades. Regionally varying seasonal responses are linked to local climate constraints and their relaxation. Second, we incorporate available land surface histories including disturbances and human land management practices to understand changes in remotely sensed vegetation greenness. This investigation indicates that multiple drivers including natural (wildfire) and anthropogenic (harvesting) disturbances, changing climate and agricultural activities govern the large-scale greening trends in northern lands. The timing and type of disturbances are important to fully comprehend spatially uneven vegetation changes in the boreal and temperate regions. In the final part, we question how photosynthetic seasonality evolved into its current state, and what role climatic constraints and their variability played in this process and ultimately in the carbon cycle. We take the ‘laws of minimum’ as a basis and introduce a new framework where the timing of peak photosynthetic activity ($\mathrm{DOY}_{\mathrm{Pmax}}$) acts as a proxy for plants adaptive state to climatic constraints on their growth. The result shows a widespread warming-induced advance in $\mathrm{DOY}_{\mathrm{Pmax}}$ with an increase of total gross primary productivity across northern lands, which leads to an earlier phase shift in land-atmosphere carbon fluxes and an increase in their amplitude. The research presented in this dissertation suggests that understanding past, present and likely future changes in northern vegetation requires a multitude of approaches that consider linked climatic, social and ecological drivers and processes.

TABLE OF CONTENTS

LIST OF TABLES

LIST OF FIGURES

LIST OF ABBREVIATIONS

AET	Actual Evapotranspiration
AFDB	Alaskan Large Fire History Database
AR	Arctic region
AVHRR	Advanced Very High Resolution Radiometer
BELMANIP	Benchmark Land Multisite Analysis and Intercomparison of Products
BO	Boreal region
CAMS	Copernicus Atmosphere Monitoring Service
CMIP	Coupled Model Intercomparison Project
CNFDB	Canadian Large Fire Database
CP	Circumpolar
CR	Cropland region
DEM	Digital Elevation Model
DOY	Day of Year
EA	Eurasia
EOS	End of growing season
ESM	Earth System Model
ESRL	Earth System Research Laboratory
EVI	Enhanced Vegetation Index
FT	Freeze and Thaw
GIMMS	Global Inventory Modeling and Mapping Studies
GLDAS	Global Land Data Assimilation Systems

GMAO	Global Modeling and Assimilation Office
GOES	Goddard Earth Observing System
GOME	Global Ozone Monitoring Experiment
GPP	Gross Primary Productivity
GSSNDVI	Growing Season Summed NDVI
GSSWI	Growing Season Summed Warmth Index
IGBP	International Geosphere-Biosphere Programme
IIASA	International Institute for Applied Systems Analysis
JENA	Jena CarboScope
JJA	June, July and August
LAI	Leaf Area Index
LC	Land Cover
LOS	Length of growing season
LUE	Light Use Efficiency
MODIS	Moderate Resolution Imaging Spectroradiometer
MTE	Multi-Tree Ensemble
NA	North America
NASA	National Aeronautics and Space Administration
NDVI	Normalized Difference Vegetation Index
NIR	Near Infrared
NOAA	National Oceanic and Atmospheric Administration
NVC	Non-Vegetated Cover Fraction

PDF	Probability Density Function
PEOS	Potential end of growing season
PET	Potential Evapotranspiration
PLOS	Potential length of growing season
PPFD	Photosynthetic photon flux density
PSOS	Potential start of growing season
RAP	Ratio of AET to PET
RCP	Representative Concentration Pathway
SCA	Seasonal Cycle Amplitude
SIF	Sun-Induced Fluorescence
SOS	Start of growing season
SVC	Short Vegetation Cover Fraction
TC	Tree Cover Fraction
TE	Temperate region
TRASP	Transformed Aspect
USFS	United States Forest Service
VCF	Vegetation Continuous Field
WWF	World Wildlife Fund

CHAPTER 1: Introduction

1.1 Background

1.1.1 Changing north and vegetation dynamics

Northern terrestrial vegetation plays a critical role in the Earth system by interactively regulating global energy, water, and carbon cycles (Bonan, 2008). During the last half-century, high-latitude regions have experienced drastic temperature increases of 0.3 to 1.0 °C per decade higher than anywhere else on the Earth (Serreze & Barry, 2011). Ongoing acceleration of climate change at high latitudes results in reduced volume and area of sea ice in the Arctic ocean (Bhatt et al., 2010), warming and thawing of permafrost (Serreze et al., 2000), increases in the frequency and severity of climate-driven disturbances (Kasischke & Turetsky, 2006), widespread changes to surface water extent (Pekel et al., 2016) and soil moisture (Barichivich et al., 2014). In addition, humans have transformed more than 50 % of Earth's land surface and extensive land use/management pressures on some parts of northern territories have led substantial and drastic land surface changes as well (Hooke et al., 2012; White et al., 2017). Cascading consequences of the changes in physical environments have already affected on a broad range of ecosystem processes (Hinzman et al., 2005; Soja et al., 2007; Beck et al., 2011a; Bjorkman et al., 2018). In particular, changes in composition, structure, and functioning of vegetation lead to multi-faceted implications for the regional carbon balance (Forkel et al., 2016). These changes will feed back to climate directly through their effects on atmospheric CO_2 concentrations, and also indirectly by altering terrestrial energy budgets and hydrologic cycles (Chapin et al., 2008). Therefore, understanding changes in northern terrestrial vegetation is a key step in diagnosing and prognosticating responses of atmospheric CO_2 to global and/or regional warming.

Warming is generally thought to ease the climatic constraint on photosynthetic activity of vegetation in the northern land. Indeed, recent growing season studies based on field observation (Parmesan & Yohe, 2003), eddy covariance (Richardson et al., 2010), remote sensing (Keenan et al., 2014) and atmospheric CO_2 (Barichivich et al., 2013) have concordantly indicated that the growing season duration for northern vegetation has significantly extended over the past decades due to both advanced beginning and delayed termination. This prolonged growing season over northern land drives a longer carbon assimilation period due to the relaxation of low-temperature limits on metabolism, and in turn increased productivity is observed (Xu et al., 2013; Forkel el al., 2016). Indeed, many ground-based studies have reported vegetation changes including vegetation encroachment into non-vegetated land (Frost & Epstein, 2014; Myers-Smith & Hik, 2018), increasing biomass of existing vegetation (Pan et al., 2011), changes in community composition (Beck et al., 2011a), and/or changes in plant traits (e.g., leaf area, height, etc.) (Zhu et al., 2016; Bjorkman et al., 2018). However, longer and warmer growing seasons also promote environmental conditions that favor surface drying and thus intensified summer droughts, tree mortality and wildfires have resulted in summer productivity decline (Kasischke & Turetsky, 2006; Peng et al., 2011; Barichivich et al., 2014). Furthermore, recent studies have reported a reduced or reversed rate of regional growing season changes (Høgda et al 2013, Wang et al 2015). These dynamics are highly variable in space and over time with substantive differences in magnitude and even direction of change. Human-induced land use change and management have transformed the state of northern lands and diversify vegetation response to changing environments as well. Thus, these complexities justify the need for a comprehensive examination of the magnitude and direction of changes of northern vegetation across the continental or hemispheric landscape.

1.1.2 Satellite remote sensing of vegetation dynamics

Because northern terrestrial ecosystems are both extensive and remote, inventory data for these biomes is not widely available and acquiring field data is challenging. Hence, many studies focused on large-scale changes in these ecosystems have relied on remote sensing (Myneni et al., 1997; Goetz et al., 2005; Xu et al., 2013; Sulla-Menashe et al., 2018). Two satellite sensors, Advanced Very High Resolution Radiometer (AVHRR) and Moderate Resolution Imaging Spectroradiometer (MODIS), have been successfully and widely used to monitor vegetation changes from regional to global scale. These two sensors onboard series of sun-synchronous NOAA and NASA satellites have provided daily global observations for the Earth. Although the relatively low spatial resolution of AVHRR data is insufficient to explore local variability, the third generation Global Inventory Modeling and Mapping Studies (GIMMS) product from the AVHRR provides an incomparable opportunity to investigate long-term vegetation dynamics (from 1981 to present). The MODIS product facilitates retrieving more consistent reflectance signatures (advantages from better onboard calibration, physics-based atmospheric correction, etc.) of vegetation dynamics at the fine scale, and the combination of Terra (from 2000 to present) and Aqua (from 2002 to present) products may alleviate deficiencies in individual sensor data.

Particularly seasonal productivity surrogated by reflectance-based indices such as the normalized difference vegetation index (NDVI; Tucker, 1979) has been used to explore vegetation growing season and productivity changes. NDVI is the normalized ratio of red and near-infrared (NIR) reflectance, which is influenced by the chemical and structural components of leaves (chlorophyll and mesophyll respectively), and is thus generally considered a good proxy for photosynthetic activity (Sellers, 1987). Leaf area index (LAI) is another important measure of vegetation biophysical parameter from remote sensing because of its significant role in the exchange of fluxes of energy, mass (e.g., water, nutrient, and CO_2) and momentum between the biosphere and atmosphere (Richardson et al., 2013). Furthermore, incorporating ecosystem models based on the light use efficiency (LUE) concept given by Monteith (1972) into remotely sensed biophysical parameters and meteorological data can retrieve gross primary productivity (GPP) (Running et al., 1999). Satellite remote sensing based NDVI, LAI, and GPP have widely used to monitor changes in large-scale vegetation dynamics. In this dissertation, we use these three key measures of vegetation structure and functioning to address three questions described in the following Section 1.2.

1.2 Research objectives and dissertation structure

Two pioneering studies in the late 1990s unveiled the enhanced seasonal CO_2 amplitude (Keeling et al., 1996) and vegetation “greening” (Myneni et al., 1997) in the north. Note that the "greening" ("browning") is defined as a trend showing increasing (decreasing) vegetation greenness or productivity. The findings have inspired a broad range of research communities to understand the past and current state of northern vegetation, in particular, greening/browning pattern and its drivers, and to project its fate under changing environments in the future. Nevertheless, the response of northern vegetation structure and function to global environmental changes is one of the most critical elements that are not well incorporated in the global carbon monitoring, modeling and forecasting. Three research questions are identified in this dissertation, and chapters 2, 3 and 4 are presented here as self-contained scientific papers answering the three questions.

- *First, how has growing season changed and characterized annual total greenness (or productivity) during the last three decades?*
- *Second, what are roles of overlooked land surface changes (e.g., disturbance and human land use/management) in the remotely sensed greening/browning patterns?*
- *Third, what does photosynthetic seasonality mean? and how has it evolved and what are their implications on the large-scale carbon cycle?*

In chapter two of this dissertation, we investigate changes in metrics of growing season (onset: SOS, end: EOS and length: LOS) and seasonal total greenness from AVHRR NDVI to ultimately understand how they have characterized greening/browning patterns in the north. Particular attention is paid to evaluating the accuracy of these metrics by comparing them to multiple independent direct and indirect growing season and productivity measures. The primary objectives of this study are to *i*) evaluate the reliability of long-term growing season duration and productivity metrics inferred from satellite data, *ii*) investigate the spatiotemporal pattern and trend of changes in growing season duration and productivity, and *iii*) characterize contribution of growing season on productivity changes.

In chapter three of this dissertation, we examine what are roles of disturbance and human activity in the remotely sensed greening/browning trends in Canadian and Alaskan territories where relatively long and extensive disturbance histories exist. We measure how much leaf area has been increased or decrease across biomes and quantify how much of them are associated with disturbance event itself and following recovery processes. The primary objectives of this study are to *i*) quantify contribution of disturbance and human land use/management in the remotely sensed long-term leaf area change, *ii*) identify primary factors driving the observed spatial patterns of greening and browning, *iii*) to examine the results from the most widely used MODIS and AVHRR LAI data.

In chapter four of this dissertation, we investigate how photosynthetic seasonality evolved into its current state, and what role climatic constraints and their variability played in this process and ultimately in the carbon cycle. We take the ‘laws of minimum’ as a basis and introduce a new framework where the timing of peak photosynthetic activity ($\mathrm{DOY}_{\mathrm{Pmax}}$) acts as a proxy for plants adaptive state to climatic constraints on their growth. The objectives of this study are to *i*) evaluate the $\mathrm{DOY}_{\mathrm{Pmax}}$ framework and characterizing the timing of peak photosynthesis, *ii*) quantify changes in DOY_{Pmax} and its implication on annual GPP, and *iii*) project their changes in a future climate change scenario and CO_2 fluxes.

Finally, in chapter five, we summarize the main findings of this dissertation in the context of northern vegetation in a time of global environmental changes and discuss future research direction. This research was supported by collaborative grant NNX16AO34H, the NASA Earth and Space Science Fellowship and two NASA funded research grants for global MODIS and VIIRS LAI/FPAR production (NNX14AP80A and NNX14AI71G).

CHAPTER 2: Changes in growing season duration and productivity of northern vegetation inferred from long-term remote sensing data

2.1 Introduction

Boreal and arctic ecosystems cover 22% of the terrestrial surface and stretch over North America (NA) and Eurasia (EA). They play a crucial role in the Earth system by regulating energy-water-carbon exchanges between the land surface and the planetary boundary layer (Chapin et al., 2000). During the last half-century, these regions have experienced temperature increases of 0.3 to 1.0 °C per decade higher than anywhere else on the Earth, particularly during the winter and spring seasons (Solomon, 2007). A changing thermal regime and its consequences on physical, hydrological and biogeochemical conditions such as snow depth, soil moisture, disturbance, etc. have already affected northern vegetation structure and function (Walther et al., 2002). For example, increasing shrub cover across a broad range of hemispheric tundra area, termed as "*shrubification*" has been documented (Tape et al., 2006) and changing tree growth has been observed in NA boreal forests (Beck et al., 2011b). As these changes may feedback on regional and global climate, an accurate characterization of changes during the recent past and some idea of future changes is a critical topic of research.

As a way to diagnose vegetation response to climate change, monitoring growing season duration and productivity has drawn particular attention because these are sensitive and easily measurable indicators (Richardson et al., 2013). Field studies have indicated that the growing season duration for northern vegetation has significantly lengthened over the past decades due to both an earlier start and delayed ending (Parmesan & Yohe 2003; Menzel et al., 2006). This is generally thought to result in a longer carbon assimilation period due to a relaxation of low-temperature limits on metabolism (Nemani et al., 2003), and in turn an increase in primary productivity (Xu et al., 2013; Forkel et al., 2016). Indeed, ground observations confirm enhanced productivity from a lengthened photosynthetically active period (Richardson et al., 2010, Keenan et al., 2014).

Satellite observations have been employed to monitor and understand changes in growing season duration and productivity at large spatial scales. Remote sensing data reveal widespread lengthening of the growing season and an increase in greenness or gross primary productivity, also called “greening”, both of which are associated with warmer air temperatures in the high latitudes during the 1980s and 1990s (Myneni et al., 1997). After this period, divergent responses in productivity between boreal (decrease in greenness or productivity called “browning”) and arctic (contiguous greening) vegetation (Goetz et al., 2005; Piao et al .,2011; Bjerke et al., 2014), and a reduced or reversed rate of regional growing season changes were also reported (Høgda et al., 2013; Wang et al., 2015). Furthermore, asymmetric seasonal warming (Serreze et al., 2000) and a multitude of drivers greatly complicates the characterization of variations in growing season duration and productivity. This complexity justifies the need for a comprehensive examination of the magnitude and direction of changes across the northern hemispheric landscape using the longest satellite data set currently available.

The primary objectives of this study are to 1) evaluate the reliability of long-term growing season duration and productivity metrics inferred from satellite data, 2) investigate the spatiotemporal pattern and trend of changes in growing season duration and productivity, and 3) quantify changes across continents (EA and NA), biomes (arctic and boreal) and vegetation types. To achieve these objectives, we used a satellite dataset covering the northern high latitude region (>45°N) for the period 1982 to 2014 (33 years long). We first define pixel-wise growing season duration and productivity metrics, then introduce independent datasets to assess the reliability of metrics inferred from satellite data. Robust statistical tests and trend analyses are used to evaluate long-term vegetation dynamics.

2.2 Materials and Methods

This study is focused on vegetation in the boreal and arctic regions depicted in Figure A1.1. We define 12 sub-vegetation classes and 4 vegetation groups using the Moderate Resolution Imaging Spectroradiometer (MODIS) International Geosphere-Biosphere Programme (IGBP) land cover (Friedl et al., 2010) and Circumpolar Arctic Vegetation Map (CAVM, Walker et al., 2005). Details for vegetation map can be found in Appendix A1.1.1. All data sets used in this study are briefly described in Appendix A1.1.2 and their spatial resolutions are identically harmonized into 1/12° for comparison purpose.

2.2.1. Determination of long-term (33-year) growing season and productivity

Normalized Difference Vegetation Index (NDVI) is a radiometric measure of the amount of photosynthetically active radiation (~400 to 700 nm) absorbed by vegetation. It is calculated from contrasting reflectances at near-infrared (ρ_{nir}) and red (ρ_{red}) bands: NDVI = $(\rho_{nir} - \rho_{red}) / (\rho_{nir} + \rho_{red})$ (Tucker,1979). NDVI has been widely used in studies of phenology, productivity, biomass and disturbance monitoring as it has been proven to be a good surrogate of vegetation photosynthetic activity (Pettorelli et al., 2005). Here, we used the latest version of Global Inventory Modeling and Mapping Studies (GIMMS) NDVI dataset (NDVI3g) which is spanning from July 1981 to December 2014 with a native resolution of 1/12° at bimonthly time steps (Pinzon & Tucker, 2014).

The growing season summed NDVI (or, GSSNDVI) has been found to be a good proxy for vegetation gross primary productivity (Goward et al., 1985; Wang et al., 2004). We derived long-term GSSNDVI from 1982 to 2014 through the inferred corresponding growing season metrics: onset, end and length of growing season (SOS, EOS, and LOS, respectively). Two preprocessing steps were first performed to maintain distinct seasonal vegetation trajectory and minimize spurious signals (e.g., cloud and snow): 1) implementing the Savitzky-Golay filter to smooth the NDVI3g time series (Jönsson et al., 2004; Chen et al., 2004); 2) identifying background NDVI and replacing NDVI that varied irregularly during the winter period (Beck et al., 2006). After that, we linearly interpolated the dataset to a daily time step. We also use the daily freeze/thaw (FT) state of the ground to define the photosynthetically active period because vegetation may remain green during the dormant season.

Based on the daily NDVI and FT time series, we define pixel-wise photosynthetically active growing season metrics as follows (Figure A1.2, Zhu et al., 2016): (a) SOS is the day when the NDVI value is greater than 0.1 and has increased by 25% of the growing season amplitude; (b) EOS is the day when the NDVI value is greater than 0.1 and has decreased by 25% of the growing season amplitude; (c) the ground should be in thawed state; (d) LOS is the duration between SOS and EOS. Note that the growing season amplitude, which represents the difference between the maximum NDVI and the base level, is determined by long-term (1982-2014) mean seasonal NDVI profile. This approach can reduce possible uncertainty involvement in seasonal amplitude determination due to varying maximum NDVI state (Karlsen et al., 2006), whereas can't take account of varying base state of vegetation. Based on the extracted growing season, the pixel-wise GSSNDVI for each grid (*p*) and year (*y*) can be calculated by cumulating daily NDVI ($f_{NDVI}(t)$) over LOS as below.

$$GSSNDVI_{(p,y)} = \sum_{SOS_{(p,y)}}^{EOS_{(p,y)}} f_{NDVI}(t)_{(p,y)}$$

2.2.2 Evaluation of growing season and productivity

We used several independent datasets to evaluate the reliability of inferred SOS, EOS, LOS, and GSSNDVI metrics. For growing season metrics, we utilized three different sets of growing season metrics from MODIS products: Standard land surface phenology product (MCD12Q2, 2001-2012) and independently derived two NDVI (MOD13C1 and MCD43C4, 2000-2014) based growing season metrics via the same method used in NDVI3g. Additionally, we used growing season metrics derived from flux tower measurements of gross primary productivity (GPP; Figure A1.2, SI Section 2.5). Similarly, to evaluate the NDVI3g based GSSNDVI, we used flux tower GPP, the MODIS GPP product (MOD17A3, 2000-2014, SI Section 2.6), and a GPP product based on Multi-Tree Ensemble (MTE) approach from the Max Planck Institute (MTE-GPP, 1982-2011). Temperature based potential SOS (PSOS), EOS (PEOS), LOS (PLOS) and growing season summed warmth index (GSSWI) were also used (see Appendix A1.1.2) as the temporal coverage, i.e. the number of years, of other reference datasets was limited.

The cross-comparisons were performed at both site and continental scales. For site scale evaluation, we selected 109 sample sites based on the latest Benchmark Land Multisite Analysis and Intercomparison of Products (BELMANIP-2) scheme as it provided a good sampling across biomes and land surface types (Baret et al., 2006). For the flux tower versus satellite data comparisons, valid flux sites and data were ascertained as follows: (i) more than 95% of the days had daily GPP data, and (ii) the mean daily quality flag was more than 0.75 (Richardson et al 2010). For continental scale comparisons, all the metrics were converted to anomalies with respect to their common period and then spatially averaged over North America (NA), Eurasia (EA) and the entire circumpolar (CP) region.

2.2.3. Quantification of growing season and productivity change

We used Vogelsang's *t−PST* test (significance level of 0.1) to evaluate the 33-year temporal trends in growing season and productivity metrics. This method is a robust model for trend estimation and does not require *a priori* knowledge of stationarity and also avoids the estimation of autocorrelation parameters (Vogelsang, 1998). We also assessed trends with the Mann-Kendall test (Mann, 1945), but these results are not presented as they were largely similar to those using Vogelsang's method. In view of a hiatus in warming in the recent years (Trenberth & Fasullo, 2013), the analysis was also performed separately for the early (1982–1999) and later (2000–2014) periods to compare with the entire period of the data record (1982–2014).

2.2.4. Quantification of growing season and maximum NDVI contributions to GSSNDVI variability

It is also interesting to be answered how the retrieved growing season and maximum NDVI characterize long-term GSSNDVI changes. We here used a semi-partial regression approach to quantify relative contributions of SOS, EOS, and MAX in explaining inter-annual variability of GSSNDVI time series. This approach provides a measure of the association between two variables (e.g., an independent, X_1, and dependent variable, Y) that remains after controlling for the effects of one or more other predictor variables (X_2,..., X_k). This approach quantifies the proportion of (unique) variance accounted for by the predictor X_1, relative to the total variance of Y. We detrended time series of SOS, EOS, MAX, and GSSNDVI and applied the semi-partial regression to measure the relative contribution of SOS, EOS, and MAX on GSSNDVI changes.

2.3 Result and Discussion

2.3.1. Evaluation of NDVI3g based growing season and productivity metrics

The NDVI3g based metrics of growing season (SOS, EOS, and LOS) and seasonal total productivity (GSSNDVI) agree well with corresponding metrics derived from other evaluation datasets (Table 2.1 and Figure 2.1−2.2). Table 2.1 provides a summary of comparison for the 109 BELMANIP-2 sites distributed over the northern vegetated lands. The correspondence between NDVI3g based metrics and those from the improved MODIS NDVI (MCD43C4) is good - R^2 and RMSE of 0.96 and 5.23 days for SOS, 0.77 and 9.23 days for EOS and 0.89 and 12.37 days for LOS, respectively. Similarly, reasonable agreement is seen for SOS (R^2=0.74) and LOS (R^2=0.59) between NDVI3g and the MODIS phenology product (MCD12Q2). However, EOS from NDVI3g tended to be much later (bias=22.42 days). This could be due to varying data-fitting techniques (Savitzky-Golay vs. piecewise logistic) and/or detection methods (amplitude threshold vs. curvature; White et al., 2009; Ganguly et al., 2010).

GSSNDVI captures the spatiotemporal patterns of productivity metrics derived from the other datasets (Table 2.1). The GSSNDVI explains more than 80% of the spatial variation in the MODIS GPP product (MOD17A3; R^2=0.81). Additional comparisons with MTE-GPP indicate that GSSNDVI captures both spatial (R^2=0.85) and temporal (R=0.52) variations in gross primary productivity.

At the continental scale, the SOS metrics from NDVI3g and temperature (PSOS) agree quite well (R=0.86 in EA, R=0.80 in NA, R=0.82 in CP) (Figure 2.1a). They show a gradual transition from positive to negative anomalies, thus demonstrating the advancing onset of thermal and photosynthetic growing seasons during the last three decades. Unlike SOS, the NDVI3g based EOS metric does not exhibit a close correspondence with temperature-based PEOS over the last three decades (Figure 2.1b). Previous studies have noted that while SOS of northern vegetation is mostly controlled by preseason temperature, EOS has multiple driving factors such as photoperiod, temperature, nutrients, etc. (White et al., 1997; Gill et al., 2015). Nevertheless, a close association between LOS and PLOS is seen (R=0.74 in CP; Figure 2.1c). We also note well-synchronized temporal variations with MODIS LOS metrics from three different MODIS datasets (MCD12Q2, MOD13C1, and MCD43C4). Overall, NDVI3g based growing season metrics reveal good temporal agreements with those of MODIS although we observed some deviations in later common period (2012~), particularly for SOS and LOS. This divergence has been caused by the differences in NDVI/EVI response to vegetation growth between sensors, rather than by the processing methods (See detail explanations in Figure A1.3).

GSSNDVI at the circumpolar scale provides a reasonable representation of the long-term MTE-GPP (R=0.67) and GSSWI (R=0.79). Statistically significant strong correlations indicate cumulative growing season temperature as the driver of inter-annual and long-term variations in growing season photosynthetic activity. GSSNDVI variations also agree with those seen in four different productivity proxies from MODIS data

(Figure 2.1d). In particular, productivity proxies based on integral NDVI or EVI over the growing season (MOD13C1, MCD43C4, and MCD12Q2) show relatively stronger correlations than model-based GPP estimates (MOD17A3).

The long-term SOS, EOS, LOS and GSSNDVI anomalies reflect the impact of global climate events such as the eruption of Mt. Pinatubo in 1991 (shorter growing season and decreased productivity) (Lucht et al., 2002) and the strong El Niño event in 1997-98 (longer growing season and increased productivity) (Buermann et al., 2003). A particularly prominent feature in these metrics is the intense photosynthetic activity in NA during 2010, which is about three standard deviations above the mean GSSNDVI. This exceptional anomaly in NA is a consequence of the greatest warmth in 2010 (Blunden et al., 2011) and it is also seen in metrics of MODIS data or other previous studies (Friedl et al., 2014, Xia et al., 2015). These matching characteristics features in metrics inferred from data from different sensors are particularly noteworthy.

As for metrics from 36 FLUXNET sites (140 site years), NDVI3g explains 73%, 77% and 82% of variations in SOS, EOS, and LOS, respectively (Figure 2.2a). NDVI3g SOS and EOS estimates are, on average, 4.2 and 14.6 days later than those inferred from tower GPP data. This translates to a growing season that is 10.5 days longer. Still, NDVI3g data capture the large variation (60 to 260 days) in growing season across a range of vegetation types (mixed forests, evergreen needleleaf forests, grasses, and tundra) (Table A1.1). It is worthy to note that the pre-processing with background NDVI estimation greatly improves the quality of growing season as shown in our internal comparison (see Figure A1.4). Similarly, NDVI3g data capture about 80% of the tower-based variations in GPP. However, GSSNDVI tends to saturate and shows large variation when GPP is above 1.5kgC/m^2/year (Figure 2.2b). This saturation is a well-known behavior of vegetation index data in dense and productive vegetation types (Sellers, 1985; Myneni & Williams, 1994). The saturation has less impact in our study area because only 3.7% of the vegetation exhibits GSSNDVI greater than 150.

2.3.2. Long-term changes in growing season over northern lands

The growing season in the north has lengthened, on an average, by 8.58 days over the past 33 years (2.60 days·decade^{-1}, $p<0.05$, Table 2.2). The lengthening is greater in EA than in NA (3.04 vs. 1.83 days·decade^{-1}, $p<0.05$). Changes during spring contributed less than changes in autumn to this lengthening in the case of NA. The opposite is the case in EA. Interestingly, changes in growing season duration differed between the first two decades of the data record (1982-1999; 5.06 days·decade^{-1}, $p<0.05$), which was an exceptionally warm period (Trenberth & Fasullo, 2013) and the latter part of the data record (2000-2014; -1.08 days·decade^{-1}, $p>0.1$) during which a warming hiatus was noted (Table 2). This switch from a lengthened (i.e., advancing SOS and delaying EOS) to a shortened (i.e., delaying SOS and advancing EOS) duration was also reported in other studies (Høgda et al., 2013; Wang et al., 2015; Zhao et al., 2015). However, MODIS indicates lengthening growing season during the later period (2000-2014), although the trend estimates from both datasets are not statistically significant from zero ($p>0.1$) due to the short time-span and large inter-annual variations (Table A1.2). Interestingly, at least of the same signs are reported when observed abrupt divergence is ignored.

About 30.6% of northern vegetated land shows statistically significant (Vogelsang's *t-PS_T* test at 10% significance level) changes in SOS over the past 33 years (Figure 2.3a,b and Table A1.3). A majority of these (27.9%) shows an advancing SOS trend, that is, a trend towards earlier springtime greening. Only 2.7% show the opposite trend. The former is especially pronounced in EA while the latter is seen mostly in boreal NA. However, the degree of advancing trend in SOS over the boreal region (Max. PDFs in EA: -2.8 days$\cdot$decade^{-1}, NA: -3.0 days$\cdot$decade^{-1}) is relatively higher than in the arctic region (Max. PDFs EA: -2.5 days$\cdot$decade^{-1}, NA: -2.3 days$\cdot$decade^{-1}). This pattern was reported by previous studies (Shen et al., 2014; 2015) and it implies that an earlier SOS in a warmer region may have higher temperature sensitivity than those in a colder region. Reported less sensitive green-up response in arctic vegetation is also possibly associated with increasing snowfall in winter/spring time which may hinder much earlier green-up in warmer arctic (e.g., Bienik et al., 2015).

About 21.9% of the study region displays a significant delay in autumn senescence (EOS) over the 33-year period of record (Figure 2.3c,d and Table A1.3). The opposite is seen in about 7.8% of the study area. Boreal regions in both NA and EA show predominant delaying EOS, however, the patterns vary between arctic regions in the two continents. Large proportions (>75% of significant changes) of arctic NA show the delayed EOS trend. In EA, this is observed in only about 25% of the vegetated arctic region showing significant changes. These trends in spring greening and autumn senescence resulted in nearly 33% of the northern vegetation experiencing a lengthened growing season (Figure 2.3e,f and Table A1.3). In most such regions, the longer growing season was due to earlier springtime greening. As shown in Figure 2.3f, trends in LOS over boreal regions in both continents (Max. PDFs in EA: 3.50 days·decade^{-1}, NA: 3.75 days·decade^{-1}) have relatively greater lengthening rate than those in arctic regions (Max. PDFs in EA: 2.25 days·decade^{-1}, NA: 3.25 days·decade^{-1}).

2.3.3. Long-term changes in productivity over northern lands

The analysis indicates that growing season summed NDVI (GSSNDVI), a measure of seasonal gross primary productivity, has increased by 2.97 decade^{-1} ($p<0.01$) over the circumpolar region. The rate of increase in NA (2.32 decade^{-1}, $p<0.01$) is less than in EA (3.34 decade^{-1}, $p<0.01$) since the early 1980s (Table 2.2). GSSNDVI exhibits a continuously increasing trend throughout this period, unlike the growing season metrics which show opposite trends between the early (1982 to 1999) and later (2000 to 2014) periods of the data record. However, the GSSNDVI trend during the later period (1.87 decade^{-1}, $p>0.1$) is lower than in the earlier period (4.23 decade^{-1}, $p>0.05$). These results are concordant between AVHRR based NDVI3g data and MODIS NDVI data (Table A1.2).

About 44.4% of the northern vegetated lands exhibit significant changes ($p<0.1$). 42.0% of the area experience increasing (greening) GSSNDVI trends (Figure 2.4a and Table 2.3). Only a small proportion displays a decreasing trend (browning, 2.5%). The greening is more prominently observed in North American mixed forests to the east and arctic coastal tundra and in Eurasian needle-leaf and mixed forests, shrublands and tundra. A fragmented pattern of greening and browning, mostly over evergreen needleleaf forest and the forest-shrub ecotone, is seen in the NA boreal region, unlike its counterpart in EA, which shows widespread contiguous greening. This fragmented browning in the interior NA has been reported as consequences of increasing drought stress and fire disturbance (Goetz et al., 2005, Beck et al., 2011a).

For a large browning area located in the eastern Bering coast of Alaska (Figure 2.4a), according to Bienik et al (2015), this may be linked to delayed snowmelt due to increased snow depth in the late winter/early spring as well as increased cloud cover during midsummer. Another large patch of decreasing productivity is prominently seen in the central Siberian plateau (Figure 2.4a) which is mostly composed by open larch forest, shrub, and erect shrub tundra. This declined productivity is mostly due to the anthropogenic influence (i.e., Cu-Ni smelters) (Toutoubalina & Rees, 1999). And smaller areas with such a decline are also found around similar smelters in Kola Peninsula in the western part of Russia (Tømmervik et al., 2003).

As shown in Figure 2.4b, arctic vegetation in both NA and EA (Max. PDFs EA: 5.0% decade^{-1}, NA: 6.5% decade^{-1}) displays relatively greater greening rates (with respect to 1982) than boreal vegetation (Max. PDFs EA: 3.5% decade^{-1}, NA: 4.0% decade^{-1}). The areal proportion of boreal browning is dominant (67.9% of browning area in CP) in the northern lands. In particular, North American boreal vegetation accounts for 55.6% of the browning area in the circumpolar region.

The seasonal maximum value of NDVI (MAX) determines the seasonal trajectory of photosynthetic activity. Thus, examining changes in MAX helps to better understand spatiotemporal changes in GSSNDVI. The spatial distribution of statistically significant increasing trends in MAX, shown in Figure A1.5, closely resembles that of GSSNDVI (Figure 2.4a), especially in the coastal arctic regions. Whereas resembled trend pattern between GSSNDVI and growing season duration (Figure 2.3e) can be found in the relatively warmer vegetated area. This implies that the seasonal maximum productivity and growing season duration jointly control inter-annual variation and trend of GSSNDVI with differently characterized relative contributions (Xia et al., 2015).

Figure 2.4c displays the GSSNDVI time series of four different vegetation groups. The GSSNDVI of forests, other woody vegetation, and herbaceous vegetation are scaled to the GSSNDVI of tundra for comparison purposes. All four vegetation groups show increasing GSSNDVI trends with tundra exhibiting the largest trend (8.5% decade^{-1}) and forests displaying the lowest (5.5% decade^{-1}). This reflects the higher sensitivity of tundra vegetation productivity as compared to boreal forests (Verbyla, 2008; Beck & Goetz, 2011). There is considerable variation in the trajectory of these time series and the declining greening rate can be clearly seen after the late 1990s. These flattened or slowed change rates are coincident with recently observed warming deceleration (Trenberth & Fasullo 2013) and divergent vegetation growth responses imply differently characterized sensitivities to changing climate. For instance, continued warming may appear to no longer promote boreal forest growth, while the warming may benefit tundra growth (Beck & Goetz, 2011; Bi et al., 2013).

Our analysis indicates that 42.0% of the total northern vegetated area shows a greening trend over the past three decades (Table 2.3). This translates to a 20.9% gain in productivity since 1982. In contrast, 2.5% of browning regions resulted in a decrease of about 1.2% of gross primary productivity since 1982. Note that the quantities of productivity changes represent only regions showing significant directional changes. All forests, in particular, the mixed and evergreen needleaf forests, contributed significantly to the observed gains in productivity. Equally noteworthy is the contribution of shrublands and the forest-shrub ecotone to productivity gains in view of the large greening extent observed in these vegetation types (Table 2.3).

2.3.4. Contribution of growing season and maximum NDVI to GSSNDVI variability

Based on the semi-partial regression analysis, we identified a regionally varying contribution of each variable (SOS, EOS, and MAX) to GSSNDVI inter-annual variability (Figure 2.5a). The high explanatory power of three variables for GSSNDVI variance implies that SOS, EOS, and MAX jointly control GSSNDVI interannual variability (Figure 2.5b). Our result indicates that about 51 % of the study region is dominantly controlled by SOS (more than 50 % of the total variance is explained by SOS), while respective 13 % and 7 % of the region show EOS- and MAX-driven GSSNDVI changes during the last three decades (Table 2.4). The rest of the region (30 %) is co-controlled by three variables together (i.e., the contribution of each variable is less than 50 %). Interestingly, the western and eastern EA regions reveal a clear distinction indicating contrasting regional long-term GSSNDVI changes driven by EOS and SOS. Indeed, Garonna et al. (2014) reported asymmetric changes in SOS and EOS over Europe and found strong EOS driven LOS changes. Buitenwerf et al. (2015) also noticed regionally varying patterns of seasonal NDVI changes and their results are closely aligned with the results presented in Figure 2.5a, though they only visually described a dominant spring NDVI increment over the large portion of northern land.

This analysis further suggests a seasonally uneven NDVI enhancement over the greening regions during the last three decades. This asymmetric importance in seasonal NDVI changes may reveal seasonally varying climatic constraints on plant growth and its dynamism. In general, thermal inertia induced decoupling of radiation and temperature characterizes a unique seasonal climate environment to local vegetation, i.e., strong temperature limit on plant growth in spring season while radiation limitation in the fall season (Garonna et al., 2018). Thus, relatively strong vegetation response to spring warming under less limits of other climate constraints over the temperature-constrained ecosystems may regulate GSSNDVI's interannual variability. For the relatively warmer regions, accumulated water stress in the late growing season may explain the most of interannual variation in GSSNDVI (Garonna et al., 2018). These intrinsic physical environments indicate contrasting responses (sensitivity) of vegetation greenness to spring versus autumn warming, in turn, annual greenness changes.

2.4 Conclusion

We investigated changes in metrics of growing season (SOS, EOS, and LOS) and gross primary productivity proxy (GSSNDVI) over the boreal and arctic lands using long-term satellite observations (GIMMS NDVI3g). An accurate derivation of growing season duration from satellite data is a challenging task. Also, the vegetation index data accumulated over the derived growing season must reflect gross primary productivity. In this sense, the main discriminating point of this work is threefold: 1) this study introduced the photosynthetically active growing season definition by combining optically measured vegetation greenness and ground freeze/thaw data to properly demonstrate photosynthetic activities in northern vegetation. 2) Moreover, we incorporated yearly varying growing season to productivity characterization, thus we enable to understand the relative contribution of growing season and peak greenness on annual gross productivity variability. 3) We evaluated retrieved growing season and productivity metrics using independent multiple direct and indirect measures, particularly eddy-covariance measurements encompassing a wide range of biomes and regions. Special emphasis was placed on assuring that the derived metrics were accurate by comparing them to several independent direct and indirect reference data sets. Overall, these inter-comparison and evaluation analyses reflected that the metrics derived from NDVI3g were reasonably accurate at a range of spatiotemporal scales. Statistical analyses presented in this study provided comprehensive information about patterns in inter-annual variations and long-term trends over the past three decades. At the hemispheric scale, we observed a significant advance in SOS, delay in EOS and lengthened LOS, all of which are concordant with thermal growing season variations. The longer growing season and increasing photosynthetic activity resulted in a predominant greening trend over 42.0% of the northern vegetated area. This translated to a 20.9% gain in gross primary productivity during the last three decades. The GSSNDVI exhibited a continuously increasing trend throughout the 1982 to 2014 period, unlike the growing season metrics which showed opposite trends between the early (1982 to 1999) and later

(2000 to 2014) periods of the data record. The arctic and boreal regions showed surprisingly different variations – greater rate of productivity change and smaller rate of growing season duration change in the arctic versus the opposite in the boreal vegetation – perhaps reflective of the biome-specific temperature sensitivity of the vegetation. Together these results document large-scale spatiotemporal changes happening in the northern vegetation.

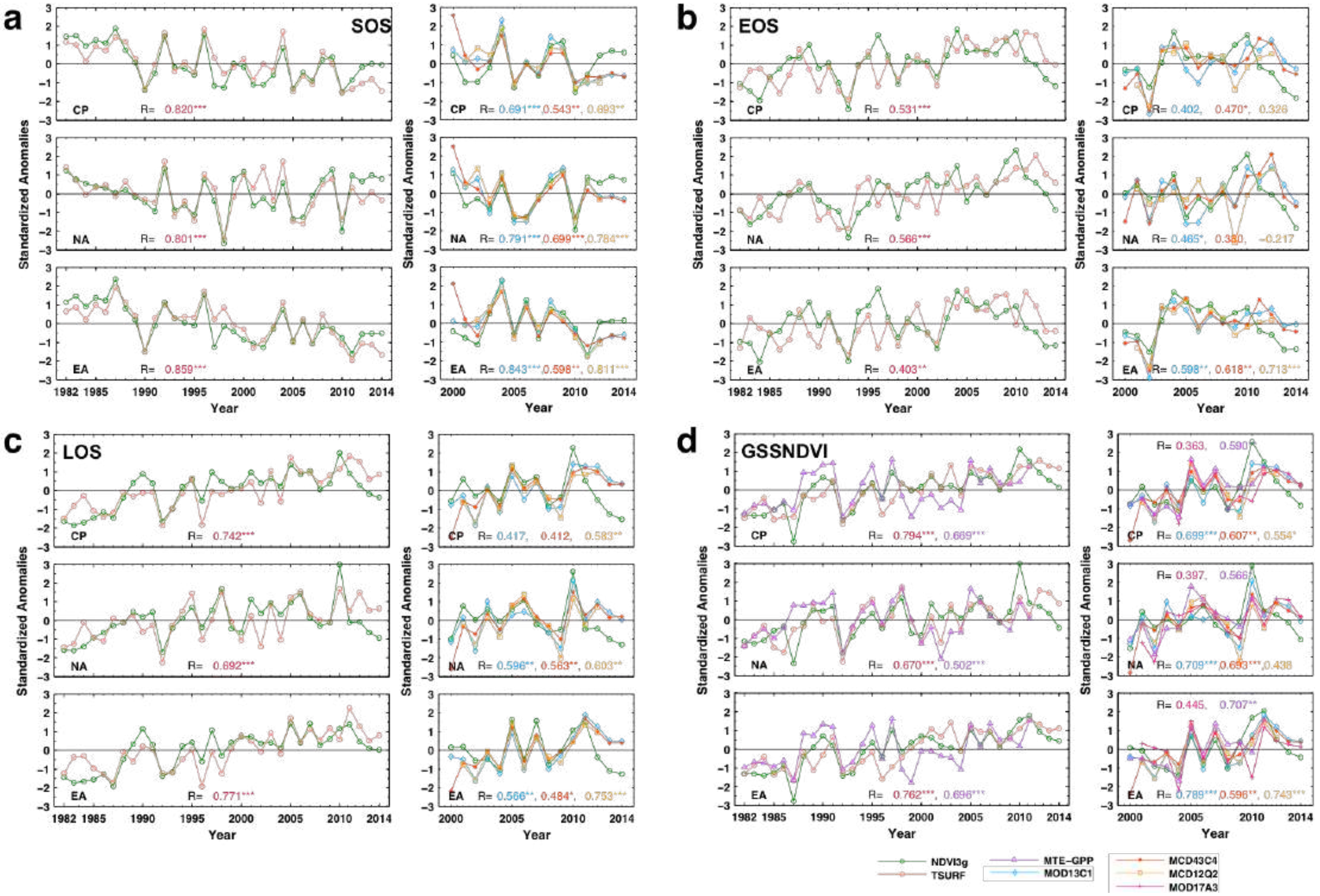

Figure 2.1 Continental scale comparison between NDVI3g and six different evaluation datasets (MCD12Q2, MOD13C1, MCD43C4, MOD17A3, TSURF, MTE-GPP). Correlation coefficients between growing season and productivity metrics from NDVI3g and evaluation datasets are calculated (*: $p<0.01$, **: $p<0.05$, *: $p<0.1$) and given with corresponding color scheme. CP, NA, and EA are for Circumpolar, North America and Eurasia regions, respectively.**

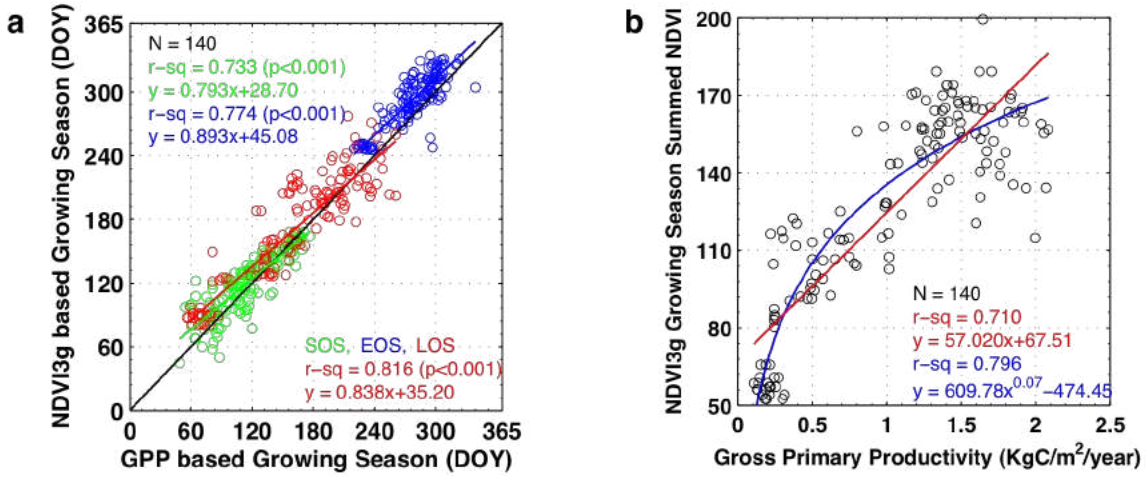

Figure 2.2 Evaluation of NDVI3g based growing season and productivity (GSSNDVI) retrievals using FLUXNET gross primary productivity (GPP) based growing season and productivity. (a) Comparison between NDVI3g and GPP-based growing season metrics over all possible observations (140 site-years), (b) Comparison between NDVI3g GSSNDVI and annual GPP over the observations.

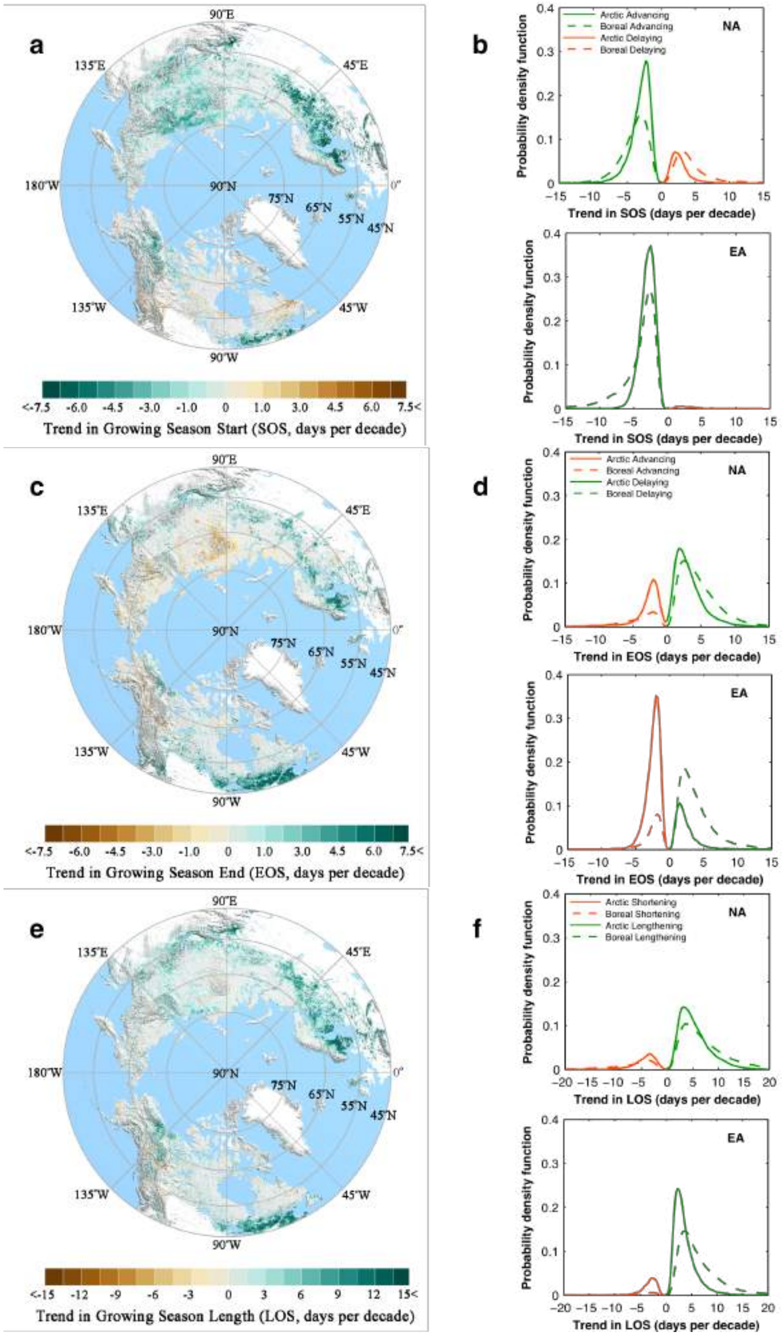

Figure 2.3 Spatial pattern of long-term (1982-2014) trends in vegetation growing season onset (SOS, a), end (EOS, c) and duration (LOS, e). The trend was calculated using Vogelsang's *t-PS_T* test at 10% significance level. Non-vegetated pixels and pixels without significant trend were shown in white and gray, respectively. Probability density function (PDF) of change rate per decade for only significant positive and negative changes is also provided for SOS (b), EOS (d) and LOS (f). PDFs are normalized to the total area showing significant changes in each continent and biome (Table A1.3). NA and EA are for North America and Eurasia. In PDFs, green and red lines represent significant positive and negative changes. Solid and dash lines stand for arctic and boreal regions, respectively.

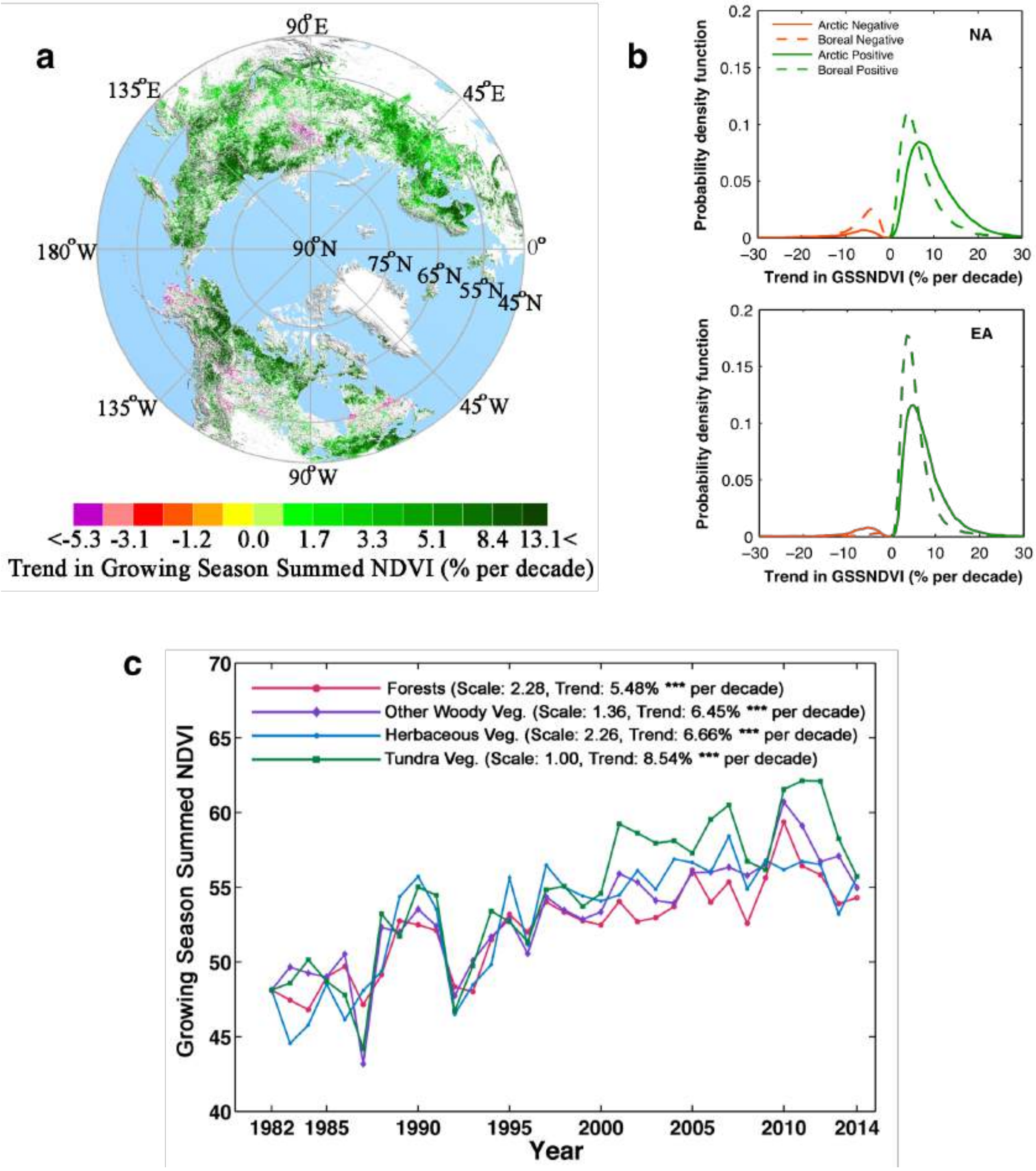

Figure 2.4 a, Long-term (1982-2014) trend in vegetation productivity (GSSNDVI) over Northern vegetated area. The trend was calculated using Vogelsang's t-PS_T test at 10% significance level. Non-vegetated pixels and pixels without significant trend were shown in white and gray, respectively. b, Probability density function (PDF) of GSSNDVI change rate per decade for only showing significant positive and negative changes. PDFs are normalized to the total area showing significant changes in each continent and biome (Table A1.3). Green and red lines represent significant positive and negative PDFs. Solid and dash lines stand for arctic and boreal regions, respectively. c, Trend in spatially aggregated GSSNDVI by grouped vegetation types from 1982 to 2014. Only significant greening and browning pixels were aggregated. For comparison purpose, the GSSNDVIs of all vegetation types were scaled to the GSSNDVI of tundra. NA and EA are for North America and Eurasia, respectively.

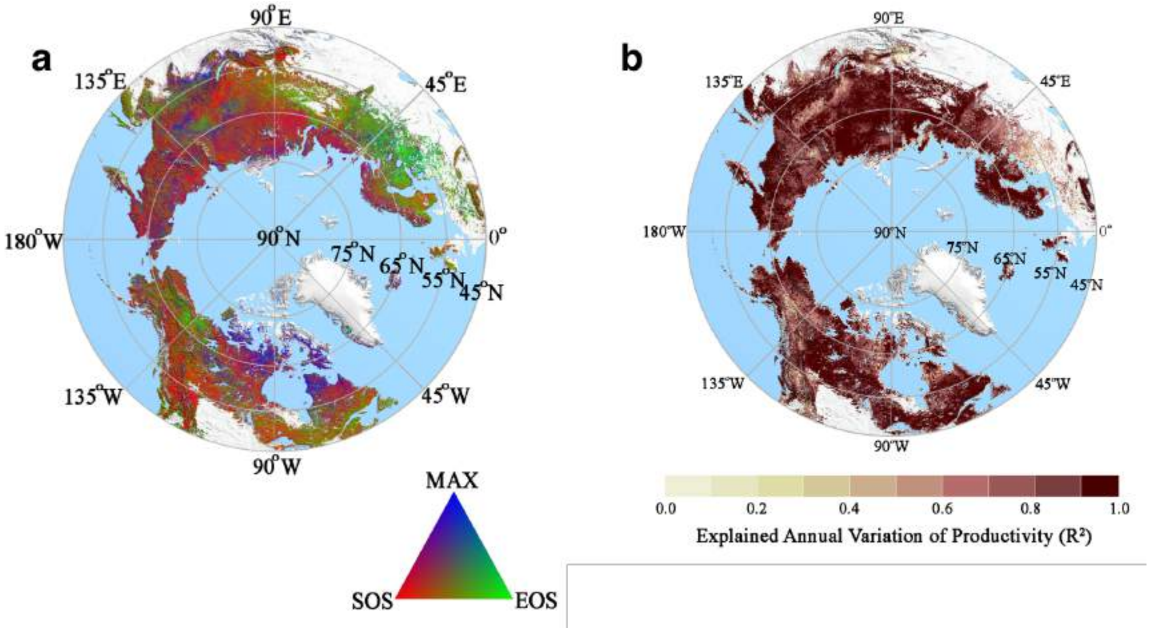

Figure 2.5 a, Map of relative contributions of onset of growing season (SOS), end of growing season (EOS), and maximum NDVI (MAX) over Northern vegetation area. b, The proportion of explained inter-annual GSSNDVI variance by three components.

Table 2.1 Evaluation of NDVI3g based onset of growing season (SOS), end of growing season (EOS), length of growing season (LOS), and growing season summed normalized difference vegetation index (GSSNDVI) at site scale. Respective results of spatial (abbreviated as S) and temporal (abbreviated as T) evaluations are indicated by the coefficient of determination (R^2) and the correlation coefficient (R).

	NDVI3g							
	SOS		EOS		LOS		GSSNDVI	
	S (R^2)	T (R)	S (R^2)	T (R)	S (R^2)	T (R)	S (R^2)	T (R)
MOD13C1[a]	0.93	0.54	0.78	0.38	0.86	0.44	0.92	0.62
MCD43C4[a]	0.96	0.70	0.77	0.34	0.89	0.50	0.92	0.64
MCD12Q2[b]	0.74	0.58	0.28	0.24	0.59	0.42	0.84	0.50
MOD17A3[c]							0.81	0.48
MTE-GPP[c]							0.85	0.52

a: NDVI based growing season and productivity (i.e., growing season summed NDVI) derivations.
b: EVI based growing season and productivity (i.e., growing season summed EVI) derivations.
c: Gross Primary Productivity (GPP) estimate.

Table 2.2 Observed 33-year long-term (1982 to 2014) growing season and productivity trends over continental scale. Trends over separated 1982-1999 and 2000-2014 periods are also calculated. The trends were evaluated by Vogelsang's *t-PS_T* test. CP, NA, and EA are for circumpolar, North America and Eurasia regions, respectively.

	1982-2014			**1982-1999**			**2000-2014**		
	CP	**NA**	**EA**	**CP**	**NA**	**EA**	**CP**	**NA**	**EA**
SOS (days·decade^{-1})	-1.61^{**}	-0.13	-2.45^{**}	-3.67^{**}	-3.20	-3.93^{**}	0.85	2.33	0.00
EOS (days·decade^{-1})	0.67^{*}	1.20^{*}	0.36	1.22	0.78	1.46	-0.69	-0.56	-0.76
LOS (days·decade^{-1})	2.60^{**}	1.83^{**}	3.04^{**}	5.06^{*}	4.74	5.24^{*}	-1.08	-2.30	-0.38
GSSNDVI (decade^{-1})	2.97^{***}	2.32^{***}	3.34^{***}	4.23^{*}	3.31^{*}	4.75^{*}	1.87	1.65	2.00

***: $p<0.01$, **: $p<0.05$, *: $p<0.1$

Table 2.3 Area and productivity (GSSNDVI) changes of vegetation classes showing statistically significant (10% level) trend in GSSNDVI. The trends were calculated pixel by pixel from GSSNDVI between 1982 and 2014 using the Vogelsang model. For area changes, positive trends indicate greening (abbreviated as G), negative trends indicate browning (abbreviated as B) and no-change (abbreviated as N). Also, the total area of each vegetation classes is given (abbreviated as T). For productivity change, productivity increase is abbreviated as I; productivity decrease is abbreviated as D. Productivity change columns show the change in productivity (%) over the area only showing significant changes (positive or negative) between 1982 and 2014. The changes were calculated by by $\sum_{p=1}^{NVC_i} 33yr \cdot T_p \cdot A_p$, where NVC_i is the total pixel number of the ith vegetation classes showing significant positive or negative changes, T_p is the yearly common productivity trend (yr^{-1}) of pixel p, A_p is the area weight (unitless) of pixel p, G_{1982} (= 9.04×10^8, unitless) and B_{1982} (= 5.89×10^7, unitless) are the total GSSNDVI of greening pixels and total GSSNDVI of browning pixels in 1982 (Table A1.4). Total vegetated area is about 26.02 million km^2.

Vegetation Class	Area				Productivity (GSSNDVI)	
	G (%)	B (%)	N (%)	T (%)	I (%)	D (%)
Mixed Forests	10.43	0.10	7.03	17.56	6.12	-0.06
Deciduous Needleleaf Forests	3.67	0.07	5.36	9.10	1.40	-0.02
Evergreen Needleleaf Forests	8.10	0.71	12.01	20.82	4.93	-0.47
Forest-Shrubs Ecotone	4.01	0.51	7.91	12.43	1.81	-0.22
Closed Shrublands	0.16	0.01	0.21	0.38	0.08	-0.01
Open Shrublands	9.72	0.71	14.41	24.84	4.11	-0.28
Grasslands/ Wetlands (North of Forests)	0.35	0.02	0.88	1.25	0.25	-0.02
Erect Shrub Tundra	2.41	0.11	2.48	5.00	1.01	-0.06
Prostrate Shrub Tundra	0.57	0.04	1.30	1.91	0.18	-0.01
Graminoid Tundra	2.13	0.12	3.11	5.36	0.87	-0.05
Wetlands	0.41	0.08	0.88	1.37	0.17	-0.04
Total	41.96	2.48	55.56	100.00	20.92	-1.23

Table 2.4 Fraction of area of categorized dominant type driving interannual variability of growing season summed NDVI (GSSNDVI) over Northern vegetation area. Relative contributions of onset of growing season (SOS), end of growing season (EOS), and maximum photosynthetic status (MAX) were calculated by semi-partial correlation analysis and normalized.

Dominant Type	Relative Contribution Range (%)			Fraction of Area (%)
	SOS	MAX	EOS	
Co- Dominant	0 – 50	0 – 50	0 – 50	29.78
EOS Dominant	0 – 50	0 – 50	50 – 100	13.07
MAX Dominant	0 – 50	50 – 100	0 – 50	6.56
SOS Dominant	50 – 100	0 – 50	0 – 50	50.59
Total				100.00

CHAPTER 3: Disturbance, cultivation, and climate drive a widespread North American vegetation greening

3.1 Introduction

Rapid warming in northern lands has affected on a broad range of ecosystem processes including composition, structure, and functioning of the arctic and boreal vegetation. The relaxation of thermal constraint on photosynthetic activity of vegetation is expected to enhance plant growth and carbon uptake (Myneni et al., 1997; Nemani et al., 2003; Forkel et al., 2016; Park et al., 2019). Extensive long-term ground studies have confirmed warming induced longer growing seasons (Xu et al., 2013; Park et al., 2016), vegetation encroachment into non-vegetated land (Frost & Epstein, 2014; Myers-Smith & Hik, 2018), increasing biomass (or growth rate) of existing vegetation (Pan et al., 2011), changes in community composition (Beck et al., 2011a), and/or changes in plant traits (e.g., leaf area, height, etc.) (Bjorkman et al., 2018).

The warmer condition in the north is not always favoring plant growth. Particularly, over the boreal region, warming-induced intensified summer drought, tree mortality and wildfires have resulted in the decline of summer ecosystem productivity (Barber et al., 2000; Kasischke & Turetsky, 2006; Allen et al., 2010). Furthermore, warmer winter increases the risk of frost damages on plants in the Arctic region and it also causes a negative impact on vegetation growth (Phoenix & Bjerke, 2016). These vegetation changes lead to multi-faceted implications for the regional/global carbon balance (Chapin et al., 2008; Forkel et al., 2016), thus, understanding changes in northern terrestrial vegetation is a key step in diagnosing and prognosticating responses of atmospheric CO_2 to global and/or regional warming.

Satellite remote sensing has been proven to be an invaluable tool to monitor such vegetation changes. The contrasting vegetation changes named ‘greening (increasing greenness or productivity)’ and ‘browning (decreasing greenness or productivity)’ are highly variable in space and over time, and indicate a complex interaction of multiple causal factors on the observed plant growth and its dynamism (Nemani et al., 2003; Zhu et al., 2016). In particular, studies based on long-term satellite records have reported that North American terrestrial ecosystems have experienced extremely heterogeneous patterns of greening and browning during the last three decades (Goetz et al., 2005; Park et al., 2016; Ju et al., 2016; Sulla-Menashe et al., 2018), yet understanding of details of satellite-observed changes and underlying mechanisms are still largely lacking or debating (Alcaraz-Segura et al., 2010; Girardin et al., 2016; Danneyrolles et al., 2019).

One of the most important yet overlooked components of North American (NA) vegetation dynamics is disturbance (Goetz et al., 2007; Johnstone et al., 2010; Beck et al., 2011a; Sulla-Menashe et al., 2018). Wildfire is the most prevalent form of stand-replacing disturbance across the North American boreal forest, significantly affecting the capacity of the boreal forest to sequester and store carbon (Bond-Lamberty et al., 2007). Over the past several decades, fire activity has increased in many NA regions (Kasischke & Turetsky, 2006), highlighting the importance of understanding its effects on vegetation changes. In addition, about one million hectares of the boreal forest is clear-cut each year in NA forests (NRC, 2018) and human-managed agricultural land is another emerging landscape that leads to a heterogeneous pattern of vegetation changes (Chen et al., 2019) suggesting a complex human-nature interaction in these interfaces. This naturally prioritizes our understandings on what underlying processes driving such variation in the remotely sensed vegetation greening/browning trends over different climate, abiotic, and biotic gradients.

In this study, we mainly use the latest version of MODIS LAI data and disturbance history records informing the timing of the event and its type to address the following research questions: a) what is the role of wildfire, harvesting, and agricultural activity in NA's vegetation changes? b) what other controllers drive spatial variations in greening/browning over the non-disturbed and non-managed landscape? We also ask whether two most widely used LAI datasets (i.e., MODIS and AVHRR) are consistent or inconsistent over NA vegetated areas. We use information related to land cover type, disturbance history, topographical features, and changes in climate in NA to characterize the role and relative contributions of disturbance history and climate change in observed geographic patterns of greening and browning. Satellite-based fractional estimates of tree and short vegetation covers are additionally used to understand composition changes in NA's ecosystems.

3.2 Data & Method

In this study, our focused area (~ 9 × 106 km^2) consists of all of Canada and Alaska (exclusive of the Aleutian Islands). We used a terrestrial ecoregion scheme (Olson et al., 2001) of the World Wildlife Fund (WWF) to discriminate the bioclimatic zones.

Based on the WWF's eco-region scheme, tundra and boreal forests/taiga ecoregions were assigned into the arctic and boreal bioclimatic zones, respectively. Temperate broadleaf and mixed forests, temperate coniferous forests, temperate grasslands, savannas, and shrublands were identified as the temperate bioclimatic zone. Croplands include croplands and mosaics of croplands and natural vegetation. Spatial distribution of four biomes is shown in Figure B1.1.

3.2.1 MODIS Leaf Area Index

The latest version (Collection 6, C6) of Terra and Aqua MODIS LAI products (MOD15A2H and MYD15A2H, Myneni et al., 2015a,b) is used in this study (Yan et al., 2016a). These LAI datasets are provided as 8-day composites with a 500-m sinusoidal projection. The datasets are further refined by rigorous checking of the quality fags of the LAI products and of the simultaneous vegetation index products, following the previously described methods (Samanta et al., 2011). This filtering provides the highest quality MODIS LAI observations that minimize any residual contamination from clouds, aerosols, snow, and shadow. The two LAI datasets (that is, four 8-day composites) are then combined into a 16-day composite by taking the mean of all valid LAIs (temporal average). The quality of C6 MODIS LAI datasets has been comprehensively evaluated against ground-based measurements of LAI and through inter-comparisons with other satellite LAI products (Yan et al., 2016b). These datasets represent the latest and highest quality LAI products that are currently available. In this study, we use the time series of 18-year MODIS LAI averaged over the summer season (June – August).

3.2.2 AVHRR Leaf Area Index

We have generated a new version of the LAI data (LAI3gV1) based on the previously described methodology (Zhu et al., 2013). The data provides global coverage with bimonthly frequency at a 1/12° spatial resolution. It spans the period from July 1981 to December 2017. Full time series of LAI3gV1 (hereafter, AVHRR LAI) data was generated by an artificial neural network algorithm that was trained with the overlapping data (2000–2017) of NDVI3gV1 and C6 Terra MODIS LAI datasets. Here, NDVI3gV1 refers to the new version of the third-generation normalized difference vegetation index data provided by Global Inventory Modeling and Mapping Studies (GIMMS) AVHRR (Pinzon & Tucker, 2014). AVHRR LAI data prior to 2000 are not evaluated due to the absence of required field data. Ground data collected as part of MODIS validation efforts after 2000 were used to test the quality of AVHRR LAI data and these have been described previously (Zhu et al., 2013).

3.2.3 MODIS Vegetation Continuous Field

The latest version of Terra MODIS C6 vegetation continuous field (VCF, Dimiceli et al., 2015) is additionally used in this study. The data is a yearly product that presents a continuous, subpixel fraction of land surface cover with a 250-m sinusoidal projection from 2000 to 2016. The fraction of land surface cover comprises by three components including the percentage of tree cover (TC), percentage of short (non-tree) vegetation cover (SVC) and percentage of non-vegetated cover (NVC). The 250-m data are aggregated to 500m and projected into a geographical projection for this study.

3.2.4 MODIS Land Cover

We introduced MODIS land cover data which has been developed by the North American Land Change Monitoring System initiative (Colditz et al., 2014). Nineteen land cover classes were defined using the Land Cover Classification System standard developed by the Food and Agriculture Organization (FAO) and two-epoch LC series (2005 & 2010) at 250 m are available. In this study, we used this LC in 2005 to investigate how varying disturbance history has changed northern landscapes and reached to LC state in 2005. Over the study region, only eleven vegetative classes are present and we recategorized these classes into five broad land cover classes (i.e., coniferous forest, deciduous forest, mixed forest, shrubland, and grassland) with a harmonized spatial resolution (500 m) by applying a majority rule.

3.2.5 Disturbance history

Disturbance history at each pixel was characterized using the combined the Alaskan Large Fire History Database (AFDB, FRAMES, 2018) and the Canadian Large Fire Database (CNFDB, Stocks et al 2002). The AFDB currently contains fire perimeters for the state of Alaska from 1940 through the present (FRAMES, 2018)). Over the Alaskan region, we additionally introduced USFS timber harvest perimeter records to demonstrate historical harvesting activities (USFS, 2019). For the Canadian territory, the CNFDB compiling Providence level data provides fire perimeters since 1910. Note that the exact year range varies by Province. The all fire perimeter vector files were rasterized. We additionally supplemented disturbance information by introducing Landsat based wall-to-wall characterization of wildfire and harvest in Canada. Time series of Landsat data were used to characterize national trends in stand-replacing forest disturbances caused by wildfire and harvest for the period 1985-2015 for Canadian terrestrial ecosystems (Hermosilla et al., 2016; White et al. 2017). Landsat data has a 30m spatial resolution, so the change information is highly detailed and is commensurate with that of human impacts. These data represent annual stand-replacing forest changes. The stand-replacing disturbances types labeled are wildfire and harvest, with lower confidence wildfire and harvest, also shared. In this study, we considered lower confidence wildfire and harvest as wildfire and harvest because they are generally found to be in the correct category (Hermosilla et al., 2016). An overview on the data, image processing, and time series change detection methods applied, as well as information on independent accuracy assessment of the data can be found in Hermosilla et al. (2016). Note that if an area was disturbed multiple times, only the latest occurrence date and type were recorded in the disturbance database.

3.2.6 Climate and Topography

Temperature, precipitation, and radiation time series were derived from a gridded (1 km x 1 km) climate product, Daymet (Thornton et al., 2018). Daymet is a data product derived from a collection of algorithms and computer software designed to interpolate and extrapolate from daily meteorological observations to produce gridded estimates of daily weather parameters. The daily data was aggregated at monthly composition, then summer time (JJA) averaged climate data was used in this study. Topography is a good proxy of site conditions because it influences organic layer thickness, carbon density, drainage and permafrost thaw by means of its control on microclimate. Here, we used the Global Multi-resolution Terrain Elevation Data (GMTED2010) product that provides 15 arc-second spatial resolution and in geographic coordinates with a WGS-84 datum. We derived elevation, slope, transformed aspect (TRASP, Roberts & Cooper, 1989), and topographic position index (TPI, Jenness, 2006). TRASP is defined as

$$TRASP = \frac{1 - (\cos(aspect - 30))}{2}$$

where aspect is in degrees. TRASP ranges from 0 to 1, with values of 0 corresponding to cooler, wetter north-northeaster aspects, and values of 1 corresponding to hotter, dryer south-southwestern aspects. Another factor that was used for the classification of the landscape into morphological categories is TPI. It shows the difference in elevation between a focal cell and all cells in the neighborhood (Jenness, 2006). In the case of plan curvature, negative curvatures illustrate concave, zero curvature represent flat, whereas, positive curvatures are known as convex.

3.2.7 Analytical Approaches

Trends in summer time (June to August) mean MODIS LAI (2000 to 2017) and AVHRR LAI3gV1 (2000 to 2017) are evaluated by the Mann–Kendall test, which is a non-parametric test to detect a monotonic trend in time series data. We used the function ‘zyp.trend.vector’ with the Yue–Pilon pre-whitening method provided by R package ‘zyp’ to conduct the trend test. The trends with $P < 0.1$ are considered to be statistically significant changes in this study. This procedure has been applied to prepare trends of climate data time series including JJA temperature, precipitation, and solar radiation for analyzing spatial patterns of greening/browning. We then quantified LAI, TC/SVC, and LC changes through a chronosequence approach with disturbance and LC information.

In order to quantify the factors modulating the spatial patterns of satellite observed LAI trends to environmental changes, the random forest regression model was used to examine the relationship between the satellite LAI trends and explanatory covariates. Note that this analysis was only applied for the non-disturbed vegetation to explore how vegetation responses vary across different climate norm, change and morphological state. Random forest regression is a non-parametric statistical method requiring no distributional assumptions on covariate in relation to the response variable (Breiman, 2001). The random forest algorithm here uses 1000 binary decision trees. In standard trees, each node is split using the best split among all variables. The explanatory covariates used are long-term means (LAI_mean, T_mean, P_mean, and R_mean) and trends (LAI_trend, T_ trend, P_ trend and R_ trend) of JJA LAI, temperature, precipitation, and solar radiation, DEM, TPI, TRASP. With the random forest regression model, variable importance ranking for variable selection was also calculated. The variable importance measures how much the error increases if we scramble the values of a variable. Larger error before and after permutation means larger importance of the variable in the forest and contribute more to predictive accuracy than other variables (Breiman, 2001). All analysis was done with the ‘treebagger’ package in Matlab. The MODIS-based LAI trend was assessed with respect to the land cover type and disturbance history, and also compared with a trend based on the most recent AVHRR LAI dataset, LAI3g (Zhu et al., 2013).

3.3 Result

3.3.1 Large scale greening and browning patterns in NA

According to MODIS LAI data, we observe the increased green leaf area over the 33.2 % (~ 3×10^6 km^2) of the vegetated regions in Alaskan and Canadian territory (~ 9×10^6 km^2) during the last two decades, while about 5 % (~ 0.5×10^6 km^2) of the study region shows a decrease of leaf area (Figure 3.1a and Table 3.1). The remaining areas (61.8 %) either have small LAI trends that are not significantly different from zero or exhibited significant year-to-year variability that precludes statistical confidence ($p \geq 0.1$). The areas showing greening in NA are 6 times larger than those showing browning, and this dominant greening pattern is more obvious in the arctic (38.7 %, 48 times larger than browning) and cropland (42.5 %, 13 times larger than browning) vegetation. Particularly, the most extensive and intensive greening has occurred primarily in most areas of Canadian Prairies (the southern regions of Alberta, Saskatchewan, and Manitoba) and tundra regions. Among tundra regions, the eastern Canadian arctic regions in Quebec and Labrador reveal the rapid increase of LAIs. For the temperate regions, greening (23.1%) is still prevalent but the ratio (3.5 times) between the areas showing greening and browning is less than the other regions. The MODIS LAI data captures very heterogeneous patches showing both greening and browning trends scattered across the Alaskan and Canadian boreal and temperate zones. Most browning patterns can be seen in the boreal forest of central Alaska, the northern parts of Alberta and Saskatchewan, and the central Manitoba. A strong negative LAI trend is visible in the forest area near Quebec City in the 2000-2017 period.

3.3.2 Disturbance associated changes in greening and browning patterns

The combined historical fire (15.9 %) and harvesting (4.9 %) data shows that about 20.8 % of the total vegetated area has experienced at least one disturbance event (either fire or harvesting) during the last decades and the undisturbed vegetation constituted 79 % of our study region (Figure 3.1b and Table 3.1). Most of the recorded fire and harvesting events have happened over the boreal (74 % of the total disturbed area) and temperate (21 % of the total disturbed area) regions, and it explains the observed heterogeneous spatial pattern of greening and browning patches. Over the boreal and temperate regions, fire is a dominant disturbance component in the boreal ecosystem while harvesting is a main disturbance type in the temperate zone. About 40 % of the regions showing either greening or browning trend is tightly associated with disturbance-induced changes over the boreal and temperate regions. Unlike the boreal and temperate regions, fire and harvesting are not a main causal factor for the observed LAI changes in AR, although few fire-related changes have been observed (e.g., 2007 Anaktuvuk River Fire) and projected to increase.

Dominant greening trends over the one-third of the vegetated area during the 18 years is translated into 9.4×10^5 km^2 net leaf area gain (Table 3.2). This is equivalent to about 6.5 % of total baseline (i.e., LAI at 2000, 14.6×10^6 km^2) leaf area of the NA vegetated area. The boreal vegetation changes contribute the half (48 %) of total net leaf area gain, and the cropland, temperate, and arctic regions are responsible for 21 %, 18 %, and 14 % of the net leaf area changes, respectively. The normalized net leaf area changes by corresponding land area give a comparable rate of vegetation changes over the unit land area. The rate of normalized leaf area changes in CR (0.64 m^2 m^{-2}) is the largest and followed by TE (0.42 m^2 m^{-2}), BO (0.26 m^2 m^{-2}), and AR (0.13 m^2 m^{-2}). About 42% (3.9×10^5 km^2) of the net leaf area gain is associated with disturbance, particularly fire and its following recovery (29%, 2.7×10^5 km^2). Note that the areal extent associated with historical disturbance events is about 20.8 % of the total vegetated area but the area is responsible for 42 % of the total net leaf area change estimate implying a rapid growth in the post-disturbance recovery phase (see details in Section 3.3.3). Surprisingly, the net leaf area gain in the disturbed boreal region is about 2.1 times larger than that of the non-disturbed boreal vegetation, while the net leaf area gains from the areas with/without disturbance are comparable in the temperate region. Varying importance of disturbance types over different biome type is also noticeable: the burned area in the boreal region and the harvested area in the temperate zone are responsible for 81 % and 79 % of the respective net leaf area gain. The net leaf area changes in AR and CR without disturbance far outweigh those with disturbance, and CR shows the highest rate of change under non-disturbed condition. This result suggests how regionally different underlying drivers characterize the remotely sensed greening/browning patterns in NA ecosystems.

Spatial details of local disturbance history, land cover, and topography help our understandings on the dominant patterns in LAI changes over different biomes. We present here four example sites for each biome (Figure B1.2-4). Site A is the Yukon Flats located in the interior Alaska where is one of the most wildfire-prone regions over NA. Site B is the area near the southeastern Ontario where heavy forestry activities have been conducted. Observed patches with greening or browning trends in MODIS LAI over Site A and B correspond well to the fire perimeters and harvested forest patches, respectively. Furthermore, the detected browning or greening trends depend on the time since the event as noticed in Section 3.3.3. Site C and D cover the northeastern part of tundra vegetation in Quebec and the southern parts of Alberta and Saskatchewan, respectively. Both sites are the areas showing the strongest greening signals from MODIS LAI over the arctic and cropland regions. Unlike Site A and B, Site C and D have not likely been disturbed by wildfire and harvesting seriously implying a strong control driven by other natural or anthropogenic factors other than disturbance. Particularly, the most greening in Site C is prevalent in the open shrub-dominated landscape while a cropland-grassland transition in Site D exhibits a strong spatial contrast in degree of greening trends. It is also worthy to note that the greening patterns observed in Site C are not randomly situated, in other words, more complex mechanisms/drivers govern such spatial pattern of vegetation changes rather than large-scale warming simply drives ubiquitous changes in this temperature limited ecosystems. Further results will be discussed in Section 3.3.6.

3.3.3 Disturbance type and timing

The observed LAI trends over the study regions are shown as a function of timing of the latest disturbance event in Figure 3.2a. We note that regions with disturbances prior to 1980 show relatively small positive LAI trends. The trend magnitudes increase for those areas burned or harvested between 1980 and 2000. Both averaged decadal trends of LAI for fire (0.38 ± 0.29 m^2 m^{-2}·$decade^{-1}$) and harvesting (0.39 ± 0.38 m^2 m^{-2}·$decade^{-1}$) peaks at after 15 (harvesting) or 20 (wildfire) years post-disturbance. They then decrease and also show negative trends, as expected, for those areas disturbed recently. See Site A and B in Figure B1.2 and 3. This implies that the trajectory of vegetation change and its state characterize the long-term LAI changes as satellite captures a snapshot (2000 – 2017) of the long-term recovery and succession. Interestingly, the following recovery rate of harvested area is faster than that of the burned area, for example, after 10 years disturbance event (i.e., disturbed in 2006 – 2010), harvested vegetation shows increase of 0.10 ± 0.34 leaf area per decade, while burned vegetation shows a smaller decrease of leaf area (–0.03 ± 0.22 m^2 m^{-2}·$decade^{-1}$). The difference in LAI trends for two disturbance types at 10 years old are statistically significant (t-test, $p < 0.001$).

The estimates of net leaf area changes over the historically disturbed area with wildfire and harvesting vary by functions of trends of LAI and total area disturbed (Figure 3.2c,d). In general, the area disturbed by harvesting is relatively stable (16 % of coefficient of variance) over the last three decades, while the inter-annual variability of the fire-disturbed area varies largely (23 % of coefficient of variance) with respect to a long-term mean of the common period (1985 – 2017). The respective total burned and harvested areas were reported to 1.49×10^6 km^2 and 4.71×10^5 km^2. Together with the rate of LAI change, the net leaf area gains peak at 1991-1995 and 2005-2010 for burned

(9.29×10^4 km^2) and harvested (5.34×10^4 km^2) areas, respectively. Interestingly, the area disturbed before 1970 is approximately 27.2×10^4 km^2, yet its contribution to net leaf area gain is minimal. This indicates a large variation in LAI change along the different disturbance and recovery states suggesting that a history of land surface change is critical to understand current vegetation changes.

3.3.4 Tree and short vegetation cover changes in recovery trajectories

To roughly investigate how vegetation composition has been changed, we introduced MODIS VCF and LC data. Our results for the decadal changes in TC and SVC indicate that positive trends in SVC until first 20 years after a disturbance event, then slow transition to negative SVC with positive TC trends can be observed (Figure 3.2b). This transition corroborates a general view of post-disturbance succession, i.e., herbaceous vegetation initially dominates after high mortality disturbance events until the newly established tree seedlings grow to dominate the canopy. Interestingly, TC and SVC changes from MODIS data differentiate recovery trajectories between two disturbance types, i.e., the area burned generally lose most of the vegetation and slowly recover with herbaceous vegetation but the area cut shows a rapid increase in SVC right after disturbance event likely thanks to remained understory vegetation or more favorable seedling conditions.

An additional investigation based on MODIS LC with a “space-time substitution” approach assuming LC at 2005 can represent a general successional LC transition and reveals distinct discrepancies between two disturbance types (Figure 3.3). Most harvesting activities detected in this study have occurred the areas where coniferous (~ 55 %) & mixed (~ 30 %) forests existing and the post-disturbed LC slowly recover coniferous forest even deciduous and mixed forests first dominate the lands. As our harvesting record only covers since 1985, a further successional transition of LC is hardly inferred. For the burned area, fires strongly prefer to burn over coniferous forests (~ 74 %) and the area burned before 1985 have turned back to a coniferous dominated forest (~45%). A greater occurrence of shrub and grassland can be seen in the recently burned area, while the recently cut area still mostly remain as forests. Our inference based on LC corroborates the finding from MODIS VCF (Figure 3.2b). Our results clearly yet roughly demonstrate this compositional transition from short vegetation to tree dominated, especially coniferous and mixed forest ecosystems over time. Also, different disturbance types show the different trajectory of the recovering process even vegetation greenness (e.g., NDVI and LAI) may not differentiate the discrepancy.

Over the non-disturbed areas showing greening, four biomes have shown different patterns of the tree and short vegetation cover changes. For the cropland region, vegetation cover including both tree and short vegetation cover increases the most (especially, SVC), i.e., non-vegetated area has rapidly diminished. Over the arctic region, short vegetation increase is most common while the boreal region shows a dominant pattern of tree cover increase. Note that we also observe a pattern of TC increase over the boreal-tundra ecotone (see Figure B1.3b-c as an example). Interestingly, the temperate zone, we observe a negative trend of tree cover but positive for short vegetation. This is likely due to unaccounted disturbances and agricultural expansions, frequent drought-induced increasing tree mortality in temperate regions.

3.3.5 LAI changes in MODIS and AVHRR

One of the key issues to be answered over these vegetation greenness changes over northern lands is consistency across different data products or sensors. As noticed earlier, AVHRR LAI is one of the most widely used datasets to investigate global vegetation changes, yet recently raised its reliability issue urges an additional comparison between the changes in MODIS and AVHRR LAIs (Park et al., 2016; Ju & Masek, 2016; Sulla-Menashe et al., 2018). A lack of accounting disturbance history in interpreting the results of previous studies based on AVHRR additionally justify this comparison. Overall, AVHRR shows a similar pattern of LAI changes compared to MODIS data indicating a dominant greening (2.3 times larger than browning) yet more browning area across Alaskan and Canadian territories during the last 18 years (Figure B1.5a and Table B1.1). This difference can be translated into 1.69 × 105 km^2 less net leaf gain during the last two decades (Table 3.2 and Table B1.2). Interestingly, degree of LAI changes in AR from AVHRR (0.25 m^2·m^{-2}) is much stronger than that of MODIS (0.13 m^2·m^{-2}) although its areal extent of greening is smaller than MODIS. This discrepancy leads to a more net leaf area gain (0.52 × 10^5 km^2) from AVHRR LAI over the arctic vegetation. For CR case, 63 % of CR area is getting greener by adding 2.59 × 10^5 km^2 more leaves during 2000 – 2017 period. This area extent and net leaf area change estimates from AVHRR LAI are 20 % and 0.66 × 10^5 km^2 larger than those of MODIS estimates. For BO region, AVHRR gives more browning and less greening areas indicating less net leaf gain from this biome type. As shown in Figure B1.5b, for the same burned area, the AVHRR results in many cases did show the effect of fires and its post-recovery process, however, LAI changes from smaller fires or clear-cut logging activities are not detected or even show opposite trends while the responses of MODIS LAI well correspond to the history of land surface changes (i.e., harvesting and fire) (see Figure B1.5c,d).

3.3.6 Biome-specific important drivers in spatial LAI changes

We use a random forest-based analysis to identify which environmental drivers characterize spatial patterns of landscape-level LAI changes (Figure 3.4). Our results point out that initial LAI is the most important feature to explain the spatial variability of LAI trends in the arctic vegetation. In other words, if there is less vegetation with lower LAI, we have seen relatively smaller changes in LAI while more LAI increase seen where more vegetation is already existing. Also, topography is another important predictor of the spatial pattern of greening trends across all biomes as hinted in Figure 3.4. While the landscape is generally flat, locations with higher slopes and elevations are negatively correlated with the frequency of detecting greening trends. North- and northeast-facing slopes are least likely to exhibit a positive trend, and western and southwestern facing slopes are the most likely in this cold environment. Topographic associations between valley bottoms and vegetation growth likely reflect more favorable edaphic conditions along the channel banks, as well as more sheltered microclimates and available water (McManus et al., 2012). Our result does not identify strong correlations between the magnitude of recent temperature changes and increases in vegetation greenness, possibly due to consistent and strong warming across the entire study region. Given favorable climatic conditions, landscape heterogeneity and species level responses may be stronger predictors of vegetation change.

3.4 Discussion

In this study, we used the latest version of MODIS LAI, VCF, LC, and AVHRR LAI to investigate underlain drivers in the remotely sensed vegetation greenness changes, called, greening/browning patterns. Most of the significant changes in different biome types are driven by different causes and we were noticed that simply vegetation greenness, i.e., LAI (or NDVI), only reflect a partial aspect of the change rather than explaining ongoing complex changes in NA vegetation (e.g., land cover transition, compositional change, etc.). Here, we further discuss relevance of our results to previous studies and what we need to consider in future studies by identifying knowledge gaps.

3.4.1 Regional drivers in North American vegetation changes

This study investigates a continental scale LAI change together with tracking its potential drivers including fire, harvesting, cultivation, and changing climate. Our data-driven results point the regionally contrasting underlain primary drivers in the Alaskan and Canadian territories. First, we've detected the greatest LAI changes during the last two decades over the cropland regions. Cropland greening is mainly attributable to the direct driver without discounting the minor contributions of the indirect drivers (e.g., CO_2 fertilization and climate change) (Rosenzweig et al., 1994). Human-driven direct management activities include quick-growing hybrid cultivars, multiple cropping, irrigation, fertilizer use, pest control, better quality seeds, and farm mechanization (Foley et al., 2011). About 1.4×10^4 km^2 increase in Canadian cropland during the last two decades is partly responsible for this observed LAI change (Statistics Canada, 2019). The observed SVC increase in cropland regions in our study supports this statistic. This emphasizes the importance of human land management/conversion and it is applicable to the managed temperate/boreal region as well (Chen et al., 2019).

Over the temperate region, forestry activity is the main driver of vegetation changes together with wildfire, while wildfire is a more important driver in the boreal vegetation change (Table 3.1 and 3.2). In Canada, about 90% of Canada's forests are located on provincial and territorial Crown lands (NRC, 2018). The provincial and territorial governments are therefore responsible for forest management for sustainable timber production, i.e., strict regulations for an allowable annual cut including both the annual level of harvest allowed on a particular area and the minimum forest age at the time of harvest. Thus, as shown in Figure 3.2d, about 8×10^4 km^2 of forested lands has been stably harvested every year. Also, by law, all forests harvested on public lands must be regenerated, thus, a half of the harvested area is artificially regenerated by planting and seeding activities (NRC, 2018). This intense human-managed forestry partially explains why we found a relatively more rapid LAI and TC change over the harvested area than the burned area.

For the boreal region, about 44 % of a total number of historical fires are initiated by lightning and this type of fire is accountable to 77 % of the total burned area

(Veraverbeke et al., 2017; NRC, 2018). It means most of the burned area is naturally combusted and recovered. Multiple studies have reported an increasing trend of wildfire frequency and burned area during the last century, and future projection under changing climate indicates a continuous its increasing trend (Veraverbeke et al., 2017). This will critically impact on carbon sequestered in woody biomass in the boreal forest. Indeed, Canadian forest service announced that their boreal forest has already transitioned to net carbon source mostly due to natural disturbances including inset outbreak and wildfire (NRC, 2018). To sum up, as reported, these natural and anthropogenic disturbances are critical components characterizing spatial patterns of the remotely sensed greening and browning, and they contribute about half of total net green leaf area gain in NA.

Previous studies have suggested that warming-induced water stress may exacerbate growth condition of coniferous boreal forests and consequentially a nontrivial pattern of decrease in vegetation greenness (Beck et al., 2011b; Buermann et al., 2014). In contrast, our result reports that about 32 % (7.2 %) of the boreal vegetation in NA is getting greener (browner) in the 2000-2017 period and only 4.5 % (18.7 %) of the region reveals browning (greening) pattern without disturbance history (Table 3.1). Ground-based studies based on dendrochronology noticed that both responsive direction and degree may differ by species, i.e., broadleaved trees like aspen favor such warmer condition while coniferous species like black spruce may not (D'Orangeville et al., 2018). In other words, a slow process of transition in stand composition with species competition may be detected as greening even some species' growth may decline or even die off (e.g., Hilmers et al., 2019). Our result based on MODIS VCF hints this point of view.

The extensive arctic greening observed in the 18-year MODIS LAI is likely due to the widely accepted changing climate, i.e., warming (Myneni et al., 1997; Xu et al., 2013; Zhu et al., 2016; Park et al., 2016). Warming-induced shrub expansion in tundra ecosystem is circumarctic phenomenon widely reported in many field studies (Sturm et al., 2001; Tape et al., 2006; Myers-Smith et al., 2011; Myers-Smith & Hik, 2018; Bjorkman et al., 2018). However, the spatial pattern of LAI changes is not aligned with regional warming pattern implying that localized microclimate, vegetation establishment, geomorphology, disturbances including herbivory, thermokarst, erosion, fire, etc. characterize the remotely sensed LAI changes. For instance, in addition to the direct warming induced stimulus on plant growth, warming-driven disturbances (e.g., glacial retreat, thermokarst) and their implications are also critical processes in understanding vegetation changes in the arctic landscape as well (Pastick et al., 2019, see more discussion in Section 3.4.2). Some regional studies have reported the decreased or browned vegetation greenness in recent years even as the climate continues to warm (Pheonix & Bjerke 2016). Early snowmelt and frosting events also have been identified as an important process in tundra browning (Pheonix and Bjerke 2016). The ecological mechanisms regulating tundra browning remain elusive.

3.4.2 Role of disturbance in compositional changes and land cover transition

Our chronological approaches based on MODIS VCF and LC support a general view of post-disturbance recovery stages implying a demographic feature is very important to understand the current state of northern vegetation and its projection to changing climate. Generally, disturbance and its regime shift could critically affect many land cover transitions because the early recovery stage after disturbance plays a large role in the structure and functioning of vegetation and its legacy effect persists for decades (Johnstone et al., 2010; Johnstone et al., 2016). It catalyzes more rapid vegetation changes by removing established plant cover in areas where newly exposed surfaces may follow an altered successional trajectory favoring current (rather than historical) climatic norms (Johnstone et al., 2010; Roland et al., 2016; Hermosilla et al., 2018). This likely has crucial implications on carbon, water and energy balances over disturbed regions, in turn, leading to regional and global consequences. For instance, many ground-based studies have informed that disturbance-induced increase of deciduousness. Deciduous forests are considered more productive indicating more carbon sequestration but higher albedo compared to coniferous species reduces positive feedback to global warming (Beck et al., 2011a). Indeed, our LC analysis informed that the areas with older disturbance events tend to be more mixed and deciduous forests even coniferous forest occurrence has increased as time goes by (Figure 3.3).

Furthermore, Goulden et al. (2011) emphasized that the relative importance of deciduous and evergreen plants shifted during post-fire succession, with deciduous herbs (grass and fireweed) and shrubs (alder and willow) assuming initial importance, and evergreens (black spruce and moss) dominating older stands. The distribution of production by plant functional type paralleled the changes in LAI and species composition. Production at the younger stands was dominated by shrubs and herbaceous plants; production at the older stands was dominated by trees. In addition, an extensive field surveying over burned and harvested areas identified that the relative contribution of each carbon pool (live biomass and deadwood) to total ecosystem carbon varied considerably between disturbance types (Seedre et al., 2014). They noticed that live biomass carbon was significantly higher following harvesting compared to fire because of residual live trees, advanced regeneration, and left shrubs and herbs. These support our finding in Figure 3.2 and Figure 3.3 suggesting a varying rate of TC/SVC and LC change across different disturbance type and timing. It thus conforms a general idea that the rate at which a forest recovers from a disturbance is influenced by a wide range of factors that are related to local site conditions, regional climate, disturbance history (intensity, type, etc.), regional species pool, and species life histories (Harper et al., 2005).

This significant role of disturbance is also critical in the arctic region. A repeated photograph-based study did not find a widespread encroachment of shrub/tree into tundra/shrub dominant landscapes during the last century (Bodie et al., 2019). They only found such transitions over the historically disturbed areas while they identified an increase of shrub/tree density over the shrub/tree established areas. Our results also support this finding as most increases of LAI correspond to the area where already more vegetation existing. Also, tree cover is barely increased in tundra-boreal ecotone and tree cover increase is evident in the area where tree stand already existing yet sparse.

3.4.3 Incomplete land history and its implications

In this study, we utilized available disturbance records over the Alaskan and Canadian territories with regionally varying temporal coverages and these data reasonably well explained MODIS LAI changes. However, still, there are many other disturbance factors we need to account for a complete picture of vegetation change. For instance, Canadian and US Forest Service have reported that insect outbreak and its impact has been increasing since the 2000s. The area damaged by insect outbreaks over Canada from 2000 to 2016 is approximately 1×10^6 km^2 and it is 3.4 times larger than total area burned and cut during the same time period (NRC, 2018). However, in our analysis, we only captured about 4 – 5 % of the area showing browning without fire and harvesting over the boreal and temperate regions. Interestingly, MODIS LAI is able to capture the recent 2014 defoliation event in Quebec and it gives a clear showcase of how insect outbreak-induced defoliation has reduced large-scale leaf area. Possible explanations for the less MODIS LAI decline (or browning) during the last two decades due to insect damages are two-fold: a) MODIS temporal coverage is likely capturing only the recovering phase over the most of damaged regions because a large portion of insect outbreaks occurs in the early MODIS era, b) Canadian forest service has counted forests where more than 20 % of leaves are defoliated, i.e., some of the reported damages may be too weak or ephemeral to be detected, thus masked by strong adjacent greening signals (Senfet al., 2015; Pastick et al., 2019).

Observed LAI trends over the areas categorized as non-disturbed may reflect a recovery from historic disturbances, despite efforts to mask out large-scale disturbances from fires and forestry operations visible during the Landsat era and a century-long fire database. For instance, Tømmervik et al. (2019) incorporated all available historical records of natural and anthropogenic disturbances since 1900 and found that legacies of human-induced land use changes over Eurasian boreal-tundra ecotone (> 67º N) are main predictors explaining the observed vegetation biomass changes rather than climate change. It is more striking because a long and old history of human influence continues to have major impacts on the current forest and tundra structure even these far-northern isolated lands considered as pristine. In our study, we found that the net leaf area changes in the area disturbed before 1970 are not noticeable (Figure 3.2), yet disturbance induced legacy effect (e.g., compositional discrepancy, see Figure 3.3) between disturbed and non-disturbed vegetation may diversify responses to environmental changes (Johnstone et al., 2016) suggesting a critical importance of the completed land surface history.

In this study, we only studied NA vegetation where the longest and spatially explicit disturbance history data available. Over the Eurasian territories, more vast regions need to be investigated to completely understand northern vegetation changes at the continental/global scale. In contrast to NA, fewer archived Landsat data over the region limits to detect historical disturbance occurrences over a whole Landsat era (Zhu et al., 2019). Reasonable disturbance detection is only available from the 2000s over EA (e.g., Hansen et al., 2013). However, we believed that a large proportion of remotely sensed vegetation changes in EA are also tightly associated with land surface history including fire, forestry, cropland expansion, herbivory, human land exploitation, etc., thus local knowledge and historical data are useful to understand these changes.

3.4.4 Confidence in multi-data-based investigation

This study confirms that the observed consistent and inconsistent patterns of vegetation changes in NA from MODIS and AVHRR LAIs. In addition to the AVHRR, a simple visual comparison practice to a Landsat based study (Ju & Masek, 2016) corroborates dominant greening patterns in NA from MODIS and confirmed low confidence in the trends in AVHRR. For instance, Landsat reproduces the extensive and intensive greening in Canadian tundra in Quebec and Labrador where AVHRR does not show significant changes during the last decades. Also, a strong greening signal in north slope from AVHRR LAI is less evident in MODIS LAI and Landsat NDVI. The observed apparent relative insensitivity of the AVHRR LAI to fires in these examples probably can be explained by the fact that the footprint of the 8-km GIMMS AVHRR pixel does not fully cover a 64 km^2 area; rather, the signal comes from an area that comprises only 7 % of the pixel size and its location varies within the 8 km cell over time (Hall et al., 2006). Previous studies reported that sensor artifacts are responsible for some of the inconsistency between vegetation changes observed from multiple satellite data (e.g., Guay et al., 2014). These artifacts are evident in AVHRR data which is due to the loss of sensor calibration, orbital drift of satellites, atmospheric contamination of vegetation signals, disjointed stitching of data from multiple sequential sensors, and harmonization of the signal from different sensors (Tian et al., 2015; Chen et al., 2019). The observed inconsistency in the AVHRR LAI, which is the most broadly used dataset for monitoring ecosystem and carbon balance changes, have broad implications for the evaluation of vegetation and carbon dynamics in this region and globally. This comparison and observed discrepancy suggest a special caution to interpret the results from AVHRR data underscoring the importance of further investigation on the properties of AVHRR and MODIS LAIs. Emerging potentials from new sensors (e.g., VIIRS) and technologies including drone and near-surface remote sensing enable to investigate finer scale vegetation changes by reducing scale discrepancy.

3.5 Conclusion

This study attempts to incorporate available disturbance histories, climate, and topography data to understand the remotely sensed vegetation changes during the last 18 years over Alaskan and Canadian territories. The latest version of 500 m MODIS LAI with strict quality controls allows us to reasonably depict details of recent vegetation changes with accounting land surface history. Our investigation clearly indicates that multiple drivers including natural (wildfire) and anthropogenic (harvesting) disturbances, changing climate, and agricultural activities together govern the dominant large-scale greening trends in NA. Timing and type of disturbances are important to fully comprehend spatially uneven vegetation changes in the boreal and temperate regions. Over the arctic ecosystems, given long-term climate norms and morphological features shaping the past and current state of vegetation are critical to understanding the observed LAI changes. The strongest greening trends in the cropland regions implies the importance of human land management in continental-scale vegetation change. The chronological analysis also reveals a gradual change in LAI as well as stand composition even only tree and short vegetation covers are discriminated. Additional comparisons to

AVHRR and Landsat (only by visual comparison) provide some degree of confidence in our study and urges more extensive and precise investigations across different sensors and datasets. The bottom line suggested by this study is that understanding the NA vegetation changes in the past, present, and future requires a multitude of approaches that consider together linked climatic, geomorphic, and social-ecological drivers and processes.

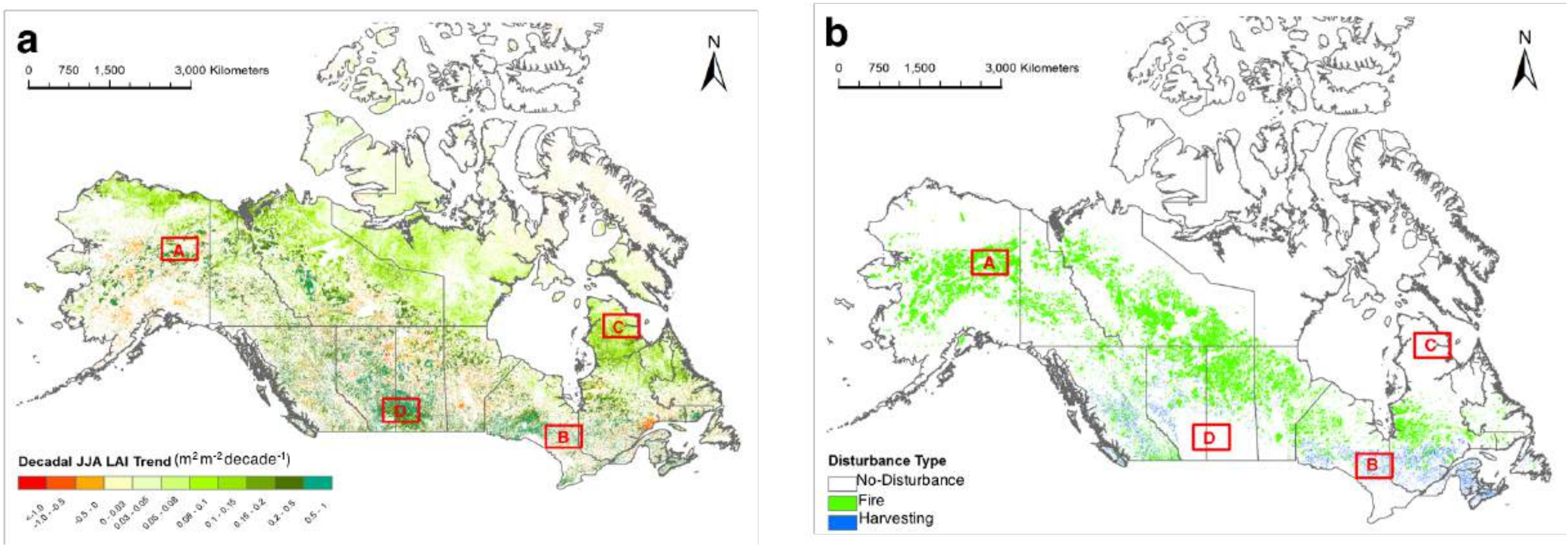

Figure 3.1 Spatial pattern of MODIS LAI trends during the last 18 years (2000 – 2017, a) and historical disturbance events (b) over NA regions. The trend and significance are derived using the non-parametric Mann–Kendall Tau-b with Sen's method. Only statistically significant changes ($p < 0.1$) are color coded. The historical disturbance information is derived from multiple databases and augmented by additional disturbances identified from Landsat data. Four red squares (A – D) in each panel are selected to showcase dominant vegetation change patterns in each biome type (i.e., Arctic, Boreal, Temperate, and Cropland biome types, See Figure S1 for biome type map).

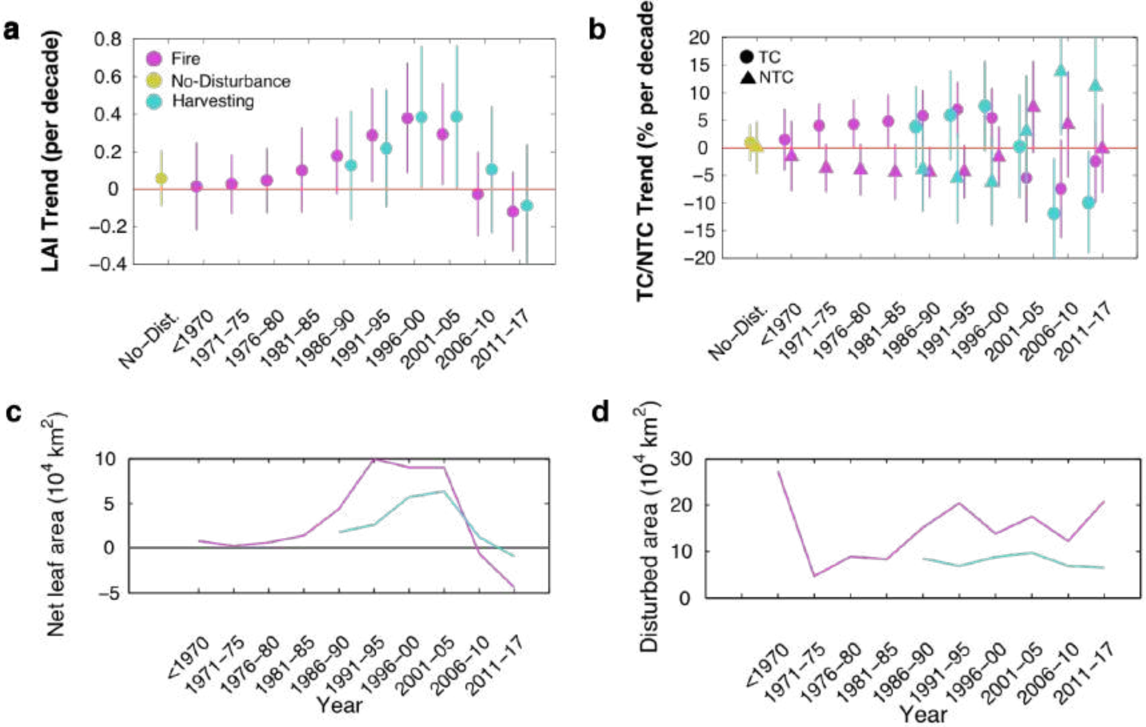

Figure 3.2 Distribution of LAI, TC, and SVC trend estimates grouped by the latest disturbance year across NA regions. Markers show the mean trend estimates of each variable and ±1SD of estimates are also given. Purple, cyan, and green stand for the vegetated area experiencing fire, harvesting, and no disturbance. Note that circle and triangle markers in below panel represent TC and SVC, respectively.

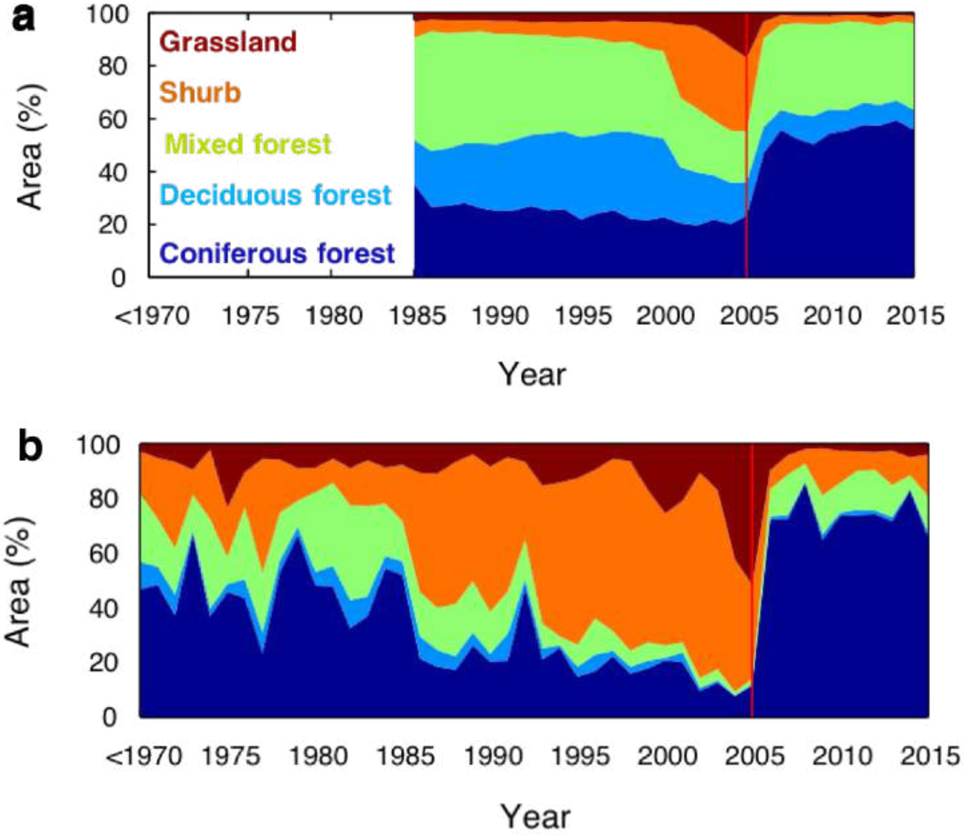

Figure 3.3 Land cover distribution grouped by the latest disturbance year across NA regions. Percent of each land cover occurrence is calculated by the total area of each group classified by disturbance year. NALCMS land cover product (circa 2005) was used.

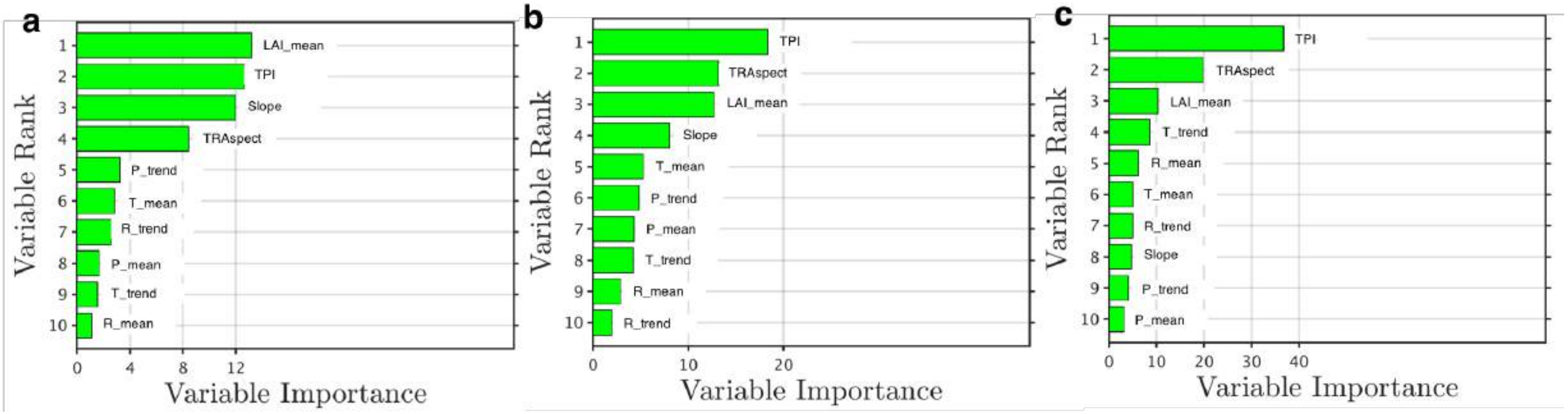

Figure 3.4 Random Forest based variable importance rank for each biome: AR (a), BO (b) and TE (c).

Table 3.1 Proportion (%) of vegetated land showing greening and browning trends in MODIS LAI with or without historical disturbance events. Note that statistically significant positive and negative changes are defined as greening (G) and browning (B), and others are insignificant changes (N.S.). Bracketed numbers in "Disturbed" column represents the solely fire-induced changes, i.e., the changes induced by harvesting can be calculated by subtracting the fire-induced changes from all disturbance-induced changes.

Biome (Area, 10^6 km^2)	Proportion of vegetated land (%)								
	All			Disturbed (fire-induced change)			Non-disturbed		
	B	N.S.	G	B	N.S.	G	B	N.S.	G
AR (2.5)	0.8	60.5	38.7	0.1 (0.1)	1.2 (1.1)	0.5 (0.5)	0.7	59.3	38.2
BO (4.5)	7.2	61	31.8	2.7 (2.4)	15.4 (13.3)	13.1 (11.6)	4.5	45.7	18.7
TE (1.3)	6.6	70.3	23.1	2.3 (0.9)	17.2 (5.6)	8.6 (2.5)	4.3	53.1	14.5
CR (0.7)	3.2	54.3	42.5	1.0 (0.9)	5.0 (4.0)	1.5 (1.1)	2.1	49.4	41.0
All (9.0)	5.0	61.8	33.2	1.8 (1.4)	10.9 (8.1)	8.1 (6.4)	3.2	50.8	25.1

Table 3.2 Net leaf area and mean leaf area index changes during the last 18 years (2000 – 2017) from MODIS LAI. Note that only vegetated areas showing greening and browning are considered in this calculation. Net leaf area and mean leaf area index changes are calculated as follows: $\boldsymbol{Net\ leaf\ area = \sum_{i=1}^{N} Trend_i \cdot Area_i \cdot Period}$, $\boldsymbol{Mean\ leaf\ area\ index = \sum_{i=1}^{N} Trend_i \cdot Area_i \cdot Period / \sum_{i=1}^{N} Area_i}$. Bracketed numbers in "Disturbed" column represents the solely fire-induced changes, i.e., the changes induced by harvesting can be calculated by subtracting the fire-induced changes from all disturbance-induced changes.

	Net leaf area (10^5 km^2)			Mean leaf area index (m^2 m^{-2})		
Biome	All	Disturbed (fire-induced change)	Non-disturbed	All	Disturbed (fire-induced change)	Non-disturbed
AR	1.30	0.06 (0.06)	1.24	0.13	0.39 (0.40)	0.13
BO	4.49	3.04 (2.47)	1.45	0.26	0.43 (0.39)	0.14
TE	1.68	0.81 (0.17)	0.87	0.42	0.55 (0.37)	0.34
CR	1.93	0.03 (0.02)	1.90	0.64	0.17 (0.11)	0.67
All	9.40	3.93 (2.71)	5.47	0.25	0.44 (0.39)	0.21

CHAPTER 4: Changes in timing of seasonal peak photosynthetic activity in northern ecosystems

4.1 Introduction

Warming is generally thought to ease climate constraint on photosynthetic activity of vegetation in northern lands. Indeed, recent growing season studies based on ground observation (Parmesan & Yohe, 2003), eddy covariance (Richardson et al., 2010; Keenan et al., 2014), remote sensing (Xu et al., 2013; Park et al., 2016), and model simulation (Duveneck & Thompson, 2017) have concordantly indicated that the growing season duration for northern terrestrial vegetation has significantly extended over the past decades due to both an earlier start and delayed termination. This prolonged growing season over northern land drives a longer carbon assimilation period due to the relaxation of low-temperature limits on metabolism, and in turn increased productivity and carbon uptake have been observed (Xu et al., 2013; Forkel el al., 2016). However, longer and warmer growing seasons also promote environmental conditions that favor surface drying, and thus intensified summer droughts, tree mortality, and wildfires have resulted in summer productivity decline (Peng et al., 2011; Barichivich et al., 2014; D'Orangeville et al., 2018). These consequential dynamics are highly variable in space and over time, and indicate a complex interaction of multiple climate constraints on plant growth and its dynamism (Nemani et al., 2003; Garonna et al., 2018; Reich et al., 2018). To accurately project the response of northern vegetation to future climate, we need to better understand how climate-vegetation interaction has evolved to its current state, and what role climatic constraints and their variability played in this process.

Photosynthetic seasonality is an integrated outcome of how plants adapt to seasonal variations in climatic constraints (Chuine & Beaubien, 2001; Jolly et al., 2005; Eagleson, 2005; Garonna et al., 2018), and is thus a critical indicator of vegetation-climate interaction. For instance, gross primary productivity (GPP) tracks the seasonal course of temperature in northern high-latitude ecosystems, while the synchrony between GPP and temperature is gradually lost southwards towards warmer and drier environments (see Figure 1 in Rotenberg & Yakir, 2010). The laws of minimum (Sprengel, 1828; Liebig, 1841; Blackman, 1905) explain these shifts in GPP with respect to varying climatic conditions (Eagleson, 2005). The laws state that although photosynthetic activity is controlled by multiple factors (e.g., radiation, temperature, water availability, etc.), the prevailing rate is set by the most deficient of these factors (Sprengel, 1828; Liebig, 1841; Blackman, 1905). This suggests that the timing (Day of Year) of peak photosynthetic rate (DOY_{Pmax}) during the seasonal course corresponds to the period when the primary climatic factor controlling plant growth is least limiting. This simple yet intuitive indicator has an indispensable role not only indicating the timing and magnitude of resource availability (i.e., constraint) but also the capacity of terrestrial ecosystem productivity (Xia et al., 2015; Zhou et al., 2017). Ongoing climate change in the north is expected to alter the state of climatic constraints on plant growth, and therefore, changes in DOY_{Pmax} and productivity. Previous studies have observed trends toward an earlier peak of the growing season (Buitenwerf et al., 2015; Gonsamo et al., 2018). However, the underlying mechanisms for spatially varying relations between its changes and implications on seasonal total productivity and carbon cycle are still largely unknown.

In this study, we take the ‘laws of minimum’ as a basis and introduce a new framework where the timing of peak photosynthetic activity (DOY_{Pmax}) acts as a proxy for plant’s adaptive state to climatic constraints on its growth. Two basic principles formulate this new framework (Figure 4.1). First, under non-limiting climatic conditions, DOY_{Pmax} will show a tendency to coincide with the period of seasonal peak radiation load so as to result in maximum photosynthetic capacity conditions (Eagleson, 2005; Bauerle et al., 2012) (Case 1 in Figure 4.1). Second, if a climatic factor acts as the primary constraint to photosynthetic activity, DOY_{Pmax} should shift towards the period in the seasonal course at which that limiting resource is more available (Eagleson, 2005; Rotenberg & Yakir, 2010) (Cases 2–4 in Figure 4.1). In this framework, the timings of peak GPP (DOY_{Pmax}) and three climatic factors including temperature (DOY_{Tmax}), radiation (DOY_{Rmax}), and water availability (DOY_{Wmax}) serve as key proxies for climate resource availability. We only introduce these three abiotic controls of GPP because it is widely known that they interact to primarily impose complex and varying limitations on vegetation activity (Nemani et al., 2003). Thanks to reduced water losses during the cold season over northern terrestrial ecosystems and thermal inertia, a sequential order of the timings of peak climatic factors ($DOY_{Wmax} < DOY_{Rmax} < DOY_{Tmax}$) simplifies our framework (Figure C1.1). In other words, this suggests that positioning of DOY_{Pmax} with respect to DOY_{Rmax} ($\delta DOY_{P,R} = DOY_{Pmax} - DOY_{Rmax}$) can indicate the primary climatic constraint on ecosystems, i.e., water ($\delta DOY_{P,R} < 0$) or temperature ($\delta DOY_{P,R} > 0$).

$\delta DOY_{P,T}$ defined as $DOY_{Pmax} - DOY_{Tmax}$ is additionally introduced to subdivide dominant temperature constrained northern ecosystems.

Our primary objectives of this study are two-fold: 1) to examine the proposed framework using independent multiple datasets and understand how northern vegetation seasonality has been characterized; 2) to investigate changes in DOY_{Pmax} and its impact on seasonal total productivity and carbon cycle. To accomplish the objectives, we apply the proposed framework to GPP dynamics from the satellite observed vegetation photosynthetic activity to evaluate its validity and changes in DOY_{Pmax}. Two independent sources of vegetation productivity (tower measured GPP and satellite driven Sun-Induced Fluorescence, SIF) are used to further test the framework. We use the atmospheric CO_2 observations at Point Barrow (71.3° N, 156.6° W) and two state-of-the-art CO_2 inversion estimates to investigate the potential impact of shifting DOY_{Pmax} on terrestrial ecosystem carbon cycle. A set of Earth System Models (ESMs) is additionally introduced to evaluate the reproducibility of the observed DOY_{Pmax} changes and their consequences under historical and future climate scenarios.

4.2 Materials and Methods

4.2.1 Study area and bioclimatic zones

Only non-agricultural vegetation over north of 30°N is considered in this study to minimize human-induced influence. Three bioclimatic zones including arctic, boreal and temperate regions were used to present outcomes of this study. To discriminate the bioclimatic zones, we combined a terrestrial ecoregion scheme (Olson et al., 2001) of the

World Wildlife Fund (WWF) and the Moderate Resolution Imaging Spectroradiometer (MODIS) International Geosphere-Biosphere Programme (IGBP) land cover data (Friedl et al., 2010) (Collection 5.1). We first used MODIS IGBP to keep only non-agricultural vegetation classes (Class 1-10, and 16). Then, based on the WWF's eco-region scheme, tundra and boreal forests/taiga ecoregions were assigned into the arctic and boreal bioclimatic zones, respectively. Temperate broadleaf and mixed forests, temperate coniferous forests, temperate grasslands, savannas, and shrublands were identified as the temperate bioclimatic zone. We further excluded the pixels containing more than 25% of cropland based on the International Institute for Applied Systems Analysis (IIASA) cropland fraction data (Fritz et al., 2015).

4.2.2 Multi-scale GPP and its proxy: satellite and tower measurements

In this study, we mainly used 17-year (2000 to 2016) time series of GPP data from the MODIS aboard NASA's Terra satellite (Running et al., 2015) to examine the framework and to investigate $\mathrm{DOY}_{\mathrm{Pmax}}$ change in northern lands. The latest version (Collection 6) of MODIS GPP with 8-day temporal composite was spatially aggregated into 0.05 degree grid. Its high temporal frequency is advantageous to capture the seasonal variation of photosynthetic activity. MODIS GPP is based on a production efficiency model that uses the product of the absorbed photosynthetically active radiation by vegetation and a light use efficiency factor. The quality of MODIS GPP data sets has been comprehensively evaluated against multiple eddy-covariance tower measurements of GPP and through inter-comparisons with other GPP products (Zhao et al., 2005;

Heinsch et al., 2006).

We additionally introduced satellite-driven SIF and eddy-covariance based GPP data to verify our framework and results from MODIS GPP. The SIF is retrieved near the λ = 740 nm far-red peak in chlorophyll fluorescence emission from the Global Ozone Monitoring Experiment-2 (GOME-2) instrument onboard Eumetsat's MetOp-A satellite. The monthly SIF record (version 27, level 3) covering 2007 to 2016 was used in this study (Joiner et al., 2016). SIF is an electromagnetic emission in the 650-800 nm range originating from plant photosynthetic machinery, and it is theoretically linearly correlated with the electron transport rate of photosynthetic activity (Zhang et al., 2014).

The eddy-covariance tower measurements from the FLUXNET2015 database (tier 1, Pastorello et al., 2017) were used in this study. FLUXNET is a global network of micrometeorological tower sites that use eddy covariance methods to measure the exchanges of carbon, water, and energy between terrestrial ecosystems and the atmosphere (Baldocchi et al., 2001). We used GPP estimates based on the flux partitioning approach proposed by Lasslop et al. (2010). A total of 92 sites (those with more than 3 site-year measurements) were selected for the evaluation of our DOY_{Pmax} framework spanning a large climatic and biome gradient (Figure C1.2a).

4.2.3 Multi-scale climate data

We used daily climate datasets provided by Global Modeling and Assimilation Office (GMAO) Reanalysis of NASA (Gelaro et al., 2017). The current version of GMAO is an hourly time step dataset generated by Goddard Earth Observing System-5

(GEOS-5) data assimilation system. We aggregated the native hourly data into the daily scale to retrieve pixel-wise phases of climate variables. Surface air temperature and down-welling photosynthetically active radiation were employed in this analysis. Daily climate datasets were used to characterize DOY_{Tmax} and DOY_{Rmax}. We also obtained potential evapotranspiration (PET) and actual evapotranspiration (AET) to quantify water availability on plant growth by calculating a ratio of AET to PET (RAP) (Prentice et al., 1992). Both AET and PET were obtained by Global Land Data Assimilation Systems (GLDAS, Version 2.1) (Rodell et al., 2004). We characterized summer climate using mean temperature and RAP during June–August for investigating how DOY_{Pmax} positioning varies as functions of climate constraints, i.e., temperature and water availability. For the tower measured GPP, the ancillary microclimate datasets including air temperature and incoming radiation (Photosynthetic photon flux density, PPFD) simultaneously measured with GPP were additionally obtained.

4.2.4 Earth System Model simulated historical and future GPP

We also introduced a set of the most recent climate-carbon simulations of ESMs contributing to the fifth phase of the Coupled Model Intercomparison Project, CMIP5 (Taylor et al., 2012). Seven ESMs, which are available at CMIP5 archive, were used in this study: NorESM1-M, MIROC-ESM, CanESM2, HadGEM2-ES, IPSL-CM5A-MR, MPI-ESM-MR and CCSM4. The datasets provided monthly GPP output (1980 to 2099) for simulations of both Historical and Representative Concentration Pathway (RCP) 4.5 (Thomson et al., 2011). Data from the Historical and RCP4.5 scenario periods were combined to generate continuous variable fields from 1980 to 2099. All model outputs were processed at the native spatial resolutions and aggregated into regional scales (i.e., arctic, boreal, and temperate regions) for trend and correlation estimates.

4.2.5 Timings of peak seasonal photosynthetic activity and climate

We extracted three metrics indicating a maximal state of seasonal photosynthetic activity (DOY_{Pmax}), radiation (DOY_{Rmax}), and temperature (DOY_{Tmax}) at two different scales: site and regional scale. For both scales, to reduce noise and maintain a distinct seasonal feature of GPP (or SIF) and climate datasets, the singular spectrum analysis was first implemented at yearly basis (Vautard et al., 1992). The singular spectrum analysis is a nonparametric approach that does not need a priori specification of models of time series, thus it is data-adaptive. It first decomposes a time series into oscillatory components and noises according to the singular value decomposition, thereafter reconstructs specific components (i.e., seasonal signal) from the original time series. This non-parametric approach has been widely used to reconstruct the time series of GPP and other environmental variables by reducing their noise components (Keenan et al., 2014; Zhou et al., 2017). Time series of GPP and meteorological datasets were used to retrieve DOY_{Pmax}, DOY_{Rmax}, and DOY_{Tmax} on a yearly basis. Note that multi-year averaged daily GPP, radiation, and temperature time series were used for FLUXNET retrievals. For the case of monthly data (SIF and CMIP5 GPP), we assigned middle of the month as the day of the year for each month and then implemented the same procedures used in MODIS and FLUXNET. Finally, $\delta DOY_{P,R}$ (i.e., $DOY_{Pmax} – DOY_{Rmax}$) and $\delta DOY_{P,T}$ (i.e.,

$DOY_{Pmax} - DOY_{Tmax}$) were also calculated. We additionally retrieved pixel-wise growing season length from MODIS GPP by applying a fixed threshold, i.e., 10% of the multi-year average maximum GPP (Zhou et al., 2017).

4.2.6 Atmospheric CO_2 concentration and fluxes: zero-crossing date and seasonal amplitude

Daily atmospheric CO_2 concentration at Point Barrow (71.3° N, 156.6° W) was obtained from the *in-situ* measurement dataset provided by the National Oceanic and Atmospheric Administration / Earth System Research Laboratory (NOAA / ESRL). The spring downward CO_2 zero-crossing date ($DOY_{Zero\text{-}Crossing}$) was extracted by following the approach described in Piao et al. (2008). We first detrended the interannual trend in the atmospheric CO_2 concentration with a quadratic polynomial curve, four harmonics in the seasonal function, and time-filtered residuals. We then used the harmonics plus the residuals (detrended CO_2 seasonal cycle) to define the downward CO_2 $DOY_{Zero\text{-}Crossing}$ as the day on which the detrended curve crossed the zero line from positive to negative. All aforementioned processes were achieved by the use of the standard package CCGCRV from NOAA/ESRL (Thoning et al., 1989). We used $DOY_{Zero\text{-}Crossing}$ as an indicator of proximal DOY_{Pmax} for three reasons, although $DOY_{Zero\text{-}Crossing}$ is not an accurate term of peak photosynthesis timing. First, seasonal trajectory of GPP strongly governs changes in net biome productivity seasonality and its trend (Ito et al., 2016; Forkel et al., 2016). Second, $DOY_{Zero\text{-}Crossing}$ can be determined more accurately and it is roughly corresponding to the time of maximum carbon uptake by the biosphere (Ito et al., 2016).

Third, a relative change in the phase of the cycle identified at one point (e.g. $DOY_{Zero-Crossing}$) will be matched by relative phase changes at all other points since the shape of the seasonal cycle does not change significantly (Barichivich et al., 2012). We further extracted the seasonal cycle amplitude (SCA) because its changes reflect vegetation GPP driven changes in net carbon uptake (Forkel et al., 2016).

We additionally used two gridded carbon fluxes from atmospheric CO_2 inversion products: the Copernicus Atmosphere Monitoring Service (Chevallier et al., 2010) (CAMS, version v15r2, 1979-2015) and the Jena CarboScope (Rödenbeck et al., 2003) (JENA, version s81_v3.8, 1981-2015). Atmospheric CO_2 inversions estimate net carbon exchange fluxes between surface and atmosphere by utilizing CO2 concentrations at measurement sites, combined with an atmospheric transport model and prior information on fossil fuel carbon emissions and carbon exchange between the atmosphere and land (and ocean). We used daily mean net flux estimates on a spatial resolution of 3.75° latitude and 5° longitude (JENA) and 1.875° latitude and 3.75° longitude (CAMS) over the vegetated land surface. Both products were firstly aggregated into regional scales then $DOY_{Zero-Crossing}$ and SCA of carbon fluxes were respectively extracted. Note that the flux amplitude is indirectly related to the amplitude in the atmospheric CO_2 concentration, as the atmospheric concentration is roughly the integral of the fluxes (Welp et al., 2016).

4.2.7 Analytical approach

Based on the extracted MODIS DOY_{Pmax}, we first tested the validity of framework by relating it to summer climate conditions (i.e., temperature and water availability). The first principle we formulated for the framework justifies using summer season as a period when the primary climate constraint dictates vegetation photosynthetic seasonality, and therefore, DOY_{Pmax}. Both seasonal total (GPP_{Total}) and maximum GPP (GPP_{Pmax}) were calculated to investigate the spatial and temporal relations between DOY_{Pmax} and vegetation productivity. In order to capture the seasonal distribution of GPP with a simple metric, we evaluated the ratio (GPP_{Ratio}) of total GPP during the first half (January 1st to the long-term mean DOY_{Pmax}) to that of the whole year. Additionally, the length of growing season together with GPP_{Pmax} was considered to explain the observed pattern between DOY_{Pmax} and GPP_{Total} (e.g., Xia et al., 2015). All explored relationships were explained as functions of $\delta DOY_{P,R}$ and $\delta DOY_{P,T}$. Independent eddy-covariance tower GPP and GOME-2 SIF based retrievals were used for further testing of the framework. Note that we limited the use of these independent data only for verifying the framework and not the change analysis because of limited temporal frequency and coverage of the data.

For the time series analysis, all trends in time series were computed as the slope of linear trends based on ordinary least squares regression. The significance of the trend was computed by using the non-parametric Mann-Kendall trend test. The standard error of the trend slope is also reported. We estimated the decadal trend based on the 5-year moving average approach to reduce the potential impact of first, last and outlier points. The Kendall's rank correlation coefficient (r) was used to measure the ordinal association between given two quantities. To understand how warming-induced DOY_{Pmax} shift has characterized northern land vegetation productivity, we investigated changes in temperature, DOY_{Pmax}, GPP_{Total}, and GPP_{Ratio}. This analysis was applied to both MODIS and ESMs based retrievals. A trend in $DOY_{zero\text{-}crossing}$ of three CO_2 data was respectively computed and correlation analysis between annual variations in $DOY_{zero\text{-}crossing}$ and SCA was performed.

4.3 Results

4.3.1 Spatial pattern of MODIS DOY_{Pmax} and its determinants

A distinct spatial gradient exists in DOY_{Pmax} and in its positioning with respect to the seasonal course of radiation and temperature (Figures 4.2a and Figure C1.2a,b). Overall, DOY_{Pmax} in arctic ecosystems is more closely aligned with DOY_{Tmax} ($\delta DOY_{P,T} = -9.3 \pm 5.5$ days, mean ± 1 s.d.) than DOY_{Rmax} ($\delta DOY_{P,R} = 29.1 \pm 8.5$ days), while in the boreal ecosystems it shows a much closer alignment with peak radiation levels ($\delta DOY_{P,T} = -13.3 \pm 5.4$ days, $\delta DOY_{P,R} = 12.9 \pm 10.5$ days). In the temperate regions, $\delta DOY_{P,R}$ is negative (-9.5 ± 27.0 days), i.e., DOY_{Pmax} precedes DOY_{Rmax}. Temperature and water availability (i.e., RAP) limiting photosynthetic activity elucidate the observed regional variations in DOY_{Pmax} positioning. Every 1 °C increase in temperature results in a $\delta DOY_{P,R}$ change of -5.7 ± 0.1 days (slope ± SE, Figure 4.2b). In regions with negative $\delta DOY_{P,R}$, every 1% decrease in water availability results in a $\delta DOY_{P,R}$ change of -1.8 ± 0.1 days (Figure 4.2c). These results follow the two tenets of our framework, as outlined earlier complying with the laws of minimum (Sprengel, 1828; Liebig, 1841; Blackman, 1905). This suggests that the use of DOY_{Pmax} and its positioning in relation to DOY_{Rmax}

and $\mathrm{DOY}_{\mathrm{Tmax}}$ represents a feasible approach to assess plant's adaptive state to climatic constraints.

4.3.2 Climate constraints, MODIS DOY_{Pmax} and seasonal vegetation productivity

Emerging climatic constraints to plant growth are directly linked to changes in both $\mathrm{GPP}_{\mathrm{Total}}$ (Figure 4.2d) and $\mathrm{GPP}_{\mathrm{Pmax}}$ (Figure C1.2c). Regions with large $\mathrm{GPP}_{\mathrm{Pmax}}$ are associated with tight synchrony between $\mathrm{DOY}_{\mathrm{Pmax}}$ and $\mathrm{DOY}_{\mathrm{Rmax}}$, i.e., both energy and water accessibility are least limiting (Bauerle et al., 2012). Ecosystems under either temperature- ($\delta\mathrm{DOY}_{\mathrm{P,R}} > 0$) or water-limited ($\delta\mathrm{DOY}_{\mathrm{P,R}} < 0$) environments show lower photosynthetic capacity by complying the general idea of climatic constraints to plant growth. Such interaction limiting photosynthetic activity is also tightly associated with growing season duration (Figure C1.2d). It is interesting to note that in areas with the largest $\mathrm{GPP}_{\mathrm{Total}}$ (~ 1.07 kg C m^{-2}), $\mathrm{DOY}_{\mathrm{Pmax}}$ slightly precedes $\mathrm{DOY}_{\mathrm{Rmax}}$ ($\delta\mathrm{DOY}_{\mathrm{P,R}} \approx -7$ days) because of a joint control by growing season length and $\mathrm{GPP}_{\mathrm{Pmax}}$ (Xia et al., 2015). The longest growing season duration (~ 6.5 months) is found when $\delta\mathrm{DOY}_{\mathrm{P,R}}$ is approximately equal to -17 days. This is known as 'phenological trade-off', i.e., a longer growing season imposed by warmer environment may result in a higher $\mathrm{GPP}_{\mathrm{Total}}$, but warmer and drier summers may suppress $\mathrm{GPP}_{\mathrm{Pmax}}$, potentially offsetting the increased amount of $\mathrm{GPP}_{\mathrm{Total}}$ (Duveneck & Thompson, 2017).

4.3.3 Confirmed patterns from two independent data: SIF and Eddy-Covariance tower GPP

Flux tower-measured GPP data from the eddy-covariance network and GOME-2 SIF confirm the above patterns observed in MODIS GPP products, thus lending further support for the proposed $\mathrm{DOY_{Pmax}}$ framework (Figures 4.3 and Figure C1.3).

4.3.4 Changes in MODIS DOY_{Pmax} during last 17 years

Trend analyses reveal a widespread shift in MODIS $\mathrm{DOY_{Pmax}}$ towards earlier in the growing season dominating across 60.6 % of the northern vegetated area during last 17 years, and 32.8 % of the area showing a significant negative trend ($P < 0.1$, Figure 4.4). These changes are seen across all three bioclimatic zones, i.e., 31.9 %, 38.7 % and 26.8 % of the arctic, boreal and temperate regions, respectively. At a hemispheric scale, we detected a significant trend towards an earlier peak photosynthetic rate of −1.66 ± 0.30 days decade^{-1} (slope ± s.e., $P < 0.001$) (Figure 4.5a), with regionally varying degree of advancing trends: a steeper change in the boreal region (−2.46 ± 0.47 days decade^{-1}, $P < 0.001$) relative to the temperate (−1.07 ± 0.26 days decade^{-1}, $P < 0.001$) and arctic regions (−1.09 ± 0.29 days decade^{-1}, $P < 0.001$). These changes are mostly associated with warming in the lands north of 30°N (Figure 4.4b and Figure 4.5b). The sensitivity of $\mathrm{DOY_{Pmax}}$ to warming was detected to be greater in the temperate (−4.27 ± 1.50 days °C^{-1}, $P < 0.001$) than in the arctic (−3.88 ± 1.29 days °C^{-1}, $P < 0.001$) and boreal (−3.91 ± 1.02 days °C^{-1}, $P < 0.001$) regions. Note that regionally varying warming rates (TE < AR < BO) lead to a different order of trend and sensitivity estimates. These changes in

DOY_{Pmax} are interpreted as shifts in $\delta DOY_{P,R}$ across the arctic (−1.98 ± 7.30 days, mean ± SD, t-test, $P < 0.001$), boreal (−3.21 ± 5.83 days, $P < 0.001$) and temperate (−1.28 ± 12.76 days, $P < 0.001$) regions (Figure C1.4a,b). We find that the observed shift in DOY_{Pmax} is mainly responsible for the changes in $\delta DOY_{P,R}$ (and $\delta DOY_{P,T}$) because of relatively stable DOY_{Rmax} and DOY_{Tmax} changes (Figure C1.4 and Table C1.1). According to the principles in our framework, the shifts resulting a newly established photosynthetic seasonality with respect to seasonal climate factors imply changes in vegetation response to varying climatic constraints, i.e., reduced relative importance of thermal constraint in the arctic and boreal vegetation while enhanced role of water availability in the temperate regions (Garonna et al., 2018; Piao et al., 2017; Fu et al., 2015; Allen et al., 2010) (Figures 4.2b,c and 4.5a). Note that some regions transitioning from positive to negative $\delta DOY_{P,R}$ might experience a critical tipping point where the ecosystems move from temperature- towards water-limited ecosystems (Figure C1.5).

4.3.5 Implications of changing MODIS DOY_{Pmax} on seasonal vegetation productivity

The changes in DOY_{Pmax} have regionally varying impacts on GPP_{Total}. An 'earlier peak–larger productivity' pattern is dominant over the arctic (−0.004 ± 0.002 kg C m^{-2} day^{-1}, slope ± s.e., $P < 0.05$) and boreal (−0.006 ± 0.002 kg C m^{-2} day^{-1}, $P < 0.05$) regions under a warming climate (Figure 4.5c). The framework proposed earlier informs that more favorable thermal conditions enable vegetation to increase its synchrony with seasonality in incoming radiation, with the seasonal course of photosynthetic activity tending toward the peak of radiation. Widely reported growing season extension (likely inferred from $\mathrm{DOY}_{\mathrm{Pmax}}$ shift, Figure C1.2d) partly explains such 'earlier peak–larger productivity' relation across the arctic and boreal regions (Xu et al., 2013; Park et al., 2016). Warmer temperatures might also enhance access to key nutrients (e.g., nitrogen), thus stimulating photosynthetic rates over the course of the entire growing season (Natali et al., 2012). A weaker 'earlier peak–less productivity' pattern in the temperate regions emerges due to complex climate-vegetation interactions (Figure 4.5c). Here, warmer conditions without moisture-stress result in an earlier $\mathrm{DOY}_{\mathrm{Pmax}}$ and larger $\mathrm{GPP}_{\mathrm{Pmax}}$ and $\mathrm{GPP}_{\mathrm{Total}}$. In other parts, where moisture stress is stronger, a significant decline in both $\mathrm{GPP}_{\mathrm{Pmax}}$ and $\mathrm{GPP}_{\mathrm{Total}}$ is seen despite earlier $\mathrm{DOY}_{\mathrm{Pmax}}$ (e.g., southwestern Eurasia) (Angert et al., 2005). In order to capture the seasonal distribution of GPP with a simple metric we evaluated the ratio ($\mathrm{GPP}_{\mathrm{Ratio}}$) of total GPP during the first half (January 1st to the long-term mean $\mathrm{DOY}_{\mathrm{Pmax}}$) to that of the whole year. We find that $\mathrm{DOY}_{\mathrm{Pmax}}$ occurring one day earlier in the season increases $\mathrm{GPP}_{\mathrm{Ratio}}$ by 0.28 ± 0.07 (temperate, slope ± SE, $P < 0.001$) to 0.58 ± 0.08 % (boreal, $P < 0.001$), clearly indicating an advance in gross carbon assimilation activity (Figure 4.5d) (Duveneck & Thompson, 2017). This is an important indicator, as the photosynthetic activity is tightly linked to the atmosphere via carbon, water and energy cycles. Thus, phase shifts in carbon, water and energy cycles could be anticipated (Richardson et al., 2013).

4.3.6 Changes in phase and amplitude of CO_2 seasonal cycle

We found that earlier peak photosynthesis and more carbon assimilation in the early part of the growing season altered the seasonal course of atmospheric CO_2

concentration. We used CO_2 observations from Point Barrow and two state-of-the-art CO_2 inversion datasets (i.e., CAMS and JENA). The springtime downward CO_2 zero-crossing date ($DOY_{Zero\text{-}Crossing}$) shows trends towards earlier downward $DOY_{Zero\text{-}Crossing}$ in the three CO_2 datasets (Figure 4.6a). The phase of atmospheric CO_2 at Point Barrow has advanced by 1.84 ± 0.20 days decade^{-1} (slope ± SE, $P < 0.001$) since 1972. We also observe advancing trends but steeper changes in both CAMS (−2.42 ± 0.21 days decade^{-1}, $P < 0.001$) and JENA (−3.26 ± 0.21 days decade^{-1}, $P < 0.001$). This shift corroborates the advancing DOY_{Pmax} of gross photosynthetic activity observed from space and shows the potential implications of enhanced gross carbon assimilation in the early growing season (i.e., increased GPP_{Ratio}) (Barichivich et al., 2012; Randerson et al., 1999) (Figure 4.5a,d). Furthermore, like as what we observed in the analysis of DOY_{Pmax} and GPP_{Total} (Figure 4.5c), SCA of three CO_2 data is negatively associated with $DOY_{Zero\text{-}Crossing}$ (Figure 4.6b). These phase shifts in the CO2 data and their association with the enhanced seasonal amplitudes are in accordance with several observations (Barichivich et al., 2012; Randerson et al., 1999; Graven et al., 2013) and modeling studies (Duveneck & Thompson, 2017; Zhao & Zeng, 2014) suggesting enhanced peak photosynthetic activity and its advancing shift.

4.3.7 Changes in ESMs simulated vegetation productivity and DOY_{Pmax}

We lastly ask whether state-of-the-art terrestrial biosphere models can reproduce the observed DOY_{Pmax} changes and their consequences under historical and future climate scenarios (Figure 4.7). The ESMs project an advancing DOY_{Pmax} across all northern bioclimatic zones for the period 1980 to 2030. We see a pattern of regional DOY_{Pmax} trends from ESMs analogous to satellite observations, i.e. a strong trend for shifting to earlier in the season over the boreal (−0.94 ± 0.67 days decade^{-1}, mean ± 1 s.d. across all ESMs), arctic (−0.86 ± 0.71 days decade^{-1}) and temperate (−0.58 ± 0.61 days decade^{-1}) regions. All models show a tightly linked negative relation between DOY_{Pmax} and GPP_{Total}, revealing the 'earlier peak-larger productivity' tendency as in current satellite observations. Particularly, temperature-constrained arctic and boreal regions have a tighter linkage between DOY_{Pmax} and GPP_{Total} than the warmer temperate regions. The shift in DOY_{Pmax} also increases the GPP_{Ratio}, indicating more carbon assimilation in the early part of the growing season than in the later period (Duveneck & Thompson, 2017; Zhao & Zeng, 2014). The pace of future (2050 – 2100) DOY_{Pmax} shift and its contribution to productivity is projected to continue, but to be slower and weaker than at present.

4.4 Discussion

Our analyses from long-term satellite records and ESMs reveal a widespread shift in DOY_{Pmax} towards earlier in the growing season. The changes are associated with divergent consequences on GPP_{Total} depending on different states of climate constraints on plant growth. For high latitude arctic ecosystems, the advancement in DOY_{Pmax} likely continues in a warmer future climate as seen in the ESM simulations. Our framework translates the change into a continuous relaxation of temperature limit on arctic vegetation photosynthetic activity. A recent remote sensing-based study supports our study by identifying a 16.4% decline in the area of vegetated land that is limited by temperature (Keenan & Riley, 2018). Yet, our framework suggests a reduction in the relative importance of temperature control on plant photosynthetic activity rather than a transitional state where other climate constraints primarily govern the ecosystem (Figure C1.4a). Indeed, long-term ground-based studies in the Arctic tundra have shown that temperature is a primary driver of shrub growth and its expansion in arctic environment, while soil moisture controls the sensitivity of growth response to warming (Myers-Smith et al., 2015).

Some of boreal ecosystems (northwest Russia and south Fennoscandia, south and southeast Canada) show a transition from positive to negative $\delta DOY_{P,R}$ during last two decades (Figure C1.5). This transition does not necessarily signify a decline of GPP_{Total} because of the “phenological tradeoff” mechanism (Figure C1.2d). However, it is critical to monitor these ecosystems continuously because our framework suggests that there may be a tipping point where they move from temperature- towards water-limited ecosystems. That is, continuous warming and drying conditions may exacerbate moisture stress, and therefore, productivity reduction in these ecosystems. Interestingly, a recent tree-ring based study revealed that while 2 °C of warming may increase overall forest productivity, additional warming could reverse this trend and lead to substantial moisture stress (D’Orangeville et al., 2018). Also, multiple warming experiments confirm the dynamism of climate constraints on plant growth in the southern boreal forest and highlight the vulnerability of the ecosystem to excess warming and drying (e.g., Reich et al., 2018).

Warmer and drier conditions over temperate vegetation, where negative $\delta DOY_{P,R}$

is dominant, generally result in a decrease of plant growth. Widespread increase of tree mortality of this susceptible ecosystem to worsening moisture stress has been reported (Allen et al., 2010). Most epidemic climate-induced tree mortality events occur over the regions where water availability is the primary climate constraint on photosynthetic activity (i.e., $\delta DOY_{P,R} < 0$, see Figure C1.5). It agrees with the 'earlier peak–less productivity' pattern in warmer temperate vegetation from MODIS data. However, the relation was not reproduced by the ESMs. The models projected that warming-induced earlier peak photosynthesis leads to an enhanced seasonal total productivity (Figure 4.7a). Recent studies have shown that current terrestrial carbon-cycle models substantially overestimate (underestimate) positive (negative) effects associated with warming (Buermann et al., 2018). It is possibly because these models inadequately capture the effects of the seasonal build-up of water stress on seasonal vegetation growth.

Our analyses of $DOY_{zero\text{-}crossing}$ and SCA confirm the advancing and enhancing CO_2 seasonal cycle in northern lands (Barichivich et al., 2012; Graven et al., 2013; Forkel et al., 2016). An additional remark made here for ongoing changes in biosphere-atmosphere interaction is an asymmetric enhancement of terrestrial photosynthetic activity. We find a widespread warming-induced DOY_{Pmax} advancement and GPP_{Total} increase across northern lands, and these changes possibly play a role in ongoing shift and amplified atmospheric CO_2 seasonal cycle. This is because peak photosynthesis rate explains about 78% of the variation of seasonal total productivity and only 21% can be explained by growing season changes (Xia et al., 2015). Our results confirm that a larger beneficial carbon uptake from an extended growing season is dominated by the later part of spring, when more fully developed leaf area with more favorable light and temperature is available for photosynthetic activity (Keenan et al., 2014). Together with these earlier studies, our findings suggest that an intra-seasonal scale may provide a possible but overlooked mechanism for the changes in atmospheric CO_2 seasonal cycle. Furthermore, the observed shift in the relative importance of climate constraints on plant growth may be a possible mechanism for the recently reported weakening temperature controls on spring carbon uptake across northern lands (Piao et al., 2017).

Furthermore, our framework also gives insight into the changes in growing season duration and its implication on carbon cycle. As described in Figure 4.1, thermal inertia induced decoupling of radiation and temperature characterizes a unique seasonal climate environment to local vegetation. For temperature-constrained ecosystems (see Case-2 in Figure 4.1), DOY_{Tmax}-ward DOY_{Pmax} positioning leads to strong temperature dependence in spring photosynthesis while light availability emerges as an important controller in autumnal activity (Garonna et al., 2018). This intrinsic physical environment indicates contrasting responses of photosynthetic activity to spring versus autumn warming. In this cold environment, spring warming generally stimulates carbon uptake by extending onset of growing season (Pulliainen et al., 2017). In contrast, autumnal growing season extension and its photosynthetic carbon gain will be strongly limited by radiation (Bauerle et al., 2012). Multiple studies have reported that the increase of autumn temperature results in net carbon loss indicating more respiratory loss than photosynthetic gain in northern lands (Piao et al., 2008; Commane et al. 2017). These contrasting seasonal responses also partially explain the observed and projected asymmetric enhancement of photosynthetic activity and carbon cycles in northern lands. However, further studies will be required to identify which case the autumn growing season extension can lead to increased photosynthesis sufficient to balance the higher respiration carbon loss.

Most of ESMs as well as MODIS GPP estimate used in this study do not include photosynthetic temperature acclimation process. This physiological adjustment is commonly observed as a shift in the optimum temperature for carbon assimilation rate by modulating local plant's metabolism (Yamori et al., 2014). We expect that taking the photosynthetic thermal acclimation likely lead to a slightly closer alignment between DOY_{Pmax} and DOY_{Rmax} than the one without the process. It also may reduce the observed DOYPmax sensitivity to warming (Smith et al., 2016). Nevertheless, we believe that the proposed DOY_{Pmax} framework and its changes are valid because of multiple evidence from independent datasets in this work (Figures 4.3 and Figure C1.3) and previous studies (Rotenberg & Yakir, 2010; Buitenwerf et al., 2015; Gonsamo et al., 2018). Interestingly, dendrometer based intra-annual tree growth studies also support our framework (e.g., Rossi et al., 2006). Ongoing efforts for advancements in modeling communities (Rogers et al., 2017) will help to deploy temperature acclimation modules in ESMs and thus better understandings on seasonal photosynthesis and DOY_{Pmax} changes are expected.

4.5 Conclusion

This study took the ‘laws of minimum’ as a basis and introduced a new framework where the timing (Day of Year) of peak photosynthetic activity (DOY_{Pmax}) acts as a proxy for plant’s adaptive state to climatic constraints on its growth. Our analyses confirmed that spatial variations in DOY_{Pmax} reflect spatial gradients in climatic constraints as well as seasonal maximum and total productivity. We found a widespread warming-induced advance in DOY_{Pmax} (−1.66 ± 0.30 days decade-1, $P < 0.001$) across northern lands, indicating a spatiotemporal dynamism of climatic constraints to plant growth. We showed that the observed changes in DOY_{Pmax} are associated with an increase in total gross primary productivity through enhanced carbon assimilation early in the growing season, which leads to an earlier phase shift in land-atmosphere carbon fluxes and an increase in their amplitude. Such changes are expected to continue in the future based on our analysis of Earth System Model projections. This is a critical development because the shifts in peak photosynthesis may cause cascading perturbations in Earth system components that include carbon, water and energy balances (Richardson et al., 2013), as well as ecological interactions (Walther, 2010). The framework proposed here is one of the first attempts to introduce the time of peak photosynthesis as an indicator of a plant’s adaptive state to climatic constraints and provides a simplified yet realistic framework for the complex mechanisms by which various climatic factors constrain plant growth.

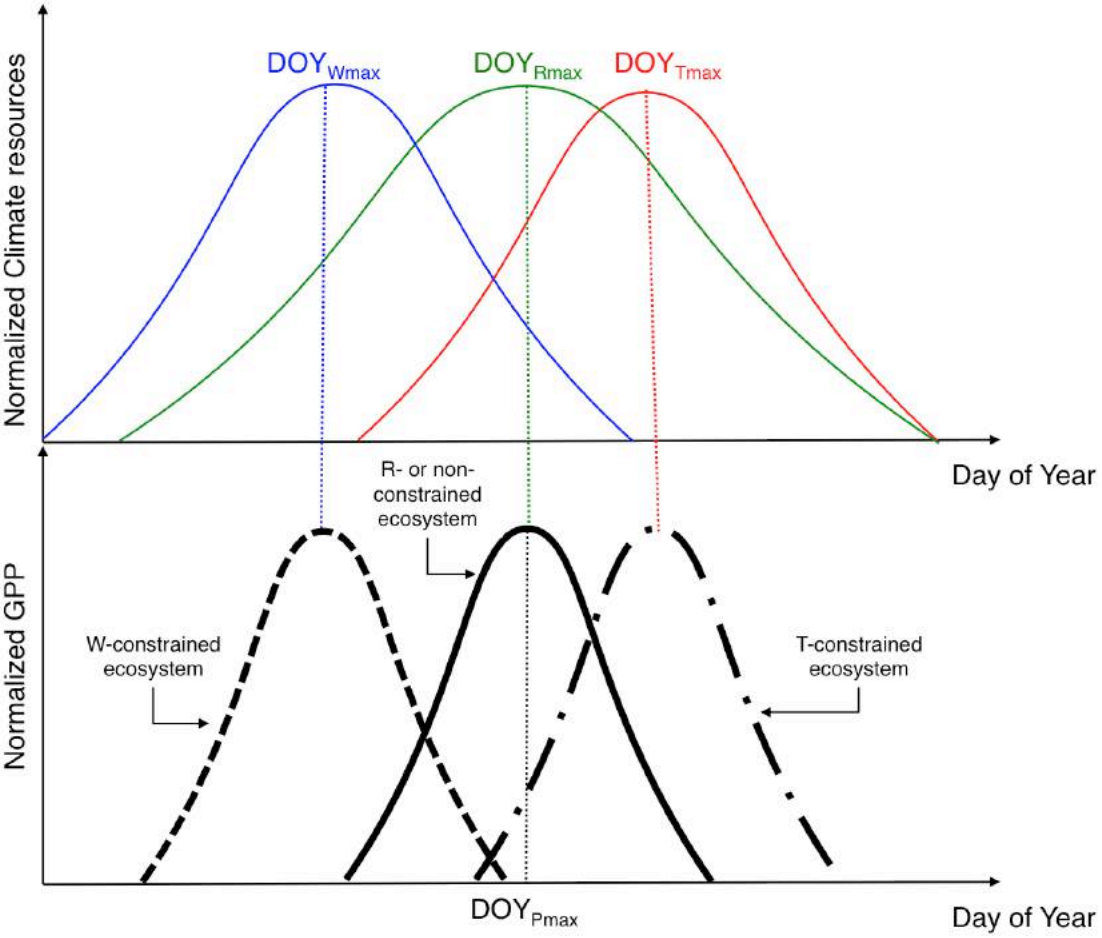

Figure 4.1 Conceptual illustration of the proposed DOY$_{Pmax}$ framework. Seasonal cycle of temperature (T, red), radiation (R, green), water availability (W, blue) and GPP (P, black) over common northern terrestrial ecosystems. Vertical lines indicate when each variable reaches a maximum state. DOY$_{Pmax}$, DOY$_{Tmax}$, DOY$_{Rmax}$, and DOY$_{Wmax}$ stand for the day of year when GPP, temperature, radiation, and precipitation reach respective maximum state during each seasonal course of the year. Four idealized cases are shown to demonstrate how photosynthetic seasonality of the ecosystem under given climate constraint differs from each other: non- (solid line, Case 1), temperature- (dot-dash line, Case 2), water- (long-dash line, Case 3), and radiation- (solid line, Case 4) constrained ecosystems.

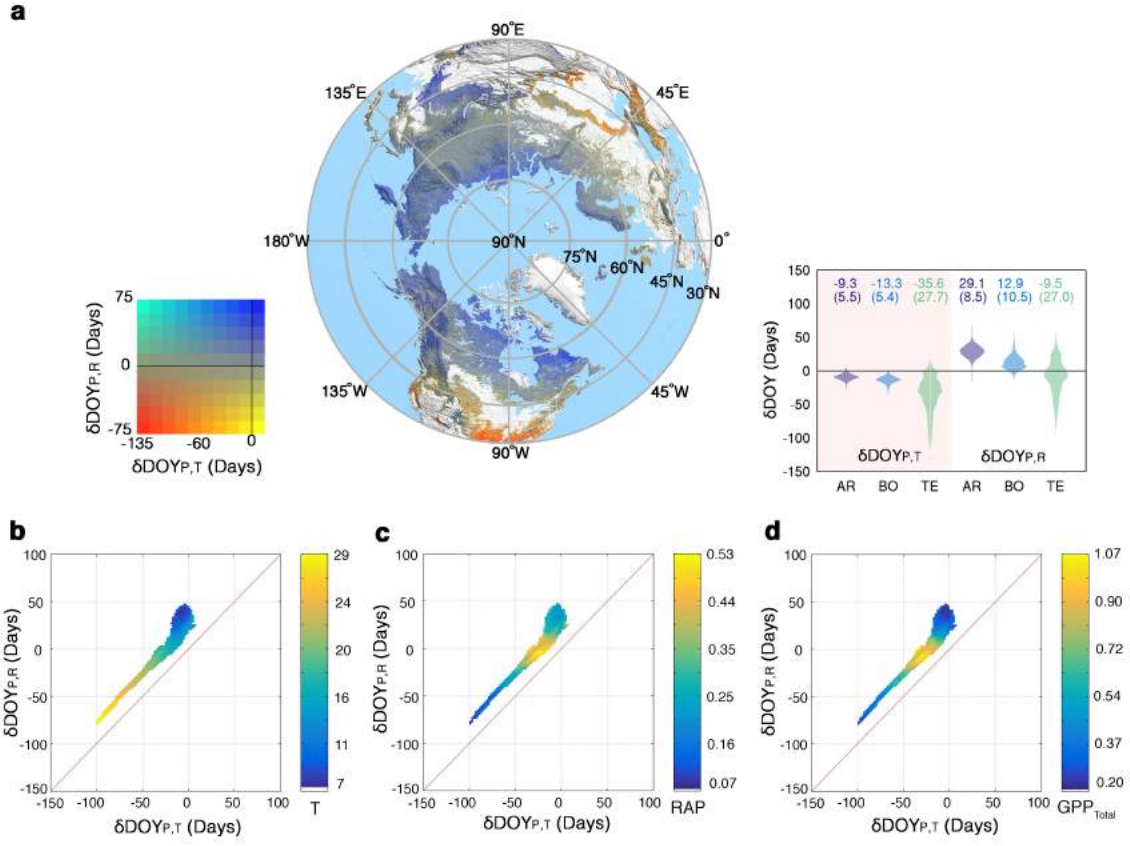

Figure 4.2 Relative positioning of peak photosynthetic activity timing with respect to the seasonal course of temperature and radiation, and its relation to climatic constraints and productivity. a, Geographical distribution of $\delta DOY_{P,T}$ ($DOY_{Pmax} - DOY_{Tmax}$) and $\delta DOY_{P,R}$ ($DOY_{Pmax} - DOY_{Rmax}$) for northern ecosystems. Regional distribution of $\delta DOY_{P,T}$ and $\delta DOY_{P,R}$ over Arctic (AR), Boreal (BO) and Temperate (TE) regions is given in the inset violin plot with mean and 1 SD (bracket). b, Positioning of DOY_{Pmax} seen as the relation between $\delta DOY_{P,R}$ and $\delta DOY_{P,T}$, with respect to temperature (°C). c, Same as b but for water availability (i.e., RAP). d, Same as b but for GPP_{Total} (kg C m^{-2}). MODIS-derived outcomes are used for these panels.

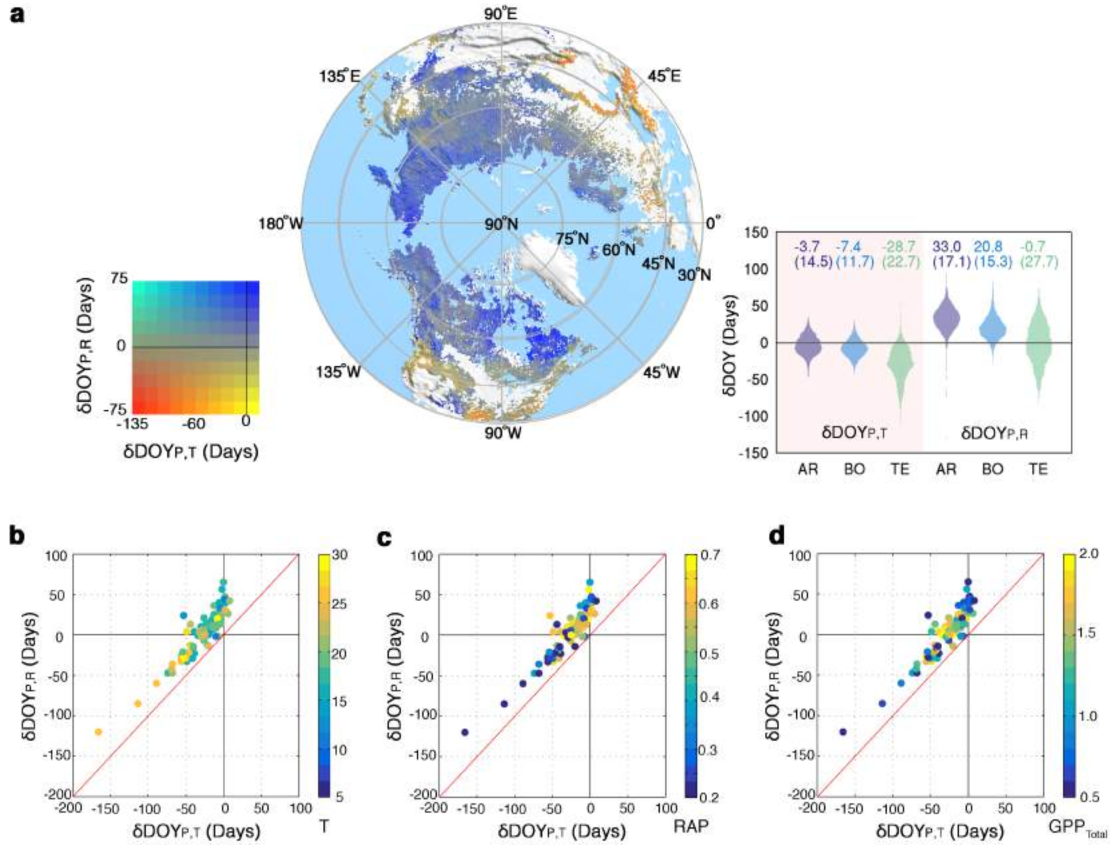

Figure 4.3 a, Same as Figure 2a but for the independent satellite Sun-Induced Fluorescence (SIF). b-d, Same as Figure 4.2b-d but for the eddy covariance tower measurement. Total 92 FLUXNET sites (Figure C1.2a) were used and each dot represents a single site.

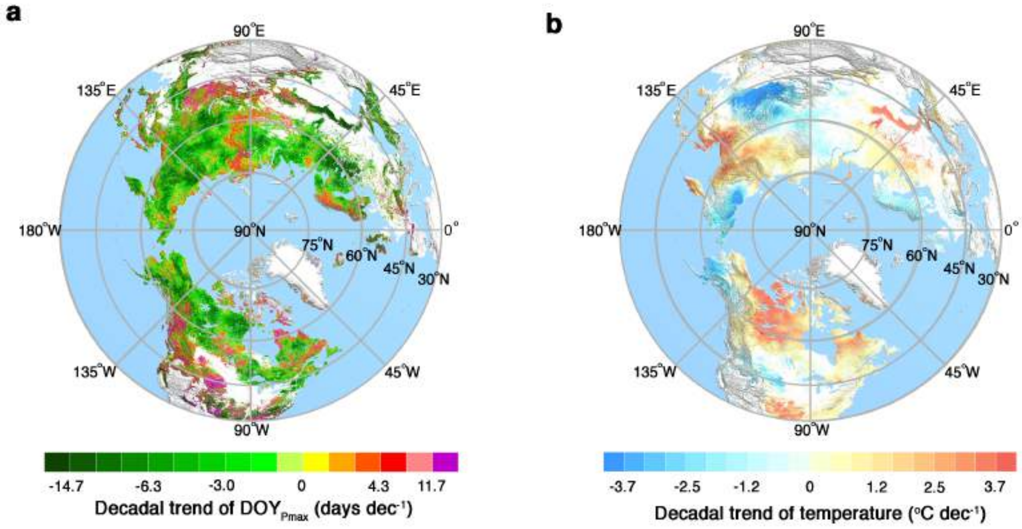

Figure 4.4 Spatial pattern of changes in DOY$_{Pmax}$ and temperature during the last 17 years (2000 – 2016). a, Decadal trend of MODIS based DOY$_{Pmax}$ over northern land during the last 17 years. b, Same as a but for summer temperature (June – August). The trend was derived based on ordinary least squares regression.

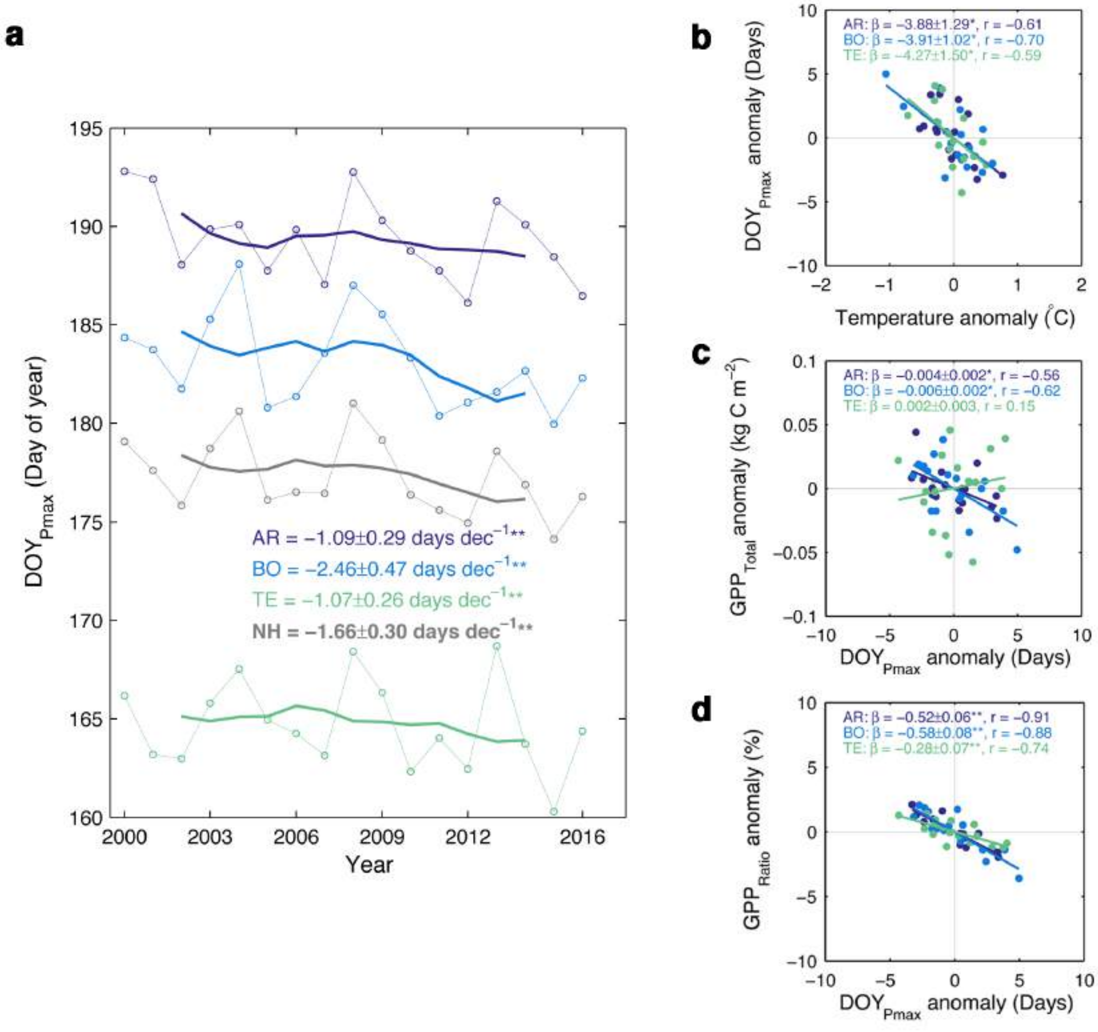

Figure 4.5 Changes in DOY$_{Pmax}$ during last 17 years (2000 – 2016) and their implications on northern vegetation productivity. a, Inter-annual variation of DOY$_{Pmax}$ by regions (Arctic: AR, Boreal: BO, Temperate: TE, Northern Hemisphere: NH) and its trend over the last 17 years. The decadal trend is estimated based on the 5-year moving average approach to reduce the potential impact of first, last and outlier points. Thin solid line with markers and thick solid line represent annual DOY$_{Pmax}$ and 5-year moving average. Calculated trend (slope ± SE) based on ordinary least squares regression is given with its significance level (double asterisks denote $P < 0.001$, single asterisks denote $P < 0.05$). The significance was computed by using the non-parametric Mann-Kendall trend test. b, Relation between regional DOY$_{Pmax}$ and summer temperature (June – August) anomalies. c–d, Same as b but for respective relation between DOY$_{Pmax}$ and GPP$_{Total}$, and DOY$_{Pmax}$ and GPP$_{Ratio}$ anomalies. Significance of the slope estimate (β ± SE) is denoted as double ($P < 0.001$) and single ($P < 0.05$) asterisks. The Kendall's rank correlation coefficient (r) between two variables is also given. Dark blue, light blue, green and gray stand for AR, BO, TE, and NH, respectively.

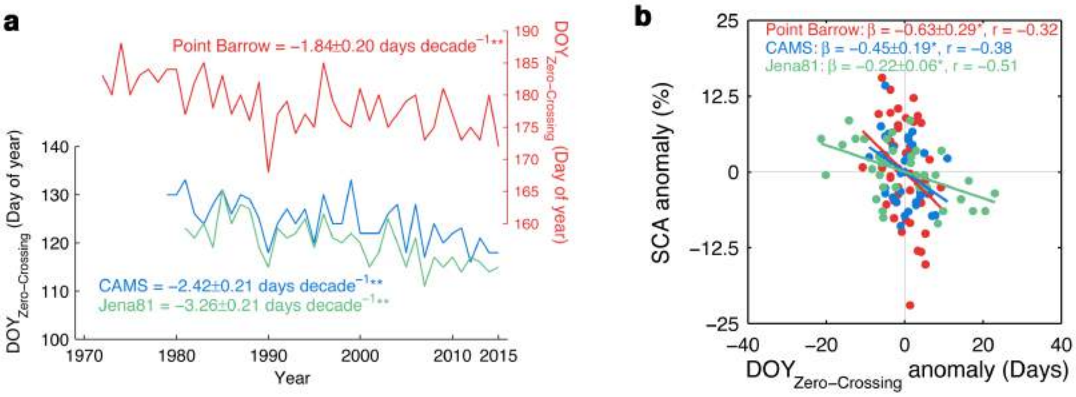

Figure 4.6 Analysis of atmospheric CO_2 concentration at Point Barrow and two CO_2 inversion estimates. a, Time series of $\text{DOY}_{\text{Zero-Crossing}}$ observed at Point Barrow atmospheric observatory and two independent CO_2 inversion datasets (CAMS and JENA). Note that the CO_2 fluxes for $\text{DOY}_{\text{Zero-Crossing}}$ retrieval of the inversion datasets are based on regionally integrated fluxes over the arctic and boreal zones, and all trend estimates are based on the 5-year moving average approach. Calculated trend (slope ± SE) based on ordinary least squares regression is given with its significance level (double asterisks denote $P < 0.001$, single asterisks denote $P < 0.05$). The significance was computed by using the non-parametric Mann-Kendall trend test. b, Relation between $\text{DOY}_{\text{Zero-Crossing}}$ and seasonal cycle amplitude (SCA) of atmospheric CO_2 concentration and flux estimates. SCA anomaly was expressed as a percentage of the long-term mean. Significance of the slope estimate (β ± SE) is denoted as double ($P < 0.001$) and single ($P < 0.05$) asterisks. The Kendall rank correlation coefficient (r) was used to measure the degree of association. Red, blue, and green stand for CO_2 data from Point Barrow, CAMS, and JENA, respectively.

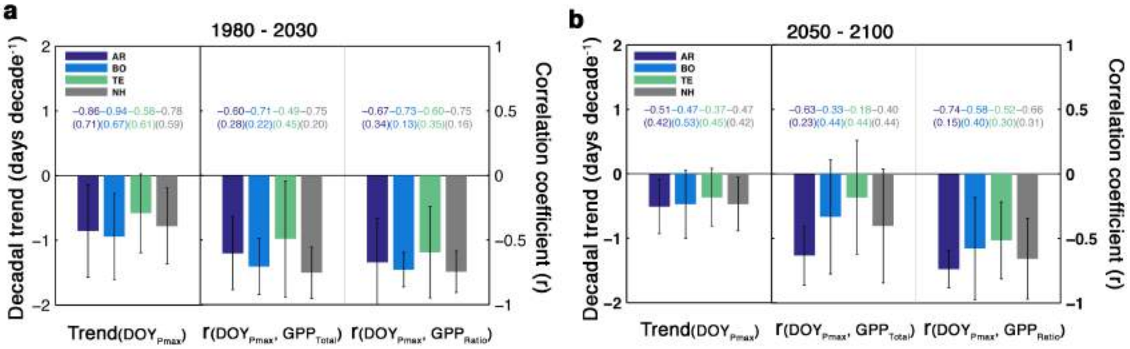

Figure 4.7 Analysis of multiple CMIP5 ESMs during two separate periods: a, 1980-2030 and b, 2050-2100. Decadal trend of DOY$_{Pmax}$ (left) and its association to GPP$_{Total}$ (center) and GPP$_{Ratio}$ (right) over northern lands inferred from the seven ESMs. Bar charts with error bars depict mean ± 1 SD across all ESMs. The Kendall rank correlation coefficient (r) was used to measure the degree of association. Dark blue, light blue, green and gray stand for AR, BO, TE, and NH, respectively.

CHAPTER 5: Concluding remarks

Recent changes in physical environments associated with substantial warming in northern lands have affected on a broad range of ecosystem processes, particularly, changes in structure, composition, and functioning of vegetation. These changes have been detected from satellite and have shown spatiotemporally varying trends (i.e., greening or browning) and complex mechanisms. Incomplete understanding of underlying processes driving such changes is the primary motivation for this research. This dissertation contributes to the growing body of literature on remote sensing-based monitoring of northern terrestrial ecosystems by tackling three scientific questions: how growing season has changed and characterized annual total greenness (**Chapter 2**), as well as how multiple agents driven environmental pressures (fire, harvesting, cultivation, etc.) have driven northern vegetation changes (**Chapter 3**) and how photosynthetic seasonality has been changing and modulating atmospheric CO_2 exchange (**Chapter 4**). This dissertation research uses a set of long-term remote sensing data as a fundamental tool to investigate changes in growing season, greenness and productivity of northern vegetation. Ground observations (e.g., eddy covariance and atmospheric CO_2 concentration) and multiple state-of-the-art Earth System Models (ESMs) are also introduced to imbue confidence in the findings from satellite observations. Results from the research presented in this dissertation provide improved understandings regarding spatial and temporal patterns of changes in growing season, greenness and productivity of northern vegetation. Here, we summarize the major findings and remained pressing issues as well as future directions of my research.

- **Chapter 2:** Complex snow-scape and permafrost dynamics complicate the remote sensing-based detection of vegetation growing season over high-latitude environments. Incorporating both snow and freeze/thaw conditions into vegetation greenness helps to adequately characterize northern vegetation growing season. We found that the remote sensing record from AVHRR reveals extensive lengthening trends of growing season and enhanced annual total greenness during the last three decades. Regionally varying seasonal responses are linked to local climate constraints and their relaxation. These results highlight spatially and temporally varying vegetation dynamics and are reflective of biome-specific responses of northern vegetation during the last three decades.
- **Chapter 3:** Disturbance and human land use/management are often neglected in large-scale studies monitoring northern vegetation dynamics under changing climate. Our approach incorporating land surface histories (disturbance and agricultural activity) revealed that natural (wildfire) and anthropogenic (harvesting) disturbances, changing climate and agricultural activities together govern the large-scale greening trends in northern lands. We also showed that the timing and type of disturbances are important to fully comprehend spatially uneven vegetation changes in the boreal and temperate regions. This study suggests climatic, social and ecological causes and processes are important to understand the underlain process of changes in remotely sensed vegetation greenness.

- **Chapter 4:** It is important to understand how photosynthetic seasonality evolved into its current state, and what role climatic constraints and their variability played in this process and ultimately in the carbon cycle. We take the ‘laws of minimum’ as a basis and introduce a new framework where the timing of peak photosynthetic activity (DOY_{Pmax}) acts as a proxy for plants adaptive state to climatic constraints on their growth. Our analyses confirm that spatial variations in DOY_{Pmax} reflect spatial gradients in climatic constraints as well as seasonal maximum and total productivity. The result captures a widespread warming-induced advance in DOY_{Pmax} with an increase of total gross primary productivity across northern lands, which leads to an earlier phase shift in land-atmosphere carbon fluxes and an increase in their amplitude. Such changes are expected to continue in the future based on our analysis of ESM projections.

This dissertation research also identified three key features that should be considered for future observing systems, data production and analytical approach to tackle further questions potentially raised from the dissertation research.

- First, spatial scale of observing system is critical for improving the process-oriented understandings on vegetation changes because of its degree of detective capability. For instance, AVHRR and MODIS have provided 8 km to 250 m vegetation indices and they are unable to identify smaller-scale land surface changes (e.g., land cover change, species specific phenology response etc.) usually hidden (or unobservable) in medium resolution remote sensing studies. The opening of the Landsat archive, continuous operation of Landsat/Sentinel series and recent development of high computing powers will help us to track vegetation changes with high spatial details (< 30 m) and longest records (since 1972) where sufficient images are available (e.g., Melaas et al., 2013). This advantageous data and computational power will enhance our capability to differentiate heterogeneous and finer land surface processes and their causes. In the same vein, there is another pressing need to gather geo-referenced microclimate data to minimize the gap between remote sensing and meteorological observations (Zellweger et al., 2019). Significant efforts on incorporating ground- and satellite- measurements will enable an improved understanding of the drivers of microclimate dynamics and how they deviate from the macroclimate, which will have important implications for estimating the velocity, and thus impact of climate change on vegetation changes.

- Second, biophysical metrics beyond the use of NDVI help to better understanding of northern vegetation dynamics. This dissertation revealed that disturbance induced changes in species composition and land cover changes implying rapid modification in spectral state of vegetation communities. For instance, we observed grass and shrub dominated successional state after fire disturbance (Figure 3.3). Increases of unit leaf area of plant functional types (e.g., grass vs. deciduous forest) may lead to a large difference in spectral response that is used to calculate the vegetation indices. In other words, identical increase of NDVI for different plant functional types mean different biophysical changes. This suggests a more robust parameterization of spectral characteristics in canopy structure modeling. MODIS LAI algorithm sophisticatedly formulates biome-specific canopy structure and spectral characteristics by accounting the discrepancy (Knyazikhin et al., 1998), but we may need to carefully revisit the parameterization for the regions with disturbance induced rapid land cover changes. Furthermore, integrating optical remote sensing to active sensors including lidar and radar is beneficial to reconstruct canopy structure, composition and functioning (Choi et al., 2016). Ongoing efforts on spatially finer and temporally more frequent global SIF measurements also will promote our understandings on the seasonal and diurnal variation in vegetation photosynthetic activity (Yang et al., 2015).

- Third, the trend estimation of vegetation greenness and its interpretation may need to be carefully revisited in future study. Most of important ecological processes associated with disturbances in the northern lands generally show sudden decline of spectral vegetation indices then a rapid increase of the indices in the following multiple years (~ 10 years), yet many studies using satellite datasets like our study look across multiple decades. The time period under consideration, whether a disturbance has occurred, and when it occurred during that time period can also influence whether a trend is detected (and the direction of that trend). To adequately interpret these vegetation changes, we may need to implement time-segmented approach such as polynomial break point analysis suggested by Verbesselt et al. (2010). This approach can be a potential solution to segment each ecological process and enhance our understandings on northern vegetation changes.

All of the studies presented in this dissertation are independently extendable as stand-alone research projects and I will continue the work along with the following directions.

(1) Improving phenology in Earth System Models: There are urgent needs for improving the representation of phenology in ESMs because uncertainties from incomplete phenology characterization in the models have significantly impacted on carbon, water, and energy exchange (Richardson et al., 2012). Resulting phenology retrievals from AVHRR and MODIS in this dissertation can effectively characterize long-term trends and anomalies in growing season phenology of northern vegetation. Implementing spatiotemporally explicit phenology retrievals from remote sensing will help to adequately parameterize phenology modules (e.g., Spring Warming model, Hunter & Lechowicz, 1992) in ESMs and ultimately will characterize how changes in phenology arising from changes in climate will affect regional carbon, water, and energy budgets of northern lands. In parallel, the land surface phenology from the remote sensing and ESM models can be evaluated with a subset of sites in the FLUXNET database having distinct carbon exchange seasonality, near-surface remote sensing (e.g., PhenoCam, PEN) and ground observations (e.g., PEP725, NPN). Note that the timing of peak photosynthesis (DOY_{Pmax}) introduced in Chapter 4 is another good indicator to evaluate the models' performance in simulating the photosynthetic seasonality. The improved phenology modules can be used to simulate how conventional modules may influence carbon, water and energy cycles in northern lands under future climate scenarios. Furthermore, implementing the growing season detection approach into the

geostationary satellites (e.g., Himawari, GOES and Geo-Kompsat2) will be an emerging avenue to track seasonal vegetation and associated matter exchanges with highly frequent observations.

(2) Albedo and radiative forcing in the rapidly changing landscapes: Spectral properties of land surface constituents such as leaves, soils, and vegetation structure determine surface reflectivity, i.e., albedo. The results from Chapter 3 clearly demonstrate how disturbance events lead to rapid changes in not only vegetation structure (e.g., LAI) but also compositional or land cover transition through the disturbance itself and following recovery processes. The extensive greening pattern associated with shrub expansion, i.e., compositional change, in the artic region is expected to result in substantial changes in the albedo and radiative forcing. Furthermore, warming-induced shifts in vegetation phenology together with changing snow-scape lead to significant impacts on land surface albedo. The MODIS albedo product is readily useable to monitor how disturbance and changed LAI alter land surface energy budget and ultimately land-atmosphere feedback. Particularly, it will be interesting to explore how the albedo varies as functions of different disturbance types and intensity, vegetation composition and different seasons.

(3) Carbon balance in the disturbance frequent landscapes: In the 3rd chapter, we quantified how much of net leaf area has been changed during the last two decade and mainly scrutinized the trends of LAI as functions of disturbance timing and types. For accurate carbon monitoring, there are urgent needs for a synergistic combination between mechanistic models and remote sensing observations for explicitly depicting

spatiotemporally complex land surface processes (e.g., fire, harvesting, etc.) in these disturbance frequent environments. I have involved in developing an integrative approach to fuse multiple optical and active remote sensing data into the mechanistic modeling scheme, called Allometric Scaling Resource Limitation that encode principles of metabolic scaling, structural stability, allometry and constraints from resource limitations (Ni & Park et al., 2014; Choi et al., 2016). Future research on this fusing approach ultimately aims to map time series of forest height and aboveground biomass with a reasonable accuracy using NASA's two promising spaceborne lidar missions (i.e., ICESat2 and GEDI). Together with this modeling work, experimentally deployed eddy covariance towers over the disturbed area with chronological variations may provide a chance to evaluate the model performance by carbon exchange over variation in successional trajectory.

(4) Multi-sensor based comparative and multi-scale studies: Chapter 2 and 3 reveal some degree of discrepancy in growing season metrics and LAIs from MODIS and AVHRR records. The observed inconsistency and recently raised reliability issue in AVHRR (e.g., Tian et al., 2015), which is the most broadly used dataset for monitoring ecosystem and carbon balance changes, have broad implications for the evaluation of vegetation and carbon dynamics. An extensive evaluation across sensors and data is an emerging challenge to be addressed in research communities by interpreting complex, variable but inherently scale dependent remotely sensed land surface changes. Bridging patterns of spatiotemporal changes in the coarse (e.g., AVHRR) and moderate (e.g., MODIS) satellite data to high-resolution (e.g., Landsat/Sentinel) satellite observation will

shed light on finer land surface processes hidden in a large and blurry pixel. Some emerging opportunities already have been made through developing international research networks (e.g., High Latitude Drone Network; HiLDEN) and it will enhance our process-oriented understandings in northern vegetation changes by giving details of land surface changes.

Continuous and accurate monitoring of vegetation dynamics is a keystone for improving our understanding of the past and current state, and the fate of the earth's terrestrial ecosystems in the future. This dissertation tried to identify and answer the overlooked yet important three research questions. From the lessons earned from this dissertation research and the plan I identified above, I will continuously explore the northern vegetation changes using remote sensing together with other potential data or approaches that help capturing and interpreting real changes in the northern vegetation.

Appendix A: Chapter 2. Changes in growing season duration and productivity of northern vegetation inferred from long-term remote sensing data

This section contains supplementary text, tables and figures for the “**Chapter 2**”.

A1.1 Supplementary Data and Methods

A1.1.1 Study region and vegetation cover map

This study focuses on northern vegetated region (>45°N), which includes Boreal and Arctic ecosystems. To define both regions, we compiled the latest version of the MODIS International Geosphere-Biosphere Programme (IGBP) land cover map (Friedl et al 2010) and the Circumpolar Arctic Vegetation Map (CAVM) (Walker et al 2005). MODIS IGBP identified 17 land cover classes including 11 natural vegetation classes, three developed and mosaicked land classes, and three non-vegetated land classes. The CAVM map was used to identify the tundra vegetation and associated characteristics of the circumpolar region as a supplement to the IGBP classes. Arctic (8.16 million km^2) is defined as the vegetated area north of 65°N, excluding crops and forests, but including the tundra south of 65°N. Boreal region (17.86 million km^2) is defined as the vegetated area between 45°N and 65°N, excluding crops, tundra, broadleaf forests, but including needleleaf forests north of 65°N. Grasslands south of the mixed forests are excluded as these are not conventionally considered as Boreal vegetation. Combined vegetation map of the Arctic and Boreal regions with 14 different vegetation classes (additionally aggregated into 4 vegetation groups) are described in Figure A1.1.

A1.1.2 Data

A1.1.2.1 GIMMS NDVI3g: In this study, we mainly used the Global Inventory Modeling and Mapping Studies (GIMMS) NDVI dataset obtained from the Advanced Very High Resolution Radiometer (AVHRR) sensors onboard the NOAA satellite series (7 to 19). The latest version of GIMMS NDVI data (a.k.a. NDVI3g) spans 1981–2014 with a native resolution of 1/12° at bimonthly temporal resolution (Pinzon & Tucker 2014). Recently resolved high latitude discontinuity issue and improved snowmelt and cloud detection have granted a better observation for northern high latitude vegetation dynamic research. Based on given growing season and productivity definition, obtained metrics were used to investigate long-term northern vegetation phenology and productivity changes.

A1.1.2.2 MODIS Phenology (MCD12Q2): The MODIS Land Cover Dynamics (MCD12Q2) product (a.k.a., MODIS Global Vegetation Phenology product) provides estimates of the timing of vegetation phenology based on Nadir-BRDF Adjusted Reflectance (NBAR) enhanced vegetation index (EVI). Four different phenological phases provided are the onset of greenness increase (same as SOS in this study), onset of greenness maximum, onset of greenness decrease and onset of greenness minimum (same as EOS in this study). Cumulative EVI area provided in MCD12Q2 is conceptually overlapped with GSSNDVI of NDVI3g. Native resolution is 500m and temporal coverage spans from 2001 to 2012 (12 years). For comparison purpose, annual growing season and productivity metrics are spatially harmonized with GIMMS NDVI3g data

(1/12°). We have to note that MODIS phenology uses different quality control, seasonal trajectory fitting (logistic model) and phenology detection (curvature-based approach). Details can be found in Zhang et al (2003) and Ganguly et al. (2010).

A1.1.2.3. MODIS NDVI (MOD13C1): MODIS Collection 5 standard NDVI product which spans from 2000 to 2014 with 16-day temporal composite at 0.05 degree is used in this study. For comparison purpose, it is harmonized with GIMMS NDVI3g spatial resolution (1/12°) via bicubic method. Growing season (i.e., SOS, EOS, and LOS) and productivity (i.e., GSSNDVI) are obtained by exactly same definition and method used in NDVI3g.

A1.1.2.4. MODIS NBAR NDVI (MCD43C4): Nadir Bidirectional Reflectance Distribution Function (BRDF)-Adjusted Reflectance (NBAR), which spans same temporal coverage (2000-2014) with MOD13C1 is used in this study. Spatial resolution (0.05°) is adjusted into NDVI3g (1/12°) and then growing season (i.e., SOS, EOS, and LOS) and productivity (i.e., GSSNDVI) metrics are obtained via identical definition and method used in GIMMS NDVI3g.

A1.1.2.5. FLUXNET GPP: We used gap-filled daily tower GPP data at 39 flux tower sites (140 site-years observation) distributed across northern hemisphere to validate remotely sensed growing season and a proxy of GPP based on GIMMS NDVI3g. Selection of valid site and data is performed by following two criteria: (i) more than 95 %

of the days had daily GPP data, and (ii) the mean daily quality flag was more than 0.75 (Richardson et al 2010). The daily data was then aggregated to monthly and later to yearly time step. Details of the individual towers are provided in Table A1.2. The data used in this study is obtained from FLUXNET “Fair-Use” data archive and the spatial distribution of the flux towers is shown in Figure S1.

A1.1.2.6. MODIS GPP (MOD17A3): Terra MODIS Net Primary Production (MOD17A3) provides 15 years (2000-2014) long annual 1km GPP estimate based on light-use efficiency model. Theoretical and practical details underpinning this product can be found in Running et al (1999). For evaluation purpose, we coarsely aggregated 1km GPP product into NDVI3g grid format (1/12°).

A1.1.2.7. Model Tree Ensemble GPP (MTE-GPP): Statistical model-based MTE-GPP is used for evaluating GSSNDVI of GIMMS NDVI3g. This model incorporates flux tower local observations, satellite retrievals of fraction of absorbed photosynthetically active radiation (fAPAR), and climate fields to upscale ground level GPP. A machine learning system where the target variable (i.e., GPP) is predicted by a set of multiple linear regressions from explanatory variable is implemented in this model. Detail information on MTE-GPP can be found in Jung et al (2011). This product provides global annual GPP from 1982 to 2011 at 0.5 degree with monthly time step. Annually aggregated and specially resampled MTE-GPP is compared with NDVI3g GSSNDVI for evaluation purpose.

A1.1.2.8. **MODIS Snow Cover (MOD10C2)**: MODIS Snow Cover 8-Day product (MOD10C2) is used to obtain snow cover information to additionally minimize snow-contamination during processing of GIMMS NDVI3g, MOD13C1, and MCD43C4 growing season and productivity determination. We first combined two consecutive 8-day composite to 16-day composite with conservative way (Minimum value composite: take lower snow cover percentage as representative). This approach can be justified, as all vegetation indices are composited by maximum value compositing approach. Then we defined a pixel as snow-contaminant pixel when snow occupies more than 20%. Identified 15-years (from 2000 to 2014) snow cover information is incorporated to determine background NDVI.

A1.1.2.9. MEaSUREs Freeze-Thaw (FT): The FT-ESDR is a NASA MEaSUREs (Making Earth System Data Records for Use in Research Environments) funded effort to provide a consistent long-term global data record of land surface freeze/thaw (FT) state dynamics for all vegetated regions where low temperatures are a major constraint to ecosystem processes (Kim et al 2012). The FT-ESDR data set provides four FT status (frozen, thawed, transitional and inverse transitional) and five filled values for the whole global with daily temporal frequency. In our analysis, we defined those days classified as frozen, transitional and inverse transitional as non-photosynthetic days. To the contrary, the other days are defined as photosynthetic days. The NDVI based growing season was adjusted by the photosynthetic/non-photosynthetic information derived from FT data set.

The rule is that a day must be in the NDVI based growing season and identified as photosynthetically active days by FT data set.

A1.1.2.10. MERRA Temperature: Daily MERRA Temperature products (Version 1) are used in this study. To obtain temperature based potential growing season and growing season summed warmth index, we firstly aggregated daily temperature to 15-day time step to smooth and enhance efficiency, then used following role to define thermal growing season metrics: (a) the start of the temperature based growing season is the day when the temperature is crossing 0 °C with rising phase; (b) the end of the temperature based growing season is the day when the temperature is crossing 0 °C decreasing phase; (c) the length of thermal growing season is the duration between start day and end day of the thermal growing season; (d) the growing season summed warmth index is the summation of temperature during the growing season.

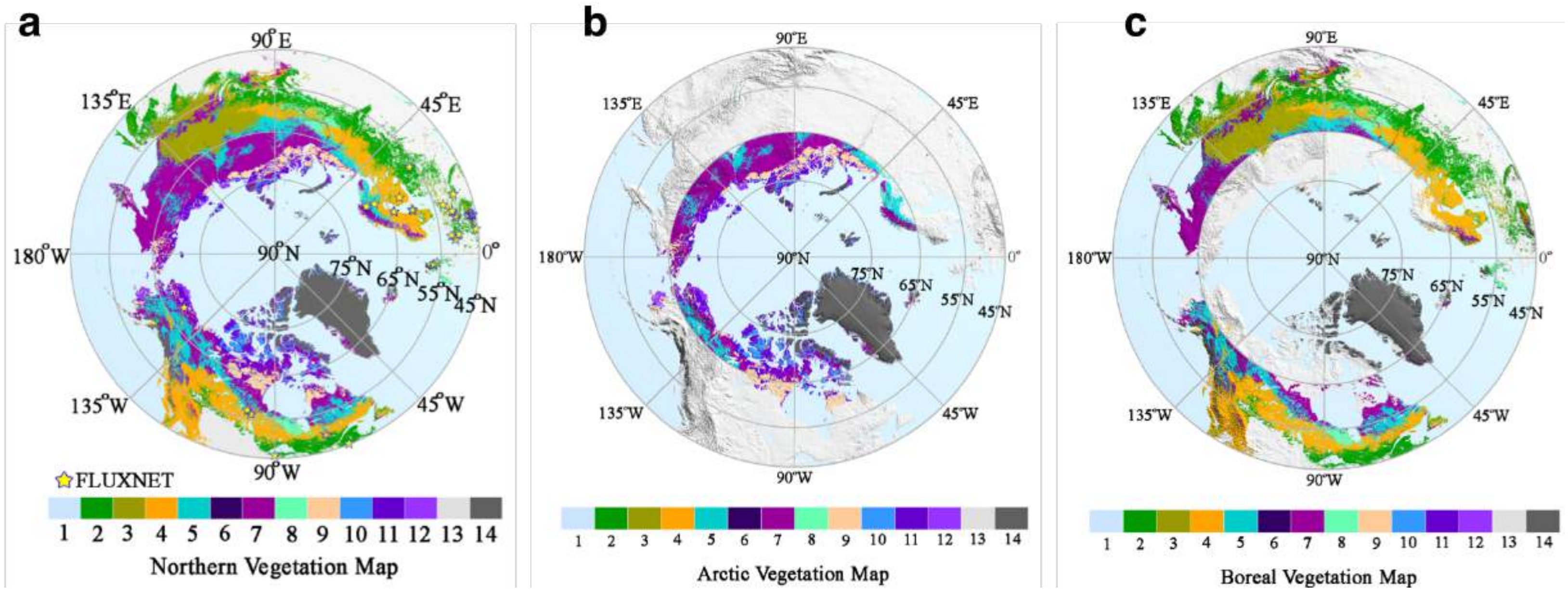

Figure A1.1 Northern Boreal and Arctic vegetation map (a). Vegetation classes 9 to 12 are as per the Circumpolar Arctic Vegetation Map (Walker et al 2005). The rest of the vegetation classes are based on the MODIS International Geosphere-Biosphere Programme (IGBP) land covers (definitions in Friedl et al 2010). Yellow star marker shows spatial distribution of used FLUXNET (N=39) sites for evaluation purposes. (b) Arctic vegetation only, (c) Boreal vegetation only. Class1: Oceans and inland lakes, Class2: Mixed Forests, Class3: Deciduous Needleleaf Forests, Class4: Evergreen Needleleaf Forests, Class5: Forest-Shrubs Ecotone, Class6: Closed Shrublands, Class7: Open Shrublands, Class8: Grasslands/ Wetlands (North of Forests), Class9: Erect Shrub Tundra, Class10: Prostrate Shrub Tundra, Class11: Graminoid Tundra, Class12: Wetlands, Class13: Other Vegetation (e.g., crops): Not considered in this study, Class14: Barren. Group1 (Forest): Class2-4, Group2 (Other woody vegetation): Class5-7, Group3 (Herbaceous vegetation): Class8, Group4 (Tundra): Class9-12.

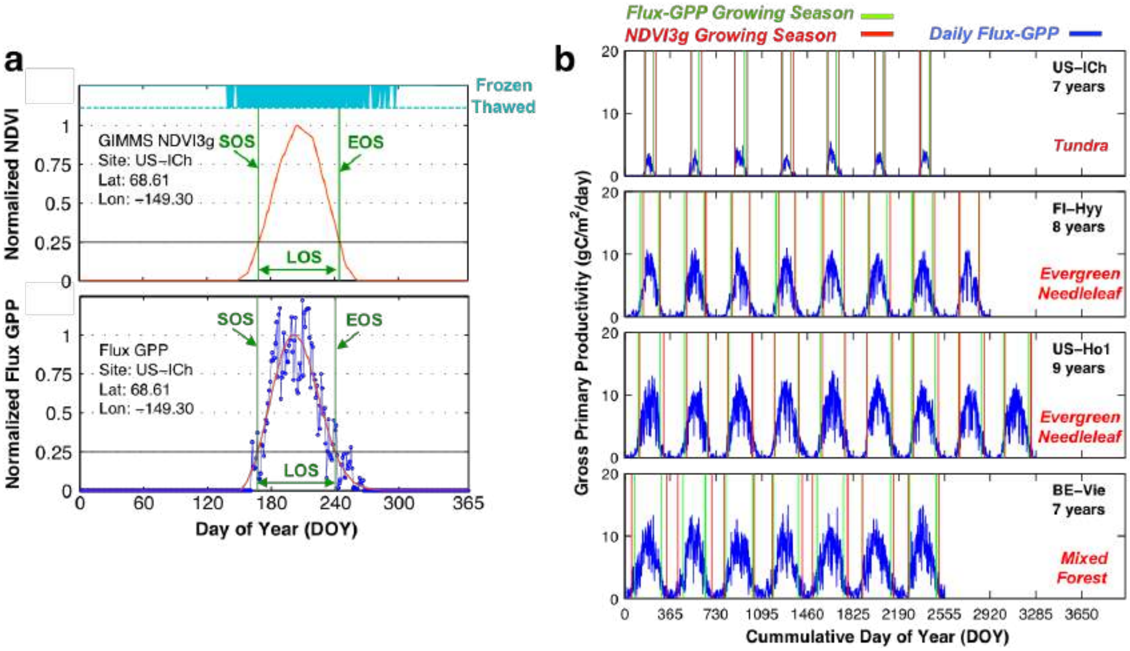

Figure A1.2 Definition of growing season and productivity from remotely sensed NDVI and FLUXNET GPP data (a). One year NDVI3g and tower measured GPP from US-ICh FLUXNET site were used for this example case. (b) Examples of retrieved NDVI3g and GPP based growing season metrics over four FLUXNET sites where have more than 6 years valid GPP observations.

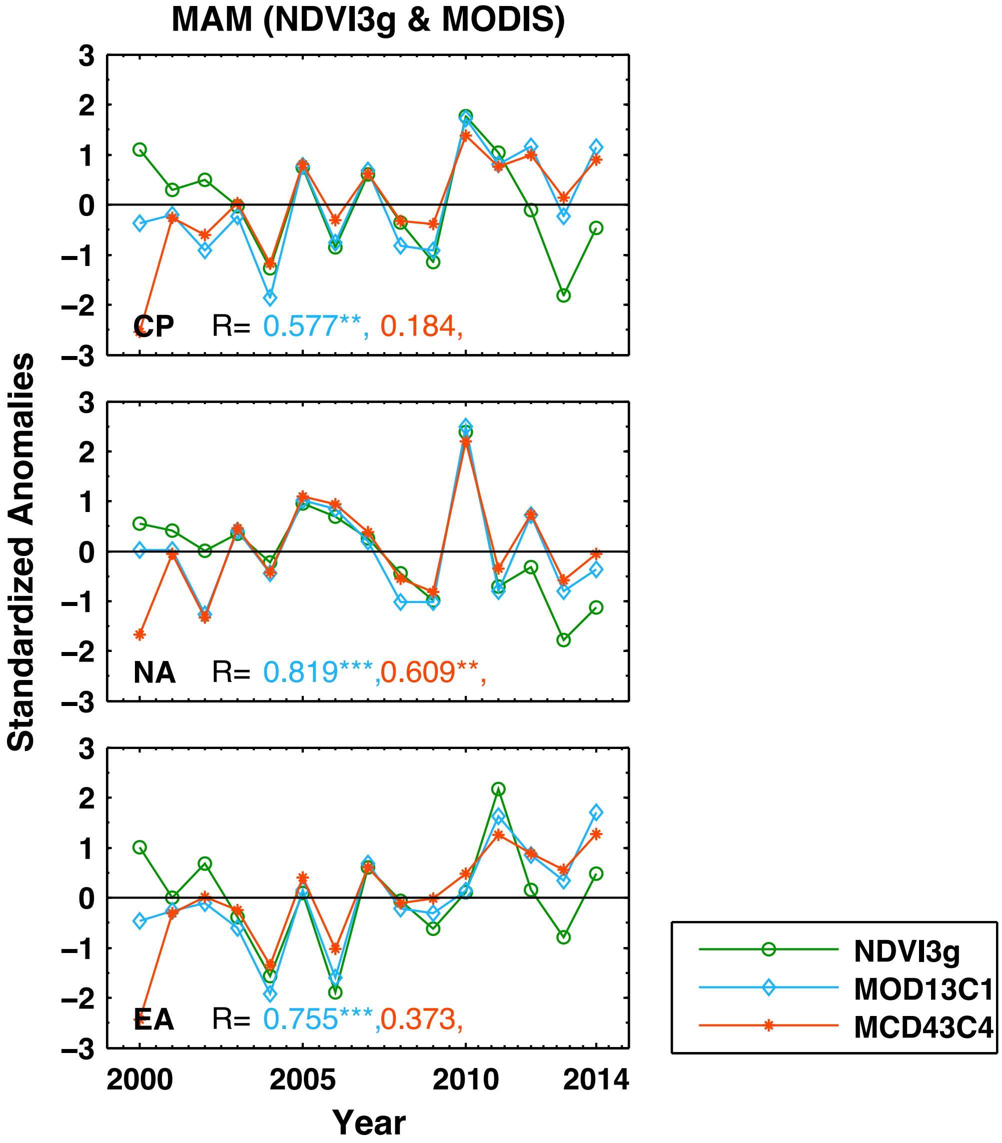

Figure A1.3 Continental scale comparison between NDVI3g and MODIS (MOD13C1 and MCD43C4) spring (March to May) NDVIs. Correlation coefficients between NDVIs from NDVI3g and MODIS datasets are calculated (*: $p<0.01$, **: $p<0.05$, *: $p<0.1$) and given with corresponding color scheme. CP, NA and EA are for Circumpolar, North America and Eurasia regions, respectively. Increase in March-May NDVIs corresponds to an advance in the green-up date while a decrease corresponds to delay. As shown in below figure, the spring AVHRR NDVI showed strong negative anomalies and the other two vegetation indices from MODIS showed slight positive anomalies during 2012–2014. Therefore, the different response to vegetation growth of the AVHRR NDVI when compared with the MODIS vegetation indices appears to be responsible for the differences in the SOS and LOS variation. This comparison clearly indicates that divergence between NDVI3g and MODIS we observed (Figure 2.1a and 2.1c) should have been caused by the differences in response of vegetation indices to vegetation growth between sensors, rather than by the processing methods.**

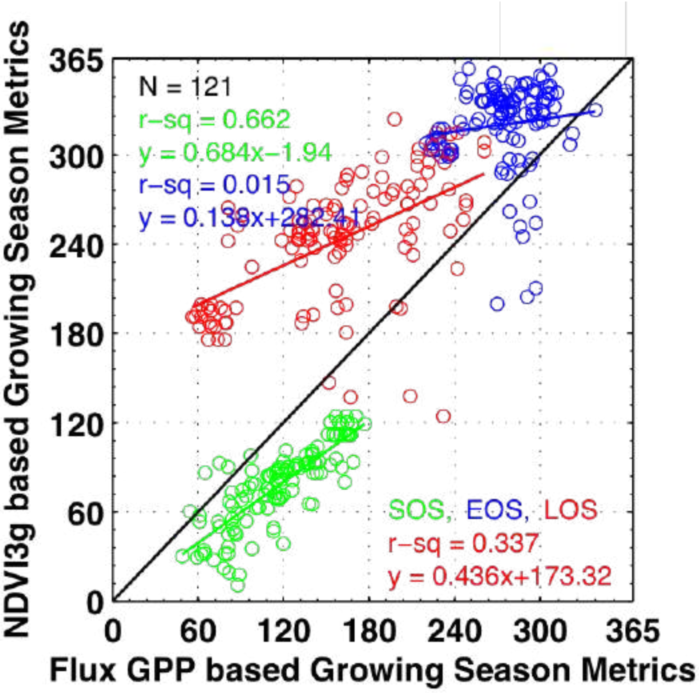

Figure A1.4 Evaluation of NDVI3g based growing season retrievals without background NDVI pre-processing using FLUXNET gross primary productivity (GPP) based growing season. This is same as Figure 2.2a but for the growing season metrics without background NDVI pre-processing.

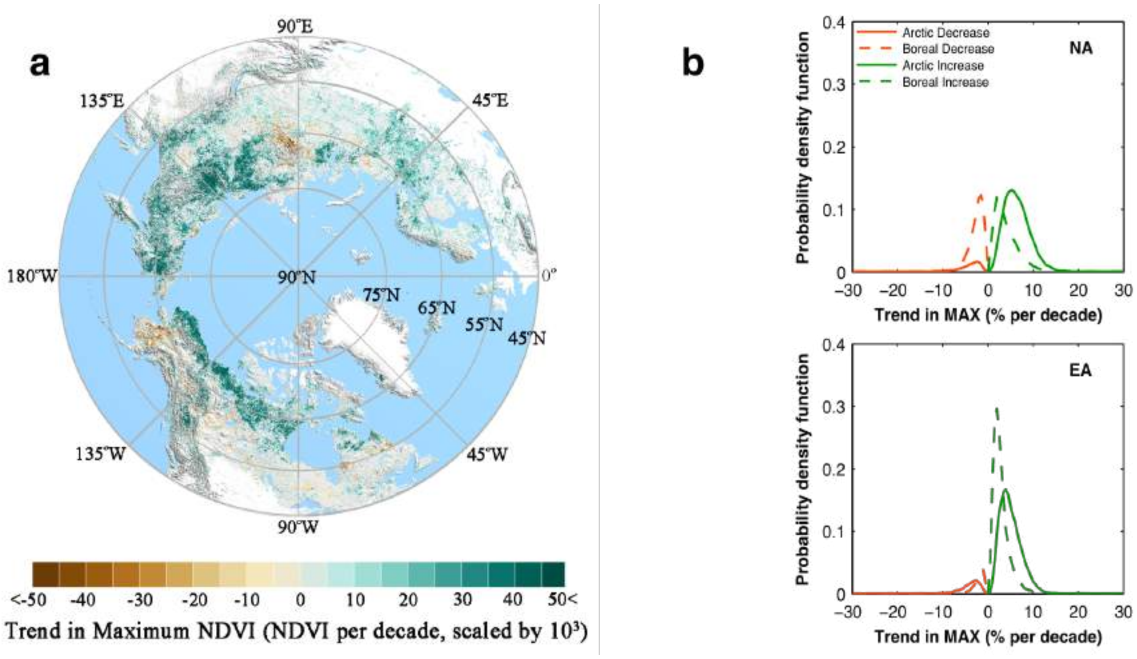

Figure A1.5 Spatial pattern of long-term (1982-2014) trends in maximum NDVI (MAX, a). The trend was calculated using Vogelsang's t-PS_T test at 10% significance level. Non-vegetated pixels and pixels without significant trend were shown in white and gray, respectively. Probability density function (PDF) of change rate per decade for only significant positive and negative changes is also provided (b). PDFs are normalized to total area showing significant changes in each continent and biome (Table A1.3). NA and EA are for North America and Eurasia. In PDFs, green and red lines represent significant positive and negative changes. Solid and dash lines stand for arctic and boreal regions, respectively.

Table A1.1. Information of selected global FLUXNET Sites (N=39, Number of observed site-years =140). Selection of valid site and data is performed by following two criteria: (i) more than 95 % of the days have daily GPP data, and (ii) the mean daily quality flag is more than 0.75 (Richardson et al., 2010).

Site	Latitude	Longitude	IGBP	N. Obs.	Site	Latitude	Longitude	IGBP	N. Obs.
AT-Neu	47.117	11.318	GRA	1	IT-Lav	45.955	11.281	ENF	2
BE-Bra	51.309	4.521	MF	3	IT-MBo	46.016	11.047	GRA	4
BE-Vie	50.306	5.997	MF	7	IT-Mal	46.117	11.703	GRA	1
CA-Man	55.880	-98.481	ENF	2	IT-Ren	46.588	11.435	ENF	5
CA-NS1	55.879	-98.484	ENF	2	NL-Loo	52.168	5.744	ENF	7
CA-NS2	55.906	-98.525	ENF	2	PL-wet	52.762	16.309	WET	2
CA-NS3	55.912	-98.382	ENF	3	RU-Fyo	56.462	32.924	ENF	7
CA-NS5	55.863	-98.485	ENF	1	SE-Deg	64.183	19.550	WET	1
CA-NS7	56.636	-99.948	OSH	2	SE-Fla	64.113	19.457	ENF	3
CA-Qcu	49.267	-74.037	ENF	4	SE-Nor	60.087	17.480	ENF	4
CA-Qfo	49.693	-74.342	ENF	3	SE-Sk2	60.130	17.840	ENF	1
CZ-BK1	49.503	18.538	ENF	1	UK-EBu	55.866	-3.206	GRA	1
DE-Bay	50.142	11.867	ENF	2	UK-Gri	56.607	-3.798	ENF	5
DE-Gri	50.950	13.513	GRA	1	US-Ho1	45.204	-68.740	ENF	9
DE-Tha	50.964	13.567	ENF	10	US-Ho2	45.209	-68.747	ENF	6
DE-Wet	50.454	11.458	ENF	5	US-ICh	68.607	-149.296	OSH	7
FI-Hyy	61.847	24.295	ENF	8	US-ICs	68.606	-149.311	OSH	7
FI-Kaa	69.141	27.295	WET	5	US-ICt	68.606	-149.304	OSH	7
FI-Sod	67.362	26.638	ENF	5	US-WCr	45.806	-90.080	DBF	2
IT-LMa	45.581	7.155	GRA	1					

Table A1.2 Continental scale trend estimation for NDVI3g and MODIS based growing season and productivity metrics over common temporal periods. We used the two different common periods (one for 2001-2012 and the other for 2000-2014) due to relatively short time span of MCD12Q2. Estimates in parentheses represent trends during 2000-2014. The trends were evaluated by Vogelsang's *t-PS_T* test. CP, NA and EA are for circumpolar, North America and Eurasia regions, respectively. ***: p<0.01, **: p<0.05, *: p<0.1, N.A.: Not available

	NDVI3g				MODIS		
	CP	NA	EA		CP	NA	EA
SOS (days·dec^{-1})	0.06 (0.85)	2.25 (2.33)	-0.98 (0.00)	MOD13C1	-2.24 (-1.98)	0.01 (-1.05)	-3.33 (-2.51)
				MCD43C4	-3.29 (-4.71)	-1.73 (-4.13)	-4.04 (-5.03*)
				MCD12Q2	-3.46 (N.A.)	-1.88 (N.A.)	-4.23 (N.A.)
EOS (days·dec^{-1})	0.95 (-0.69)	1.88 (-0.56)	0.43 (-0.76)	MOD13C1	2.45 (1.34)	2.90 (1.41)	2.19 (1.30)
				MCD43C4	2.89 (1.58)	2.71 (1.49)	2.94 (1.63)
				MCD12Q2	1.38 (N.A.)	0.72 (N.A.)	1.71 (N.A.)
LOS (days·dec^{-1})	1.41 (-1.08)	0.18 (-2.30)	1.98 (-0.38)	MOD13C1	4.96 (3.45*)	3.43 (2.73*)	5.72 (3.85*)
				MCD43C4	6.52 (6.48)	5.22* (6.09)	7.19 (6.70*)
				MCD12Q2	4.65 (N.A.)	2.42* (N.A.)	5.80 (N.A.)
GSSNDVI (dec^{-1})	4.81 (1.87)	4.36 (1.65)	5.01 (2.00)	MOD13C1	3.10 (2.21*)	2.28 (1.92*)	3.50 (2.37*)
				MCD43C4	4.03 (4.42)	3.16 (4.19)	4.46 (4.55)
				MCD12Q2	1.29 (N.A.)	0.41* (N.A.)	1.74 (N.A.)

Table A1.3. Area of long-term (1982-2014) SOS, EOS, LOS, MAX and GSSNDVI trends by continents and biomes. Significant trends are calculated by Vogelsang's *t-PS_T* test at 10% significance level. Total area focused from this study is 26.02 million km^2. CP, NA, EA, AR and BO are for circumpolar, North America, Eurasia, arctic and boreal regions, respectively. All areal quantities in percent (%) are calculated with respect to total vegetated area in CP.

Metric Type	**Trend Type**	**CP**			**NA**			**EA**		
		All	AR	BO	All	AR	BO	All	AR	BO
SOS	Sig. Positive	2.7	0.5	2.2	2.3	0.4	1.8	0.5	0.1	0.4
	Sig. Negative	27.9	8.7	19.3	5.7	1.8	3.9	22.2	6.8	15.4
	InSig. or No Change	69.4	21.3	48.1	30.3	10.1	20.3	39.0	11.2	27.8
EOS	Sig. Positive	21.9	3.1	18.8	9.9	1.9	7.9	12.1	1.2	10.9
	Sig. Negative	7.7	4.3	3.5	1.9	0.8	1.1	5.8	3.5	2.3
	InSig. or No Change	70.3	23.0	47.3	26.5	9.5	16.9	43.9	13.5	30.4
LOS	Sig. Positive	33.2	7.7	25.4	10.1	2.8	7.3	23.1	4.9	18.2
	Sig. Negative	2.7	1.2	1.6	1.7	0.5	1.2	1.1	0.6	0.4
	InSig. or No Change	64.1	21.6	42.5	26.5	8.9	17.6	37.6	12.6	25.0
MAX	Sig. Positive	28.7	11.3	17.4	8.3	4.5	3.7	20.5	6.8	13.7
	Sig. Negative	5.2	1.1	4.0	3.1	0.4	2.7	2.1	0.7	1.4
	InSig. or No Change	66.1	18.0	48.1	26.9	7.3	19.6	39.1	10.7	28.5
GSSNDVI	Sig. Positive	42.0	12.8	29.1	12.8	5.2	7.6	29.1	7.6	21.5
	Sig. Negative	2.5	0.8	1.7	1.7	0.3	1.4	0.8	0.5	0.3
	InSig. or No Change	55.6	16.8	38.8	23.7	6.7	17.0	31.9	10.1	21.7

Table A1.4. Productivity (GSSNDVI) in 1982 and productivity change between 1982 and 2014 of vegetation classes. The Greening (abbreviated as G, shown in green color), Browning (abbreviated as B, shown in red color) and No change (abbreviated as N, shown in black color) was defined by calculating productivity trend between 1982 and 2014 pixel by pixel using the Vogelsang model at 10% significance level. Increased productivity (abbreviated as I, shown in green color) and decreased productivity (abbreviated as D, shown in red color) are calculated by $\sum_{p=1}^{NVC_i} 33yr \cdot T_p \cdot A_p$, where NVC_i is the total pixel number of the ith vegetation classes showing significant positive or negative changes, T_p is the yearly common productivity trend (yr^{-1}) of pixel p, A_p is the area weight (unitless) of pixel p. Area weighted total GSSNDVI over the greening (G_{1982} = 9.04×108) and browning (B_{1982} = 5.89×107) regions in 1982 was used as denominator to calculate Table 2.3 quantities. All quantities listed in below are unitless.

Vegetation Class	GSSNDVI in 1982			GSSNDVI Change (1982-2014)	
	G	B	N	I	D
Mixed Forests	3.18×10^{8}	3.66×10^{6}	2.19×10^{8}	5.89×10^{7}	-5.40×10^{5}
Deciduous Needleleaf Forests	8.76×10^{7}	1.87×10^{6}	1.32×10^{8}	1.35×10^{7}	-2.16×10^{5}
Evergreen Needleleaf Forests	2.01×10^{8}	2.13×10^{7}	3.08×10^{8}	4.75×10^{7}	-4.55×10^{6}
Forest-Shrubs Ecotone	7.58×10^{7}	1.16×10^{7}	1.63×10^{8}	1.74×10^{7}	-2.13×10^{6}
Closed Shrublands	2.91×10^{6}	2.87×10^{5}	4.29×10^{6}	7.63×10^{5}	-6.27×10^{4}
Open Shrublands	1.44×10^{8}	1.38×10^{7}	2.17×10^{8}	3.95×10^{7}	-2.67×10^{6}
Grasslands/ Wetlands (North of Forests)	9.72×10^{6}	5.60×10^{5}	1.82×10^{7}	2.41×10^{6}	-1.47×10^{5}
Erect Shrub Tundra	3.17×10^{7}	2.17×10^{6}	3.58×10^{7}	9.77×10^{6}	-5.44×10^{5}
Prostrate Shrub Tundra	4.73×10^{6}	3.98×10^{5}	7.91×10^{6}	1.70×10^{6}	-1.13×10^{5}
Graminoid Tundra	2.36×10^{7}	1.75×10^{6}	2.95×10^{7}	8.33×10^{7}	-5.03×10^{5}
Wetlands	4.80×10^{6}	1.47×10^{6}	1.13×10^{7}	1.62×10^{6}	-3.53×10^{5}
Total	9.04×10^{8}	5.89×10^{7}	1.15×10^{9}	2.01×10^{8}	-1.18×10^{7}

Appendix B: Chapter 3. Disturbance, cultivation and climate drive a widespread North American vegetation greening

This section contains supplementary tables and figures for the "**Chapter 3**".

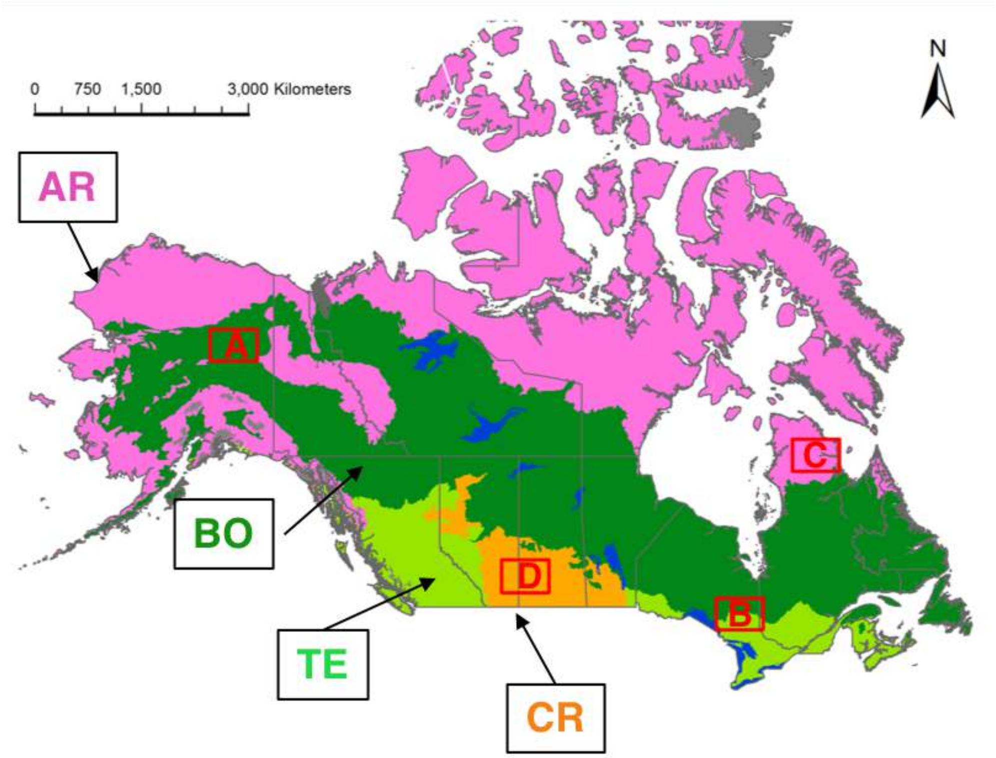

Figure B1.1 Geographical distribution of four classified biome types including Arctic (AR), Boreal (BO), Temperate (TE), and Cropland (CR) zones. Four red squares (A – D) in each panel are selected to showcase dominant vegetation change patterns in each biome type.

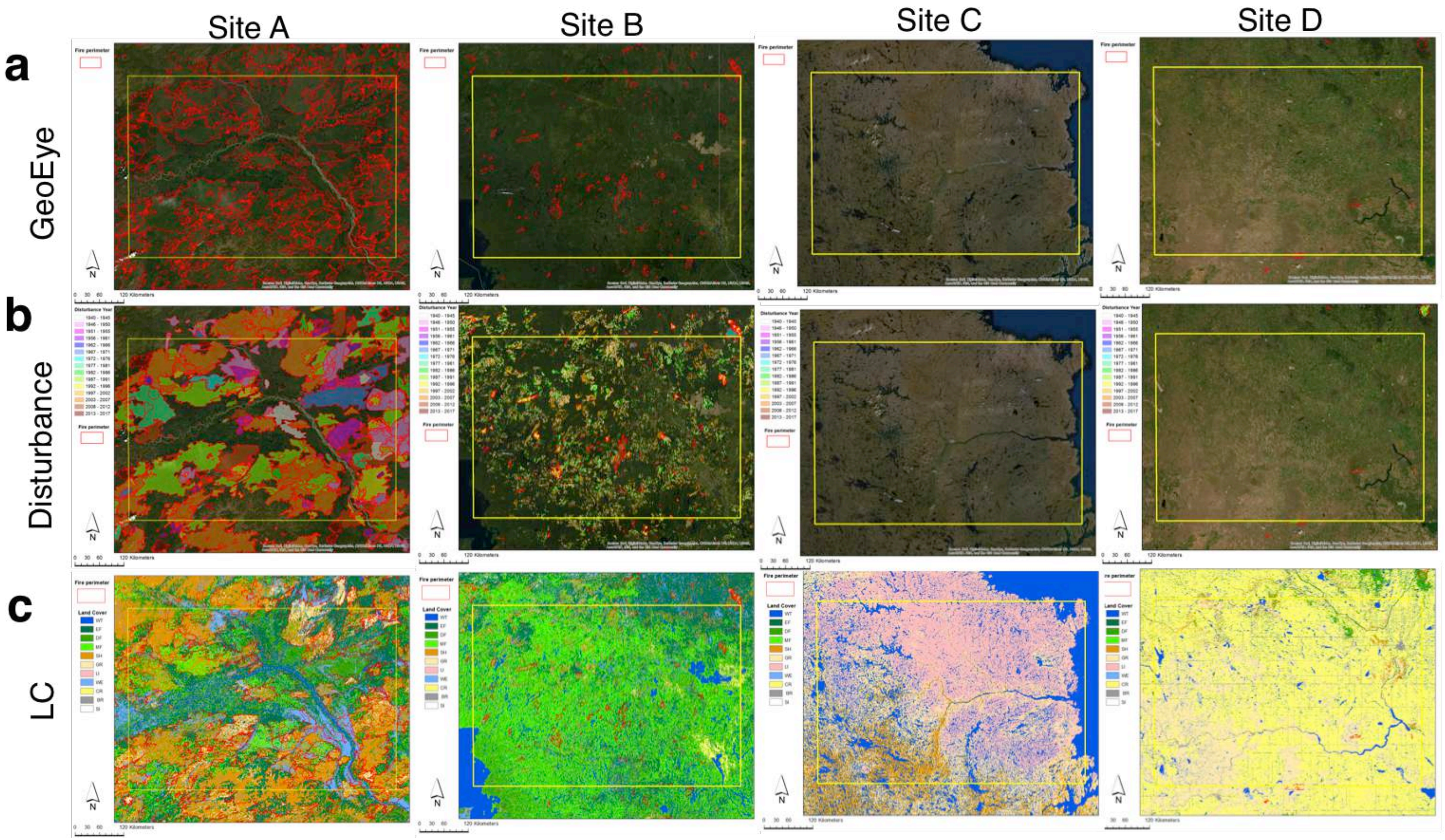

Figure B1.2 Regional subsets of high-resolution satellite image (GeoEye, a), disturbance year (b), and MODIS land cover (c) over the selected four example sites. Each column represents each site with alphabetical order (left to right, A to D) and red lines in all panels represent fire perimeters.

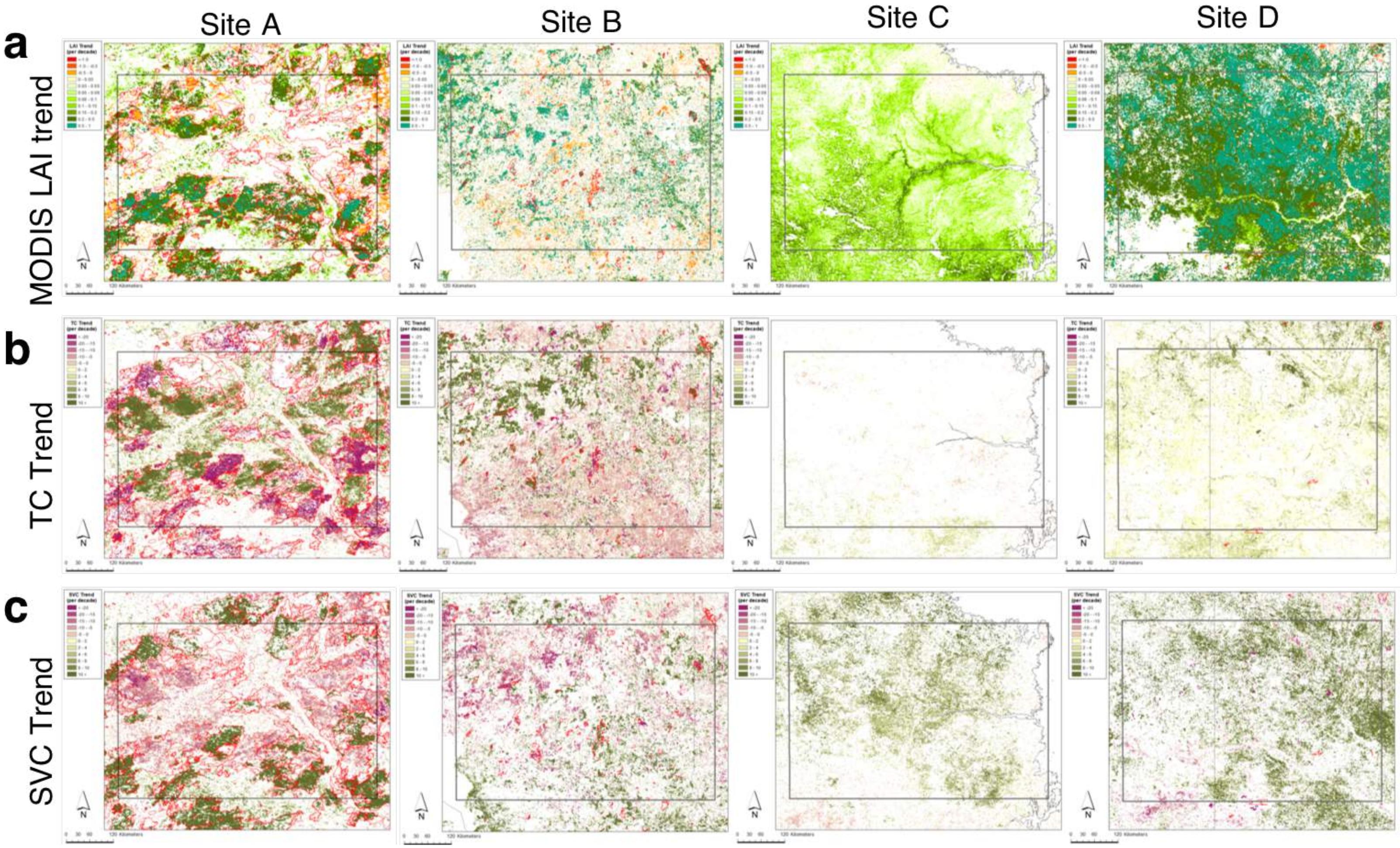

Figure B1.3 Same as Figure B1.2 but for decadal MODIS LAI (d), tree cover (TC, e) and short vegetation cover (SVC, f) trends.

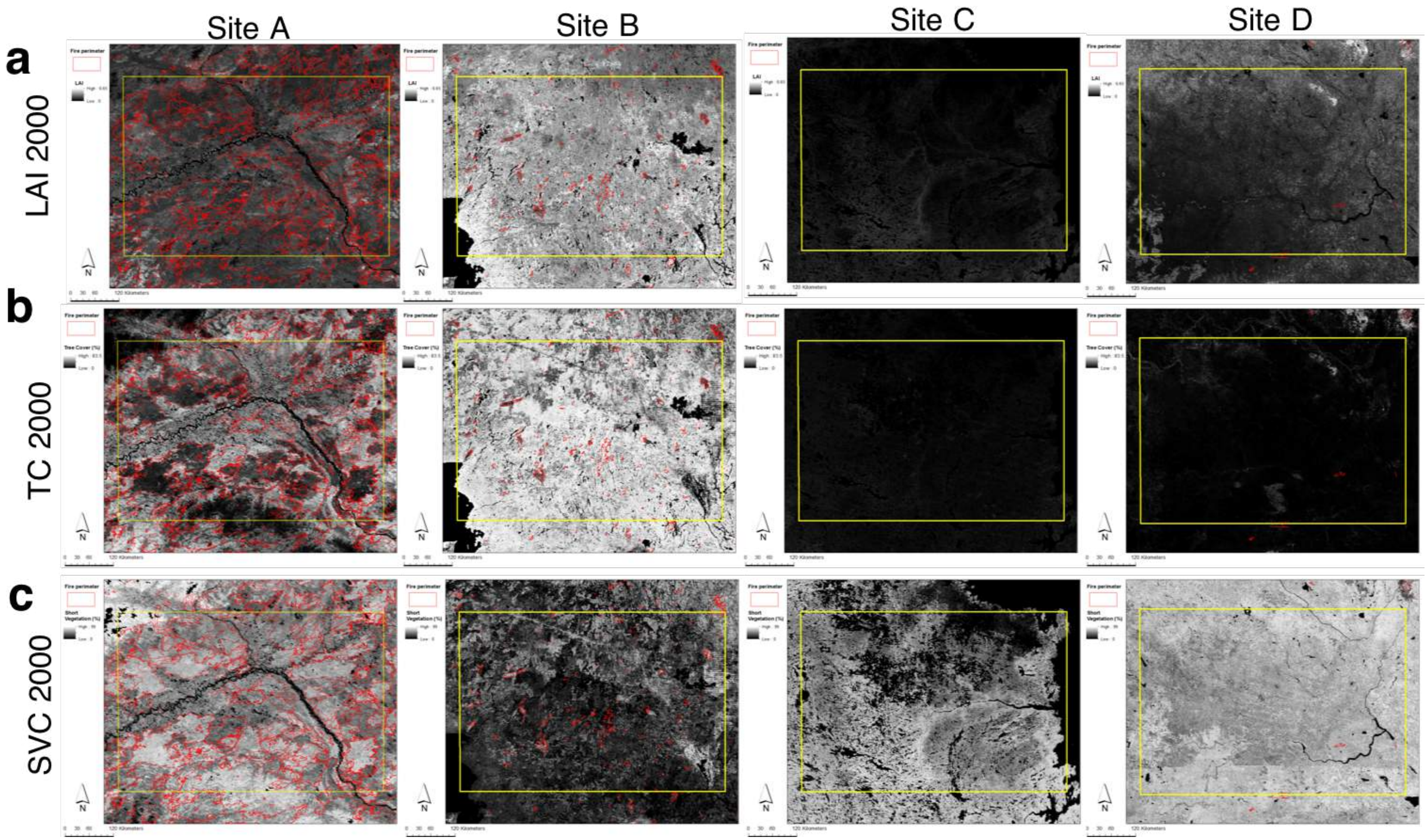

Figure B1.4 Same as Figure B1.2 but for MODIS LAI (d), tree cover (TC, e) and short vegetation cover (SVC, f) at 2000.

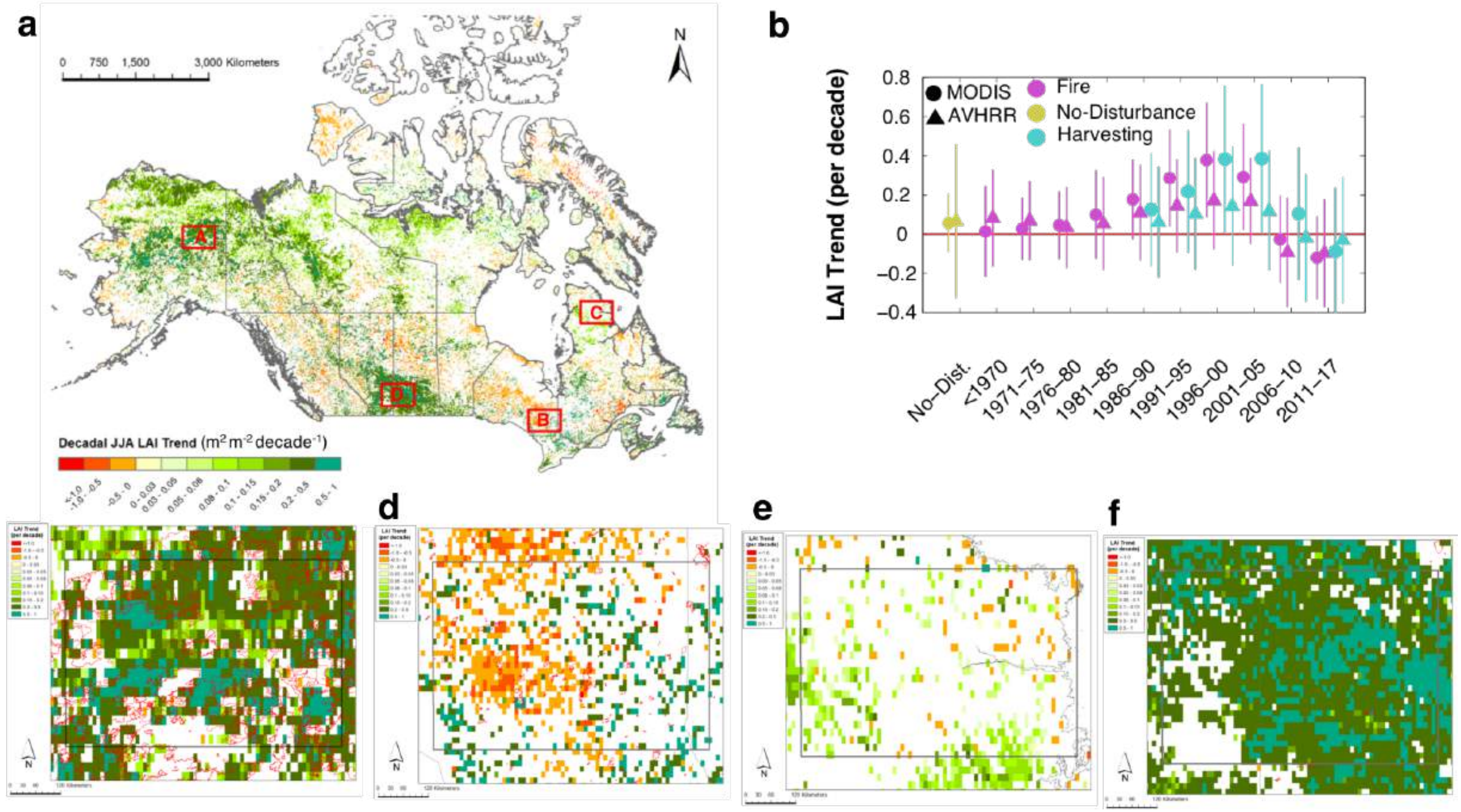

Figure B1.5 Spatial pattern of AVHRR LAI trends during last 18 years (a, same as Figure 3.1a but for AVHRR), distribution of LAI trend estimates grouped by the latest disturbance year (b, same as Figure 3.2a but for AVHRR and MODIS comparison), and four example sites showing details of vegetation changes (c-f, same as Figure 3.2c but for AVHRR).

Table B1.1 Proportion (%) of vegetated land showing greening and browning trends in AVHRR LAI with or without historical disturbance events. Note that statistically significant positive and negative changes are defined as greening (G) and browning (B), and others are insignificant changes (N.S.). Bracketed numbers in “Disturbed” column represents the solely fire-induced changes, i.e., the changes induced by harvesting can be calculated by subtracting the fire-induced changes from all disturbance-induced changes.

Biome (Area, 10^6 km^2)	Proportion of vegetated land (%)								
	All			Disturbed (fire induced change)			Non-disturbed		
	B	N.S.	G	B	N.S.	G	B	N.S.	G
AR (2.5)	5.2	70.4	24.4	0.1 (0.1)	1.0 (1.0)	0.6 (0.6)	5.0	69.4	23.8
BO (4.5)	11.7	66.1	22.1	3.7 (3.2)	18.3 (15.7)	9.2 (8.4)	8.0	47.8	12.9
TE (1.3)	11.0	68.3	20.7	3.7 (1.4)	17.9 (5.6)	6.6 (2.0)	7.3	50.8	14.1
CR (0.7)	1.6	35.8	62.6	0.6 (0.5)	4.6 (3.8)	2.2 (1.7)	1.0	31.2	60.4
All (9.0)	9.0	65.4	25.5	2.5 (1.9)	12.4 (9.2)	5.9 (4.8)	6.6	53.0	19.6

Table B1.2 Net leaf area and mean leaf area index changes during last 18 years (2000 – 2017) from AVHRR LAI. Note that only vegetated areas showing greening and browning are considered in this calculation. Net leaf area and mean leaf area index changes are calculated as follows: $\boldsymbol{Net\ leaf\ area} = \sum_{i=1}^{N} \boldsymbol{Trend_i} \cdot \boldsymbol{Area_i} \cdot \boldsymbol{Period}$, $\boldsymbol{Mean\ leaf\ area\ index} = \sum_{i=1}^{N} \boldsymbol{Trend_i} \cdot \boldsymbol{Area_i} \cdot \boldsymbol{Period} / \sum_{i=1}^{N} \boldsymbol{Area_i}$. Bracketed numbers in "Disturbed" column represents the solely fire-induced changes, i.e., the changes induced by harvesting can be calculated by subtracting the fire-induced changes from all disturbance-induced changes.

	Net leaf area (10^5 km^2)			Mean leaf area index (m^2 m^{-2})		
Biome	All	Disturbed (fire induced change)	Non-disturbed	All	Disturbed (fire induced change)	Non-disturbed
AR	1.82	0.06 (0.06)	1.75	0.25	0.33 (0.33)	0.24
BO	2.32	1.37 (1.26)	0.95	0.15	0.23 (0.24)	0.10
TE	0.98	0.27 (0.05)	0.71	0.23	0.19 (0.11)	0.25
CR	2.59	0.06 (0.05)	2.52	0.61	0.34 (0.31)	0.62
All	7.71	1.77 (1.42)	5.94	0.25	0.23 (0.24)	0.25

Appendix C: Chapter 4. Changes in timing of seasonal peak photosynthetic activity in northern ecosystems

This section contains supplementary tables and figures for the "**Chapter 4**".

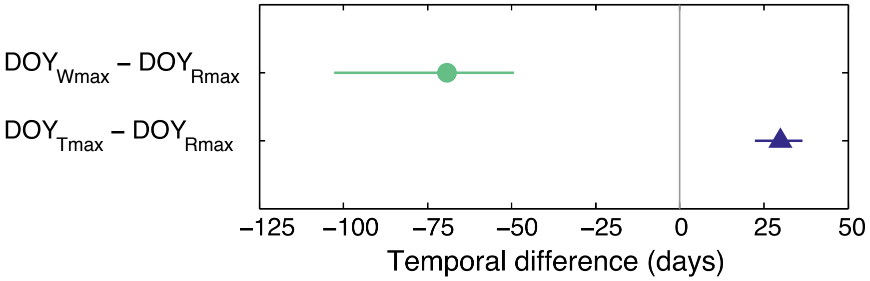

Figure C1.1 Temporal differences between the timings of peak climatic factors over northern terrestrial ecosystems. Temperature (DOY_{Tmax}), radiation (DOY_{Rmax}) and water availability (DOY_{Wmax}) serve as key proxies for climate resource availability. Reduced water losses during the cold season and thermal inertia lead to a sequential order of the timings of peak climatic factors.

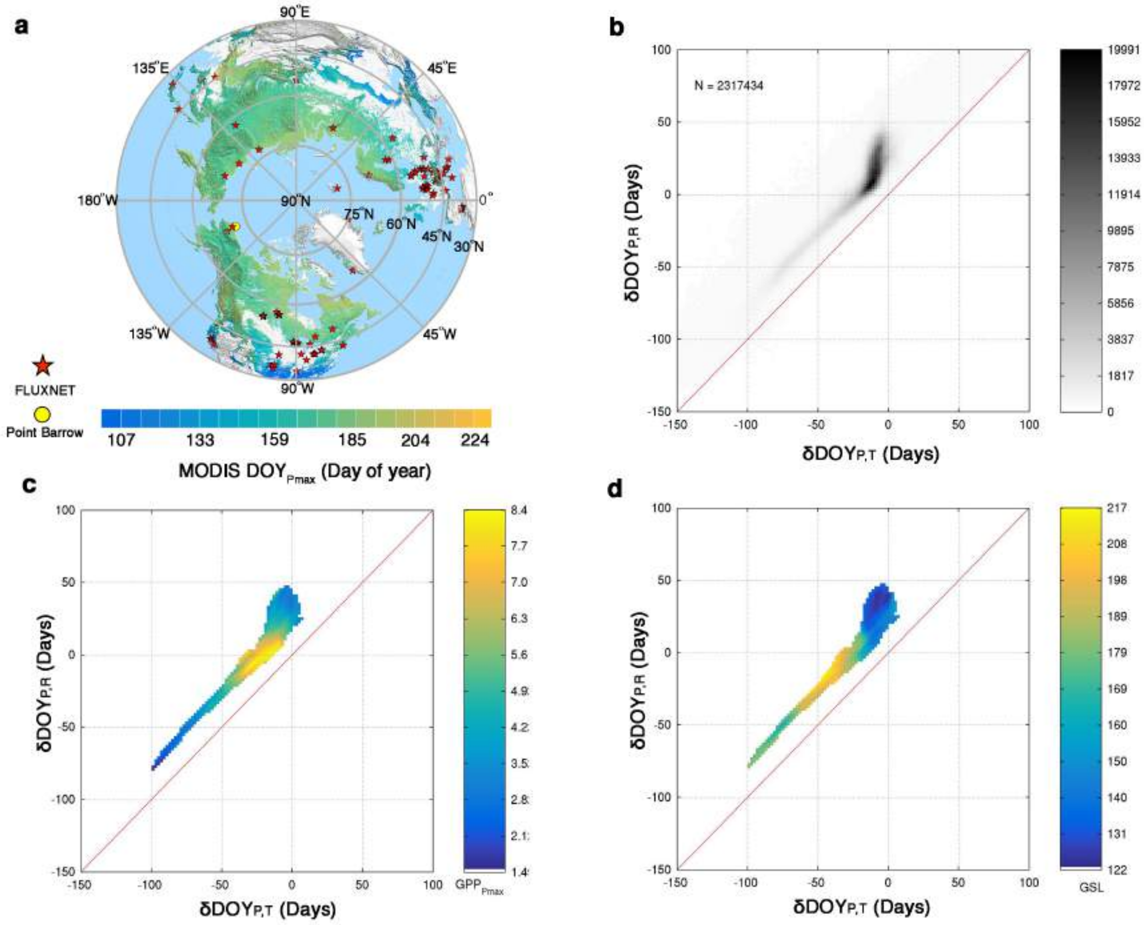

Figure C1.2. Satellite observed relation of positioning maximal photosynthetic activity to growing season length and maximal GPP. a, Spatial distribution of MODIS DOY$_{Pmax}$, FLUXNET and Point Barrow sites. Long-term (2000-2016) mean of DOY$_{Pmax}$ is used here. b, Density distribution of δDOY$_{P,T}$ and δDOY$_{P,R}$ for northern vegetation. c, Positioning of maximal photosynthetic activity (DOY$_{Pmax}$) seen as the relation between δDOY$_{P,R}$ and δDOY$_{P,T}$, with respect to maximum GPP (GPP$_{Pmax}$, g C m^{-2}). d, Same as c but for growing season length (GSL, days). MODIS derived outcomes are used for these panels.

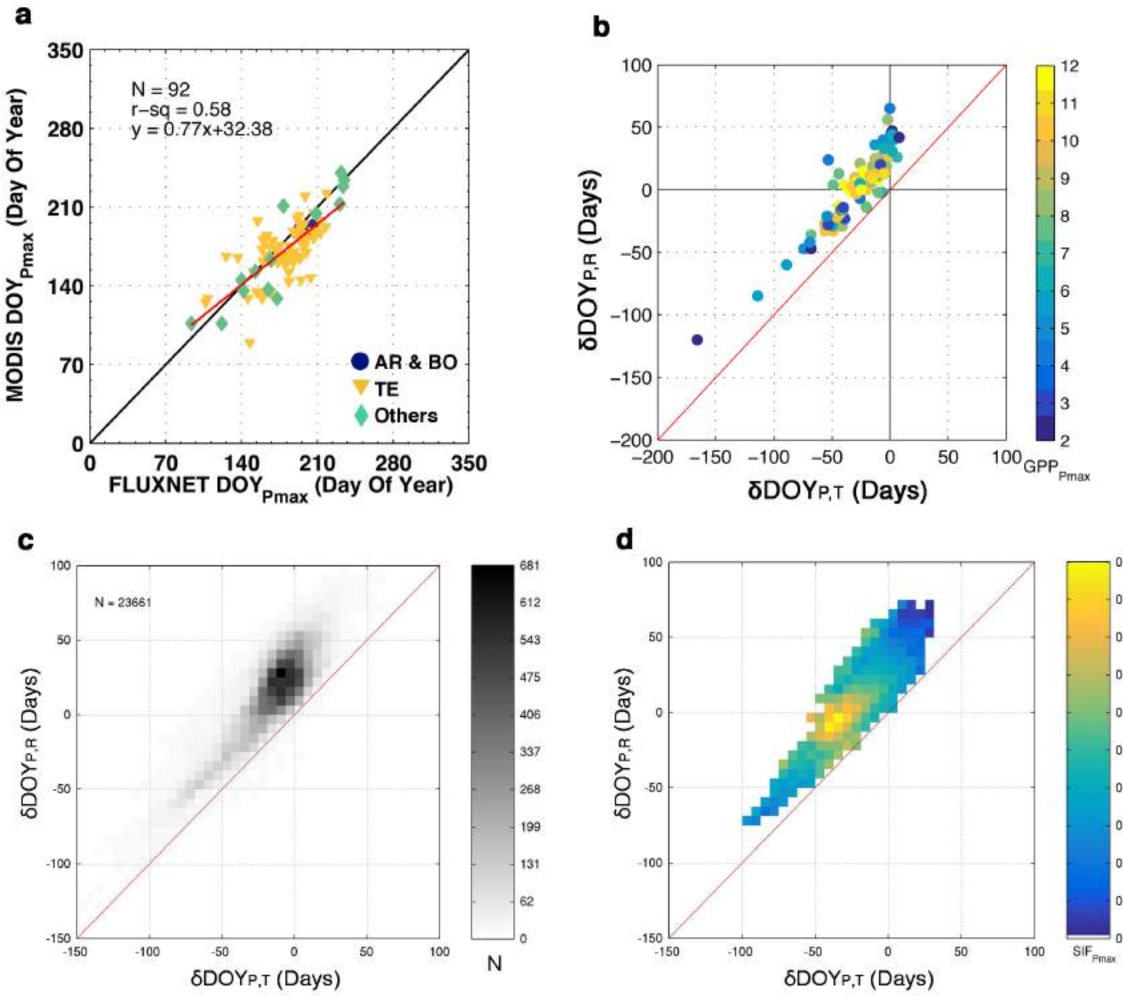

Figure C1.3 Analysis of eddy-covariance tower and GOME-2 SIF based maximal photosynthetic activity timing and its relation to productivity. a, Comparison between MODIS and FLUXNET based retrievals of DOY_{Pmax}. b, Observed positioning of maximal photosynthetic activity (DOY_{Pmax}) seen as the relation between $\delta DOY_{P,R}$ and $\delta DOY_{P,T}$, with respect to GPP_{Pmax} (g C m^{-2}). 92 FLUXNET sites are used and their geographical locations can be found in Figure C1.2a. c, Density distribution of $\delta DOY_{P,T}$ and $\delta DOY_{P,R}$ for northern vegetation based on GOME-2 SIF. d, Positioning of maximal photosynthetic activity (DOY_{Pmax}) seen as the relation between $\delta DOY_{P,R}$ and $\delta DOY_{P,T}$, with respect to maximum SIF (SIF_{Pmax}).

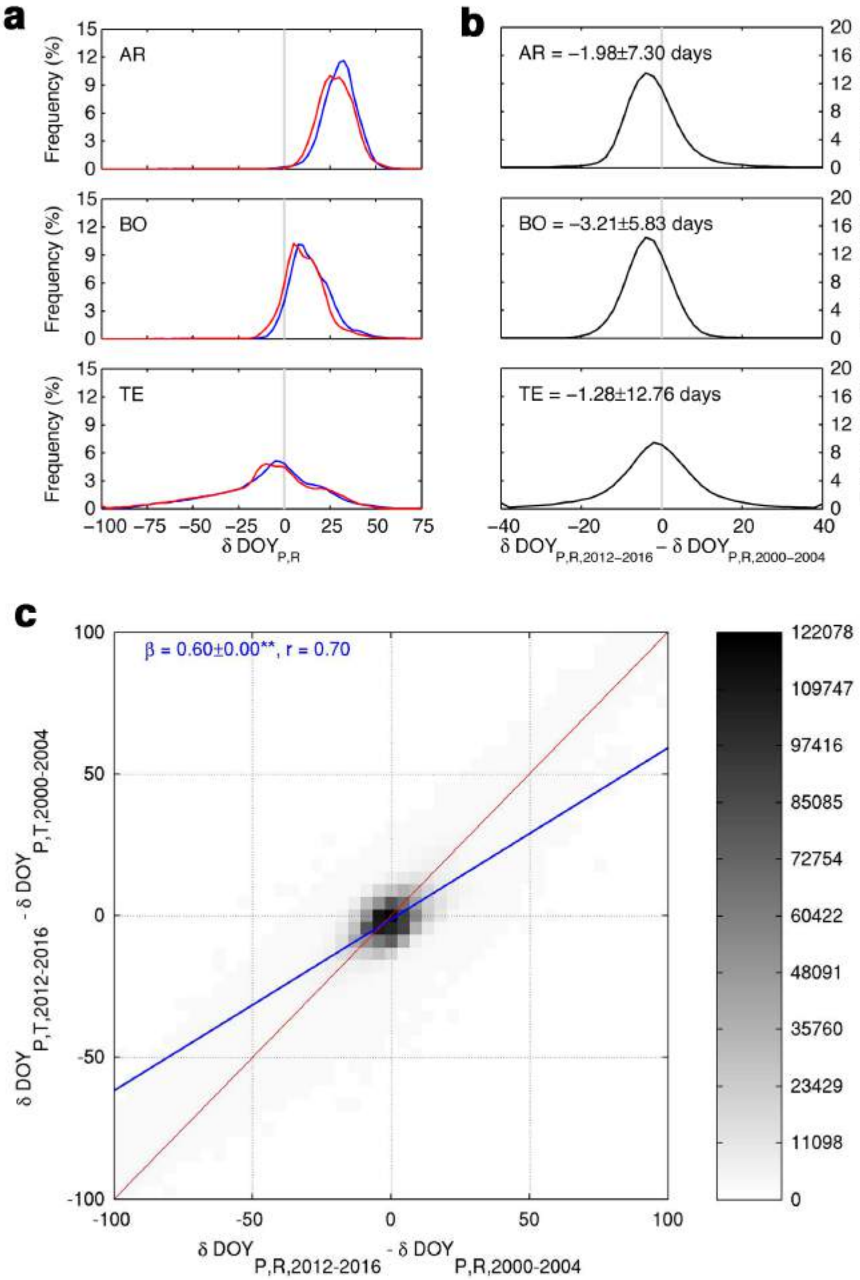

Figure C1.4 Changes in $\delta DOY_{P,R}$ and its relation to $\delta DOY_{P,T}$ during two separate periods. a, Distribution of $\delta DOY_{P,R}$ during first (2000 – 2004, blue) and last (2012 – 2016, red) 5-year periods over AR, BO and TE regions. b, Shift of $\delta DOY_{P,R}$ from the initial (2000 – 2004) to the last (2012 – 2016) period over three bioclimatic zones. Mean and 1 SD of changes in $\delta DOY_{P,R}$ are given. c, Scatter density plot between the shift in $\delta DOY_{P,R}$ from the initial to the last period and the shift in $\delta DOY_{P,T}$ during the period. Significance of the slope estimate (β ± SE) is denoted as double ($P < 0.001$) and single ($P < 0.05$) asterisks. The Kendall rank correlation coefficient (r) was used to measure degree of association.

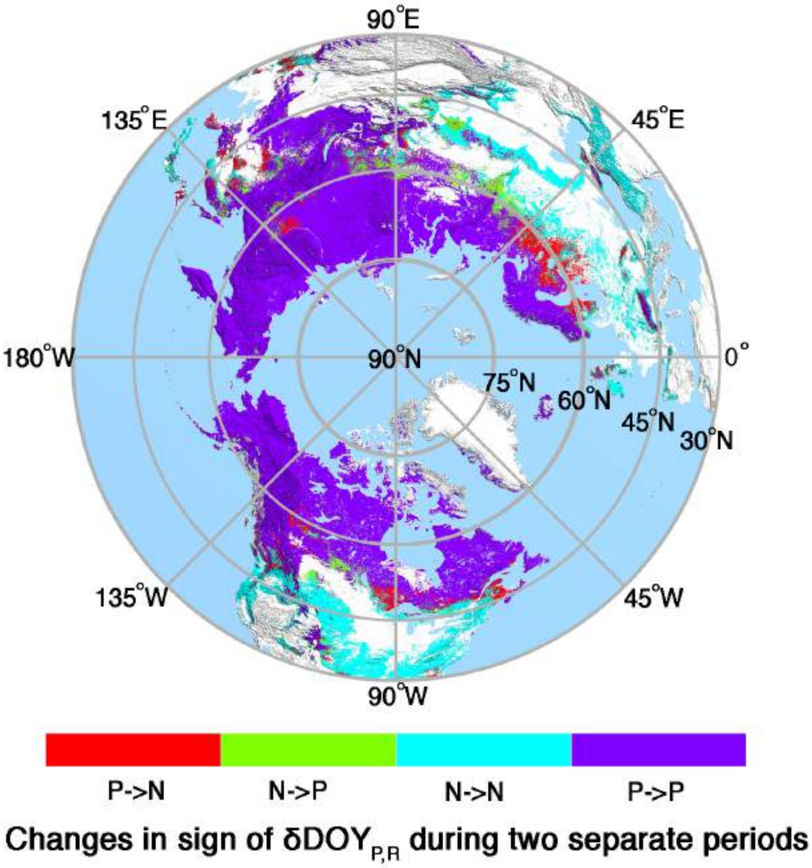

Figure C1.5 Spatial pattern of changes in sign of $\delta DOY_{P,R}$ during first (2000 – 2004) and last (2012 – 2016) periods. For example, P −>N denotes the regions where positive $\delta DOY_{P,R}$ changes into negative one.

Table C1.1 Changes in DOY_{Rmax}, DOY_{Tmax}, and DOY_{Wmax} over three different regions during last 17 years (2000 – 2016). The decadal trend is estimated based on the 5-year moving average approach to reduce the potential impact of first, last and outlier points. Calculated trend (slope ± SE) based on ordinary least squares regression is given with its significance level. The significance was computed by using the non-parametric Mann-Kendall trend test.

Biome	DOY_{Rmax} (days decade^{-1})	DOY_{Tmax} (days decade^{-1})	DOY_{Wmax} (days decade^{-1})
AR	-0.21 ± 0.45 ($P = 0.40$)	-0.43 ± 0.57 ($P = 0.46$)	-1.38 ± 0.61 ($P = 0.04$)
BO	-0.23 ± 0.31 ($P = 0.33$)	-0.34 ± 0.56 ($P = 0.57$)	-1.73 ± 1.33 ($P = 0.21$)
TE	0.05 ± 0.06 ($P = 0.27$)	0.56 ± 0.38 ($P = 0.19$)	-2.24 ± 1.18 ($P = 0.08$)
NH	-0.15 ± 0.65 ($P = 0.60$)	-0.02 ± 0.07 ($P = 0.97$)	-1.84 ± 0.55 ($P = 0.05$)

BIBLIOGRAPHY

Alcaraz‐Segura, D.O.M.I.N.G.O., Chuvieco, E., Epstein, H.E., Kasischke, E.S. and Trishchenko, A., 2010. Debating the greening vs. browning of the North American boreal forest: differences between satellite datasets. Global Change Biology, 16(2), pp.760-770.

Allen, C.D., Macalady, A.K., Chenchouni, H., Bachelet, D., McDowell, N., Vennetier, M., Kitzberger, T., Rigling, A., Breshears, D.D., Hogg, E.T. and Gonzalez, P., 2010. A global overview of drought and heat-induced tree mortality reveals emerging climate change risks for forests. Forest Ecology and Management, 259(4), pp.660-684.

Angert, A., Biraud, S., Bonfils, C., Henning, C.C., Buermann, W., Pinzon, J., Tucker, C.J. and Fung, I., 2005. Drier summers cancel out the CO2 uptake enhancement induced by warmer springs. Proceedings of the National Academy of Sciences of the United States of America, 102(31), pp.10823-10827.

Baldocchi, D., Falge, E., Gu, L., Olson, R., Hollinger, D., Running, S., Anthoni, P., Bernhofer, C., Davis, K., Evans, R. and Fuentes, J., 2001. FLUXNET: A new tool to study the temporal and spatial variability of ecosystem-scale carbon dioxide, water vapor, and energy flux densities. Bulletin of the American Meteorological Society, 82(11), pp.2415-2434.

Barber, V.A., Juday, G.P. and Finney, B.P., 2000. Reduced growth of Alaskan white spruce in the twentieth century from temperature-induced drought stress. Nature, 405(6787), p.668.

Baret, F., Morissette, J.T., Fernandes, R.A., Champeaux, J.L., Myneni, R.B., Chen, J., Plummer, S., Weiss, M., Bacour, C., Garrigues, S. and Nickeson, J.E., 2006. Evaluation of the representativeness of networks of sites for the global validation and intercomparison of land biophysical products: Proposition of the CEOS-BELMANIP. IEEE Transactions on Geoscience and Remote Sensing, 44(7), pp.1794-1803.

Barichivich, J., Briffa, K., Myneni, R., Schrier, G., Dorigo, W., Tucker, C., Osborn, T. and Melvin, T., 2014. Temperature and snow-mediated moisture controls of summer photosynthetic activity in northern terrestrial ecosystems between 1982 and 2011. Remote Sensing, 6(2), pp.1390-1431.

Barichivich, J., Briffa, K.R., Osborn, T.J., Melvin, T.M. and Caesar, J., 2012. Thermal growing season and timing of biospheric carbon uptake across the Northern Hemisphere. Global Biogeochemical Cycles, 26(4).

Bauerle, W.L., Oren, R., Way, D.A., Qian, S.S., Stoy, P.C., Thornton, P.E., Bowden, J.D., Hoffman, F.M. and Reynolds, R.F., 2012. Photoperiodic regulation of the seasonal pattern of photosynthetic capacity and the implications for carbon cycling. Proceedings of the National Academy of Sciences of the United States of America, 109(22), pp.8612-8617.

Beck, P.S. and Goetz, S.J., 2011. Satellite observations of high northern latitude vegetation productivity changes between 1982 and 2008: ecological variability and regional differences. Environmental Research Letters, 6(4), p.045501.

Beck, P.S., Atzberger, C., Høgda, K.A., Johansen, B. and Skidmore, A.K., 2006. Improved monitoring of vegetation dynamics at very high latitudes: A new method using MODIS NDVI. Remote Sensing of Environment, 100(3), pp.321-334.

Beck, P.S., Goetz, S.J., Mack, M.C., Alexander, H.D., Jin, Y., Randerson, J.T. and Loranty, M.M., 2011a. The impacts and implications of an intensifying fire regime on Alaskan boreal forest composition and albedo. Global Change Biology, 17(9), pp.2853-2866.

Beck, P.S., Juday, G.P., Alix, C., Barber, V.A., Winslow, S.E., Sousa, E.E., Heiser, P., Herriges, J.D. and Goetz, S.J., 2011b. Changes in forest productivity across Alaska consistent with biome shift. Ecology Letters, 14(4), pp.373-379.

Bergeron, Y. and Harvey, B., 1997. Basing silviculture on natural ecosystem dynamics: an approach applied to the southern boreal mixed wood forest of Quebec. Forest Ecology and Management, 92(1-3), pp.235-242.

Bergeron, Y., Chen, H.Y., Kenkel, N.C., Leduc, A.L. and Macdonald, S.E., 2014. Boreal mixedwood stand dynamics: ecological processes underlying multiple pathways. The Forestry Chronicle, 90(2), pp.202-213.

Bhatt, U.S., Walker, D.A., Raynolds, M.K., Comiso, J.C., Epstein, H.E., Jia, G., Gens, R., Pinzon, J.E., Tucker, C.J., Tweedie, C.E. and Webber, P.J., 2010. Circumpolar Arctic tundra vegetation change is linked to sea ice decline. Earth Interactions, 14(8), pp.1-20.

Bi, J., Xu, L., Samanta, A., Zhu, Z. and Myneni, R., 2013. Divergent arctic-boreal vegetation changes between North America and Eurasia over the past 30 years. Remote Sensing, 5(5), pp.2093-2112.

Bieniek, P.A., Bhatt, U.S., Walker, D.A., Raynolds, M.K., Comiso, J.C., Epstein, H.E., Pinzon, J.E., Tucker, C.J., Thoman, R.L., Tran, H. and Mölders, N., 2015. Climate drivers linked to changing seasonality of Alaska coastal tundra vegetation productivity. Earth Interactions, 19(19), pp.1-29.

Bjerke, J.W., Karlsen, S.R., Høgda, K.A., Malnes, E., Jepsen, J.U., Lovibond, S., Vikhamar-Schuler, D. and Tømmervik, H., 2014. Record-low primary productivity and high plant damage in the Nordic Arctic Region in 2012 caused by multiple weather events and pest outbreaks. Environmental Research Letters, 9(8), p.084006.

Bjorkman, A.D., Myers-Smith, I.H., Elmendorf, S.C., Normand, S., Rüger, N., Beck, P.S., Blach-Overgaard, A., Blok, D., Cornelissen, J.H.C., Forbes, B.C. and Georges, D., 2018. Plant functional trait change across a warming tundra biome. Nature, 562(7725), p.57.

Blackman, F.F., 1905. Optima and limiting factors. Annals of Botany, 19(74), pp.281-295.

Blunden, J., Arndt, D.S. and Baringer, M.O., 2011. State of the climate in 2010. Bulletin of the American Meteorological Society, 92(6), pp.S1-S236.

Bond-Lamberty, B., Peckham, S.D., Ahl, D.E. and Gower, S.T., 2007. Fire as the dominant driver of central Canadian boreal forest carbon balance. Nature, 450(7166), p.89.

Breiman, L., 2001. Random forests. Machine Learning, 45(1), pp.5-32.

Brodie, J.F., Roland, C., Stehn, S. and Smirnova, E., 2019. Variability in the expansion of trees and shrubs in boreal Alaska. Ecology, p.e02660.

Buermann, W., Anderson, B., Tucker, C.J., Dickinson, R.E., Lucht, W., Potter, C.S. and Myneni, R.B., 2003. Interannual covariability in Northern Hemisphere air temperatures and greenness associated with El Niño ‐ Southern Oscillation and the Arctic Oscillation. Journal of Geophysical Research: Atmospheres, 108(D13).

Buermann, W., Forkel, M., O'Sullivan, M., Sitch, S., Friedlingstein, P., Haverd, V., Jain, A.K., Kato, E., Kautz, M., Lienert, S. and Lombardozzi, D., 2018. Widespread seasonal compensation effects of spring warming on northern plant productivity. Nature, 562(7725), p.110.

Buermann, W., Parida, B., Jung, M., MacDonald, G.M., Tucker, C.J. and Reichstein, M., 2014. Recent shift in Eurasian boreal forest greening response may be associated with warmer and drier summers. Geophysical Research Letters, 41(6), pp.1995-2002.

Buitenwerf, R., Rose, L. and Higgins, S.I., 2015. Three decades of multi-dimensional change in global leaf phenology. Nature Climate Change, 5(4), p.364.

Chapin Iii, F.S., McGuire, A.D., Randerson, J., Pielke, R., Baldocchi, D., Hobbie, S.E., Roulet, N., Eugster, W., Kasischke, E., Rastetter, E.B. and Zimov, S.A., 2000. Arctic and boreal ecosystems of western North America as components of the climate system. Global Change Biology, 6(S1), pp.211-223.

Chen, C., Park, T., Wang, X., Piao, S., Xu, B., Chaturvedi, R.K., Fuchs, R., Brovkin, V., Ciais, P., Fensholt, R. and Tømmervik, H., 2019. China and India lead in greening of the world through land-use management. Nature Sustainability, 2(2), p.122.

Chen, J., Jönsson, P., Tamura, M., Gu, Z., Matsushita, B. and Eklundh, L., 2004. A simple method for reconstructing a high-quality NDVI time-series data set based on the Savitzky–Golay filter. Remote Sensing of Environment, 91(3-4), pp.332-344.

Chevallier, F., Ciais, P., Conway, T.J., Aalto, T., Anderson, B.E., Bousquet, P., Brunke, E.G., Ciattaglia, L., Esaki, Y., Fröhlich, M. and Gomez, A., 2010. CO2 surface fluxes at grid point scale estimated from a global 21 year reanalysis of atmospheric measurements. Journal of Geophysical Research: Atmospheres, 115(D21).

Choi, S., Kempes, C.P., Park, T., Ganguly, S., Wang, W., Xu, L., Basu, S., Dungan, J.L., Simard, M., Saatchi, S.S. and Piao, S., 2016. Application of the metabolic scaling theory and water–energy balance equation to model large ‐ scale patterns of maximum forest canopy height. Global Ecology and Biogeography, 25(12), pp.1428-1442.

Chuine, I. and Beaubien, E.G., 2001. Phenology is a major determinant of tree species range. Ecology Letters, 4(5), pp.500-510.

Colditz, R.R., Pouliot, D., Llamas, R.M., Homer, C., Latifovic, R., Ressl, R.A., Tovar, C.M., Hernández, A.V. and Richardson, K., 2014. Detection of North American land cover change between 2005 and 2010 with 250m MODIS data. PE&RS, Photogrammetric Engineering & Remote Sensing, 80(10), pp.918-924.

Commane, R., Lindaas, J., Benmergui, J., Luus, K.A., Chang, R.Y.W., Daube, B.C., Euskirchen, E.S., Henderson, J.M., Karion, A., Miller, J.B. and Miller, S.M., 2017. Carbon dioxide sources from Alaska driven by increasing early winter respiration from Arctic tundra. Proceedings of the National Academy of Sciences of the United States of America, 114(21), pp.5361-5366.

D'Orangeville, L., Houle, D., Duchesne, L., Phillips, R.P., Bergeron, Y. and Kneeshaw, D., 2018. Beneficial effects of climate warming on boreal tree growth may be transitory. Nature Communications, 9(1), p.3213.

Danneyrolles, V., Dupuis, S., Fortin, G., Leroyer, M., de Römer, A., Terrail, R., Vellend, M., Boucher, Y., Laflamme, J., Bergeron, Y. and Arseneault, D., 2019. Stronger influence of anthropogenic disturbance than climate change on century-scale compositional changes in northern forests. Nature Communications, 10(1), p.1265.

Dimiceli, C., Carroll, M., Sohlberg, R., Kim, D.H., Kelly, M. and Townshend, J.R.G., 2015. MOD44B MODIS/Terra vegetation continuous fields yearly L3 Global 250 m SIN Grid V006. NASA EOSDIS Land Processes DAAC.

Duveneck, M.J. and Thompson, J.R., 2017. Climate change imposes phenological trade‐offs on forest net primary productivity. Journal of Geophysical Research: Biogeosciences, 122(9), pp.2298-2313.

Eagleson, P.S., 2005. Ecohydrology: Darwinian expression of vegetation form and function. Cambridge University Press.

Foley, J.A., Ramankutty, N., Brauman, K.A., Cassidy, E.S., Gerber, J.S., Johnston, M., Mueller, N.D., O'Connell, C., Ray, D.K., West, P.C. and Balzer, C., 2011. Solutions for a cultivated planet. Nature, 478(7369), p.337.

Forkel, M., Carvalhais, N., Rödenbeck, C., Keeling, R., Heimann, M., Thonicke, K., Zaehle, S. and Reichstein, M., 2016. Enhanced seasonal CO2 exchange caused by amplified plant productivity in northern ecosystems. Science, 351(6274), pp.696-699.

FRAMES, 2018. Alaska Large Fire Database. Accessed February 21, 2018 <https://www.frames.gov/catalog/10465>.

Friedl, M.A., Gray, J.M., Melaas, E.K., Richardson, A.D., Hufkens, K., Keenan, T.F., Bailey, A. and O'Keefe, J., 2014. A tale of two springs: using recent climate anomalies to characterize the sensitivity of temperate forest phenology to climate change. Environmental Research Letters, 9(5), p.054006.

Friedl, M.A., Sulla-Menashe, D., Tan, B., Schneider, A., Ramankutty, N., Sibley, A. and Huang, X., 2010. MODIS Collection 5 global land cover: Algorithm refinements and characterization of new datasets. Remote Sensing of Environment, 114(1), pp.168-182.

Fritz, S., See, L., McCallum, I., You, L., Bun, A., Moltchanova, E., Duerauer, M., Albrecht, F., Schill, C., Perger, C. and Havlik, P., 2015. Mapping global cropland and field size. Global Change Biology, 21(5), pp.1980-1992.

Frost, G.V. and Epstein, H.E., 2014. Tall shrub and tree expansion in Siberian tundra ecotones since the 1960s. Global Change Biology, 20(4), pp.1264-1277.

Fu, Y.H., Zhao, H., Piao, S., Peaucelle, M., Peng, S., Zhou, G., Ciais, P., Huang, M., Menzel, A., Peñuelas, J. and Song, Y., 2015. Declining global warming effects on the phenology of spring leaf unfolding. Nature, 526(7571), p.104.

Ganguly, S., Friedl, M.A., Tan, B., Zhang, X. and Verma, M., 2010. Land surface phenology from MODIS: Characterization of the Collection 5 global land cover dynamics product. Remote Sensing of Environment, 114(8), pp.1805-1816.

Garonna, I., De Jong, R., De Wit, A.J., Mücher, C.A., Schmid, B. and Schaepman, M.E., 2014. Strong contribution of autumn phenology to changes in satellite-derived growing season length estimates across Europe (1982–2011). Global Change Biology, 20(11), pp.3457-3470.

Garonna, I., de Jong, R., Stöckli, R., Schmid, B., Schenkel, D., Schimel, D. and Schaepman, M.E., 2018. Shifting relative importance of climatic constraints on land surface phenology. Environmental Research Letters, 13(2), p.024025.

Gelaro, R., McCarty, W., Suárez, M.J., Todling, R., Molod, A., Takacs, L., Randles, C.A., Darmenov, A., Bosilovich, M.G., Reichle, R. and Wargan, K., 2017. The modern-era retrospective analysis for research and applications, version 2 (MERRA-2). Journal of Climate, 30(14), pp.5419-5454.

Gill, A.L., Gallinat, A.S., Sanders-DeMott, R., Rigden, A.J., Short Gianotti, D.J., Mantooth, J.A. and Templer, P.H., 2015. Changes in autumn senescence in northern hemisphere deciduous trees: a meta-analysis of autumn phenology studies. Annals of Botany, 116(6), pp.875-888.

Girardin, M.P., Bouriaud, O., Hogg, E.H., Kurz, W., Zimmermann, N.E., Metsaranta, J.M., de Jong, R., Frank, D.C., Esper, J., Büntgen, U. and Guo, X.J., 2016. No growth stimulation of Canada's boreal forest under half-century of combined warming and CO2 fertilization. Proceedings of the National Academy of Sciences of the United States of America, 113(52), pp.E8406-E8414.

Goetz, S.J., Bunn, A.G., Fiske, G.J. and Houghton, R.A., 2005. Satellite-observed photosynthetic trends across boreal North America associated with climate and fire disturbance. Proceedings of the National Academy of Sciences of the United States of America, 102(38), pp.13521-13525.

Goetz, S.J., Mack, M.C., Gurney, K.R., Randerson, J.T. and Houghton, R.A., 2007. Ecosystem responses to recent climate change and fire disturbance at northern high latitudes: observations and model results contrasting northern Eurasia and North America. Environmental Research Letters, 2(4), p.045031.

Gonsamo, A., Chen, J.M. and Ooi, Y.W., 2018. Peak season plant activity shift towards spring is reflected by increasing carbon uptake by extratropical ecosystems. Global Change Biology, 24(5), pp.2117-2128.

Goulden, M.L., McMillan, A.M.S., Winston, G.C., Rocha, A.V., Manies, K.L., Harden, J.W. and Bond ‐ Lamberty, B.P., 2011. Patterns of NPP, GPP, respiration, and NEP during boreal forest succession. Global Change Biology, 17(2), pp.855-871.

Goward, S.N., Tucker, C.J. and Dye, D.G., 1985. North American vegetation patterns observed with the NOAA-7 advanced very high resolution radiometer. Vegetatio, 64(1), pp.3-14.

Graven, H.D., Keeling, R.F., Piper, S.C., Patra, P.K., Stephens, B.B., Wofsy, S.C., Welp, L.R., Sweeney, C., Tans, P.P., Kelley, J.J. and Daube, B.C., 2013. Enhanced seasonal exchange of CO2 by northern ecosystems since 1960. Science, 341(6150), pp.1085-1089.

Guay, K.C., Beck, P.S., Berner, L.T., Goetz, S.J., Baccini, A. and Buermann, W., 2014. Vegetation productivity patterns at high northern latitudes: a multi ‐ sensor satellite data assessment. Global Change Biology, 20(10), pp.3147-3158.

Hall, F., Masek, J.G. and Collatz, G.J., 2006. Evaluation of ISLSCP Initiative II FASIR and GIMMS NDVI products and implications for carbon cycle science. Journal of Geophysical Research: Atmospheres, 111(D22).

Hansen, M.C., Potapov, P.V., Moore, R., Hancher, M., Turubanova, S.A.A., Tyukavina, A., Thau, D., Stehman, S.V., Goetz, S.J., Loveland, T.R. and Kommareddy, A., 2013. High-resolution global maps of 21st-century forest cover change. Science, 342(6160), pp.850-853.

Harper, K.A., Macdonald, S.E., Burton, P.J., Chen, J., Brosofske, K.D., Saunders, S.C., Euskirchen, E.S., Roberts, D.A.R., Jaiteh, M.S. and Esseen, P.A., 2005. Edge influence on forest structure and composition in fragmented landscapes. Conservation Biology, 19(3), pp.768-782.

Heinsch, F.A., Zhao, M., Running, S.W., Kimball, J.S., Nemani, R.R., Davis, K.J., Bolstad, P.V., Cook, B.D., Desai, A.R., Ricciuto, D.M. and Law, B.E., 2006. Evaluation of remote sensing based terrestrial productivity from MODIS using regional tower eddy flux network observations. IEEE Transactions on Geoscience and Remote Sensing, 44(7), pp.1908-1925.

Hermosilla, T., Wulder, M.A., White, J.C., Coops, N.C. and Hobart, G.W., 2018. Disturbance-informed annual land cover classification maps of Canada's forested ecosystems for a 29-year Landsat time series. Canadian Journal of Remote Sensing, 44(1), pp.67-87.

Hermosilla, T., Wulder, M.A., White, J.C., Coops, N.C., Hobart, G.W. and Campbell, L.B., 2016. Mass data processing of time series Landsat imagery: pixels to data products for forest monitoring. International Journal of Digital Earth, 9(11), pp.1035-1054.

Hilmers, T., Avdagić, A., Bartkowicz, L., Bielak, K., Binder, F., Bončina, A., Dobor, L., Forrester, D.I., Hobi, M.L., Ibrahimspahić, A. and Jaworski, A., 2019. The productivity of mixed mountain forests comprised of *Fagus sylvatica*, *Picea abies*, and *Abies alba* across Europe. Forestry 92(5), pp.512–522.

Hinzman, L.D., Bettez, N.D., Bolton, W.R., Chapin, F.S., Dyurgerov, M.B., Fastie, C.L., Griffith, B., Hollister, R.D., Hope, A., Huntington, H.P. and Jensen, A.M., 2005. Evidence and implications of recent climate change in northern Alaska and other arctic regions. Climatic Change, 72(3), pp.251-298.

Høgda, K., Tømmervik, H. and Karlsen, S., 2013. Trends in the start of the growing season in Fennoscandia 1982–2011. Remote Sensing, 5(9), pp.4304-4318.

Hooke, R.L., Martín-Duque, J.F. and Pedraza, J., 2012. Land transformation by humans: a review. GSA Today, 22(12), pp.4-10.

Hunter, A.F. and Lechowicz, M.J., 1992. Predicting the timing of budburst in temperate trees. Journal of Applied Ecology, pp.597-604.

Ito, A., Inatomi, M., Huntzinger, D.N., Schwalm, C., Michalak, A.M., Cook, R., King, A.W., Mao, J., Wei, Y., Post, W.M. and Wang, W., 2016. Decadal trends in the seasonal-cycle amplitude of terrestrial CO2 exchange resulting from the ensemble of terrestrial biosphere models. Tellus B: Chemical and Physical Meteorology, 68(1), p.28968.

Jenness, J., 2006. Topographic Position Index (tpi_jen. avx) extension for ArcView 3. x, v. 1.3 a. Jenness Enterprises.

Johnstone, J.F., Allen, C.D., Franklin, J.F., Frelich, L.E., Harvey, B.J., Higuera, P.E., Mack, M.C., Meentemeyer, R.K., Metz, M.R., Perry, G.L. and Schoennagel, T., 2016. Changing disturbance regimes, ecological memory, and forest resilience. Frontiers in Ecology and the Environment, 14(7), pp.369-378.

Johnstone, J.F., Chapin, F.S., Hollingsworth, T.N., Mack, M.C., Romanovsky, V. and Turetsky, M., 2010. Fire, climate change, and forest resilience in interior Alaska. Canadian Journal of Forest Research, 40(7), pp.1302-1312.

Joiner, J., Yoshida, Y., Guanter, L. and Middleton, E.M., 2016. New methods for the retrieval of chlorophyll red fluorescence from hyperspectral satellite instruments: simulations and application to GOME-2 and SCIAMACHY. Atmospheric Measurement Techniques, 9(8).

Jolly, W.M., Nemani, R. and Running, S.W., 2005. A generalized, bioclimatic index to predict foliar phenology in response to climate. Global Change Biology, 11(4), pp.619-632.

Jönsson, P. and Eklundh, L., 2004. TIMESAT—a program for analyzing time-series of satellite sensor data. Computers & Geosciences, 30(8), pp.833-845.

Ju, J. and Masek, J.G., 2016. The vegetation greenness trend in Canada and US Alaska from 1984–2012 Landsat data. Remote Sensing of Environment, 176, pp.1-16.

Jung, M., Reichstein, M., Margolis, H.A., Cescatti, A., Richardson, A.D., Arain, M.A., Arneth, A., Bernhofer, C., Bonal, D., Chen, J. and Gianelle, D., 2011. Global patterns of land ‐ atmosphere fluxes of carbon dioxide, latent heat, and sensible heat derived from eddy covariance, satellite, and meteorological observations. Journal of Geophysical Research: Biogeosciences, 116(G3).

Karlsen, S.R., Elvebakk, A., Høgda, K.A. and Johansen, B., 2006. Satellite ‐ based mapping of the growing season and bioclimatic zones in Fennoscandia. Global Ecology and Biogeography, 15(4), pp.416-430.

Kasischke, E.S. and Turetsky, M.R., 2006. Recent changes in the fire regime across the North American boreal region—Spatial and temporal patterns of burning across Canada and Alaska. Geophysical Research Letters, 33(9).

Keeling, C.D., Chin, J.F.S. and Whorf, T.P., 1996. Increased activity of northern vegetation inferred from atmospheric CO2 measurements. Nature, 382(6587), p.146.

Keenan, T.F. and Riley, W.J., 2018. Greening of the land surface in the world's cold regions consistent with recent warming. Nature Climate Change, 8(9), p.825.

Keenan, T.F., Gray, J., Friedl, M.A., Toomey, M., Bohrer, G., Hollinger, D.Y., Munger, J.W., O'Keefe, J., Schmid, H.P., Wing, I.S. and Yang, B., 2014. Net carbon uptake has increased through warming-induced changes in temperate forest phenology. Nature Climate Change, 4(7), p.598.

Kim, Y., Kimball, J.S., Zhang, K. and McDonald, K.C., 2012. Satellite detection of increasing Northern Hemisphere non-frozen seasons from 1979 to 2008: Implications for regional vegetation growth. Remote Sensing of Environment, 121, pp.472-487.

Knyazikhin, Y., Martonchik, J.V., Myneni, R.B., Diner, D.J. and Running, S.W., 1998. Synergistic algorithm for estimating vegetation canopy leaf area index and fraction of absorbed photosynthetically active radiation from MODIS and MISR data. Journal of Geophysical Research: Atmospheres, 103(D24), pp.32257-32275.

Lasslop, G., Reichstein, M., Papale, D., Richardson, A.D., Arneth, A., Barr, A., Stoy, P. and Wohlfahrt, G., 2010. Separation of net ecosystem exchange into assimilation and respiration using a light response curve approach: critical issues and global evaluation. Global Change Biology, 16(1), pp.187-208.

Lucht, W., Prentice, I.C., Myneni, R.B., Sitch, S., Friedlingstein, P., Cramer, W., Bousquet, P., Buermann, W. and Smith, B., 2002. Climatic control of the high-latitude vegetation greening trend and Pinatubo effect. Science, 296(5573), pp.1687-1689.

Mann, H.B., 1945. Nonparametric tests against trend. Econometrica: Journal of the Econometric Society, pp.245-259.

McManus, K.M., Morton, D.C., Masek, J.G., Wang, D., Sexton, J.O., Nagol, J.R., Ropars, P. and Boudreau, S., 2012. Satellite‐based evidence for shrub and graminoid tundra expansion in northern Quebec from 1986 to 2010. Global Change Biology, 18(7), pp.2313-2323.

Melaas, E.K., Friedl, M.A. and Zhu, Z., 2013. Detecting interannual variation in deciduous broadleaf forest phenology using Landsat TM/ETM+ data. Remote Sensing of Environment, 132, pp.176-185.

Menzel, A., Sparks, T.H., Estrella, N., Koch, E., Aasa, A., Ahas, R., Alm‐Kübler, K., Bissolli, P., Braslavská, O.G., Briede, A. and Chmielewski, F.M., 2006. European phenological response to climate change matches the warming pattern. Global Change Biology, 12(10), pp.1969-1976.

Myers-Smith, I.H., Elmendorf, S.C., Beck, P.S., Wilmking, M., Hallinger, M., Blok, D., Tape, K.D., Rayback, S.A., Macias-Fauria, M., Forbes, B.C. and Speed, J.D., 2015. Climate sensitivity of shrub growth across the tundra biome. Nature Climate Change, 5(9), p.887.

Myers-Smith, I.H., Forbes, B.C., Wilmking, M., Hallinger, M., Lantz, T., Blok, D., Tape, K.D., Macias-Fauria, M., Sass-Klaassen, U., Lévesque, E. and Boudreau, S., 2011. Shrub expansion in tundra ecosystems: dynamics, impacts and research priorities. Environmental Research Letters, 6(4), p.045509.

Myers-Smith, I.H. and Hik, D.S., 2018. Climate warming as a driver of tundra shrubline advance. journal of ecology, 106(2), pp.547-560.

Myneni, R., Knyazikhin, Y. and Park, T., 2015a. MOD15A2H MODIS/terra leaf area index/FPAR 8-day L4 global 500 m SIN grid V006. NASA EOSDIS Land Processes DAAC.

Myneni, R., Knyazikhin, Y. and Park, T., 2015b. MYD15A2H MODIS/terra leaf area index/FPAR 8-day L4 global 500 m SIN grid V006. NASA EOSDIS Land Processes DAAC.

Myneni, R.B. and Williams, D.L., 1994. On the relationship between FAPAR and NDVI. Remote Sensing of Environment, 49(3), pp.200-211.

Myneni, R.B., Keeling, C.D., Tucker, C.J., Asrar, G. and Nemani, R.R., 1997. Increased plant growth in the northern high latitudes from 1981 to 1991. Nature, 386(6626), p.698.

Natali, S.M., Schuur, E.A. and Rubin, R.L., 2012. Increased plant productivity in Alaskan tundra as a result of experimental warming of soil and permafrost. Journal of Ecology, 100(2), pp.488-498.

Natural Resources Canada (NRC), 2018. The state of Canada's forests: Annual report 2018. Accessed May 1, 2019 < http://cfs.nrcan.gc.ca/pubwarehouse/pdfs/39336.pdf >.

Nemani, R.R., Keeling, C.D., Hashimoto, H., Jolly, W.M., Piper, S.C., Tucker, C.J., Myneni, R.B. and Running, S.W., 2003. Climate-driven increases in global terrestrial net primary production from 1982 to 1999. Science, 300(5625), pp.1560-1563.

Ni, X., Park, T., Choi, S., Shi, Y., Cao, C., Wang, X., Lefsky, M., Simard, M. and Myneni, R., 2014. Allometric scaling and resource limitations model of tree heights: Part 3. Model optimization and testing over continental China. Remote Sensing, 6(5), pp.3533-3553.

Olson, D.M., Dinerstein, E., Wikramanayake, E.D., Burgess, N.D., Powell, G.V., Underwood, E.C., D'amico, J.A., Itoua, I., Strand, H.E., Morrison, J.C. and Loucks, C.J., 2001. Terrestrial Ecoregions of the World: A New Map of Life on EarthA new global map of terrestrial ecoregions provides an innovative tool for conserving biodiversity. BioScience, 51(11), pp.933-938.

Pan, Y., Birdsey, R.A., Fang, J., Houghton, R., Kauppi, P.E., Kurz, W.A., Phillips, O.L., Shvidenko, A., Lewis, S.L., Canadell, J.G. and Ciais, P., 2011. A large and persistent carbon sink in the world’s forests. Science, 333(6045), pp.988-993.

Park, T., Chen, C., Macias-Fauria, M., Tømmervik, H., Choi, S., Winkler, A., Bhatt, U.S., Walker, D.A., Piao, S., Brovkin, V. and Nemani, R.R., 2019. Changes in timing of seasonal peak photosynthetic activity in northern ecosystems. Global Change Biology 25(7), pp.2382–2395.

Park, T., Ganguly, S., Tømmervik, H., Euskirchen, E.S., Høgda, K.A., Karlsen, S.R., Brovkin, V., Nemani, R.R. and Myneni, R.B., 2016. Changes in growing season duration and productivity of northern vegetation inferred from long-term remote sensing data. Environmental Research Letters, 11(8), p.084001.

Parmesan, C. and Yohe, G., 2003. A globally coherent fingerprint of climate change impacts across natural systems. Nature, 421(6918), p.37.

Pastick, N.J., Jorgenson, M.T., Goetz, S.J., Jones, B.M., Wylie, B.K., Minsley, B.J., Genet, H., Knight, J.F., Swanson, D.K. and Jorgenson, J.C., 2019. Spatiotemporal remote sensing of ecosystem change and causation across Alaska. Global Change Biology, 25(3), pp.1171-1189.

Pastorello, G., Papale, D., Chu, H., Trotta, C., Agarwal, D., Canfora, E., Baldocchi, D. and Torn, M., 2017. A new data set to keep a sharper eye on land-air exchanges. Eos, Transactions American Geophysical Union (Online), 98(8).

Pekel, J.F., Cottam, A., Gorelick, N. and Belward, A.S., 2016. High-resolution mapping of global surface water and its long-term changes. Nature, 540(7633), p.418.

Peng, C., Ma, Z., Lei, X., Zhu, Q., Chen, H., Wang, W., Liu, S., Li, W., Fang, X. and Zhou, X., 2011. A drought-induced pervasive increase in tree mortality across Canada's boreal forests. Nature Climate Change, 1(9), p.467.

Pettorelli, N., Vik, J.O., Mysterud, A., Gaillard, J.M., Tucker, C.J. and Stenseth, N.C., 2005. Using the satellite-derived NDVI to assess ecological responses to environmental change. Trends in Ecology & Evolution, 20(9), pp.503-510.

Phoenix, G.K. and Bjerke, J.W., 2016. Arctic browning: extreme events and trends reversing arctic greening. Global Change Biology, 22(9), pp.2960-2962.

Piao, S., Ciais, P., Friedlingstein, P., Peylin, P., Reichstein, M., Luyssaert, S., Margolis, H., Fang, J., Barr, A., Chen, A. and Grelle, A., 2008. Net carbon dioxide losses of northern ecosystems in response to autumn warming. Nature, 451(7174), p.49.

Piao, S., Liu, Z., Wang, T., Peng, S., Ciais, P., Huang, M., Ahlstrom, A., Burkhart, J.F., Chevallier, F., Janssens, I.A. and Jeong, S.J., 2017. Weakening temperature control on the interannual variations of spring carbon uptake across northern lands. Nature Climate Change, 7(5), p.359.

Piao, S., Wang, X., Ciais, P., Zhu, B., Wang, T.A.O. and Liu, J.I.E., 2011. Changes in satellite ‐ derived vegetation growth trend in temperate and boreal Eurasia from 1982 to 2006. Global Change Biology, 17(10), pp.3228-3239.

Pinzon, J. and Tucker, C., 2014. A non-stationary 1981–2012 AVHRR NDVI3g time series. Remote Sensing, 6(8), pp.6929-6960.

Prentice, I.C., Cramer, W., Harrison, S.P., Leemans, R., Monserud, R.A. and Solomon, A.M., 1992. Special paper: a global biome model based on plant physiology and dominance, soil properties and climate. Journal of Biogeography, pp.117-134.

Pulliainen, J., Aurela, M., Laurila, T., Aalto, T., Takala, M., Salminen, M., Kulmala, M., Barr, A., Heimann, M., Lindroth, A. and Laaksonen, A., 2017. Early snowmelt significantly enhances boreal springtime carbon uptake. Proceedings of the National Academy of Sciences of the United States of America, 114(42), pp.11081-11086.

Randerson, J.T., Field, C.B., Fung, I.Y. and Tans, P.P., 1999. Increases in early season ecosystem uptake explain recent changes in the seasonal cycle of atmospheric CO2 at high northern latitudes. Geophysical Research Letters, 26(17), pp.2765-2768.

Reich, P.B., Sendall, K.M., Stefanski, A., Rich, R.L., Hobbie, S.E. and Montgomery, R.A., 2018. Effects of climate warming on photosynthesis in boreal tree species depend on soil moisture. Nature, 562(7726), p.263.

Richardson, A.D., Andy Black, T., Ciais, P., Delbart, N., Friedl, M.A., Gobron, N., Hollinger, D.Y., Kutsch, W.L., Longdoz, B., Luyssaert, S. and Migliavacca, M., 2010. Influence of spring and autumn phenological transitions on forest ecosystem productivity. Philosophical Transactions of the Royal Society B: Biological Sciences, 365(1555), pp.3227-3246.

Richardson, A.D., Anderson, R.S., Arain, M.A., Barr, A.G., Bohrer, G., Chen, G., Chen, J.M., Ciais, P., Davis, K.J., Desai, A.R. and Dietze, M.C., 2012. Terrestrial biosphere models need better representation of vegetation phenology: results from the N orth A merican C arbon P rogram S ite S ynthesis. Global Change Biology, 18(2), pp.566-584.

Richardson, A.D., Keenan, T.F., Migliavacca, M., Ryu, Y., Sonnentag, O. and Toomey, M., 2013. Climate change, phenology, and phenological control of vegetation feedbacks to the climate system. Agricultural and Forest Meteorology, 169, pp.156-173.

Roberts, D.W. and Cooper, S.V., 1989. Concepts and techniques of vegetation mapping. General Technical Report INT-US Department of Agriculture, Forest Service, Intermountain Research Station (USA).

Rodell, M., Houser, P.R., Jambor, U.E.A., Gottschalck, J., Mitchell, K., Meng, C.J., Arsenault, K., Cosgrove, B., Radakovich, J., Bosilovich, M. and Entin, J.K., 2004. The global land data assimilation system. Bulletin of the American Meteorological Society, 85(3), pp.381-394.

Rödenbeck, C., Houweling, S., Gloor, M. and Heimann, M., 2003. CO 2 flux history 1982–2001 inferred from atmospheric data using a global inversion of atmospheric transport. Atmospheric Chemistry and Physics, 3(6), pp.1919-1964.

Rogers, A., Medlyn, B.E., Dukes, J.S., Bonan, G., Von Caemmerer, S., Dietze, M.C., Kattge, J., Leakey, A.D., Mercado, L.M., Niinemets, Ü. and Prentice, I.C., 2017. A roadmap for improving the representation of photosynthesis in Earth system models. New Phytologist, 213(1), pp.22-42.

Roland, C.A., Stehn, S.E., Schmidt, J. and Houseman, B., 2016. Proliferating poplars: The leading edge of landscape change in an Alaskan subalpine chronosequence. Ecosphere, 7(7).

Rosenzweig, C. and Parry, M.L., 1994. Potential impact of climate change on world food supply. Nature, 367(6459), p.133.

Rossi, S., Deslauriers, A., Anfodillo, T., Morin, H., Saracino, A., Motta, R. and Borghetti, M., 2006. Conifers in cold environments synchronize maximum growth rate of tree‐ring formation with day length. New Phytologist, 170(2), pp.301-310.

Rotenberg, E. and Yakir, D., 2010. Contribution of semi-arid forests to the climate system. Science, 327(5964), pp.451-454.

Running, S., Mu, Q., & Zhao, M. (2015). MOD17A2H MODIS/Terra Gross Primary Productivity 8-Day L4 Global 500m SIN Grid V006. NASA EOSDIS Land Processes DAAC.

Running, S.W., Nemani, R., Glassy, J.M. and Thornton, P.E., 1999. MODIS daily photosynthesis (PSN) and annual net primary production (NPP) product (MOD17) Algorithm Theoretical Basis Document. University of Montana, SCF At-Launch Algorithm ATBD Documents (available online at: www. ntsg. umt. edu/modis/ATBD/ATBD_MOD17_v21. pdf).

Samanta, A., Costa, M.H., Nunes, E.L., Vieira, S.A., Xu, L. and Myneni, R.B., 2011. Comment On "Drought-Induced Reduction In Global Terrestrial Net Primary Production From 2000 Through 2009". Science 333(6046), pp.1093.

Seedre, M., Taylor, A.R., Brassard, B.W., Chen, H.Y. and Jõgiste, K., 2014. Recovery of ecosystem carbon stocks in young boreal forests: a comparison of harvesting and wildfire disturbance. Ecosystems, 17(5), pp.851-863.

Sellers, P.J., 1985. Canopy reflectance, photosynthesis and transpiration. International Journal of Remote Sensing, 6(8), pp.1335-1372.

Senf, C., Seidl, R. and Hostert, P., 2017. Remote sensing of forest insect disturbances: current state and future directions. International Journal of Applied Earth Observation and Geoinformation, 60, pp.49-60.

Serreze, M.C., Walsh, J.E., Chapin, F.S., Osterkamp, T., Dyurgerov, M., Romanovsky, V., Oechel, W.C., Morison, J., Zhang, T. and Barry, R.G., 2000. Observational evidence of recent change in the northern high-latitude environment. Climatic Change, 46(1-2), pp.159-207.

Shen, M., Cong, N. and Cao, R., 2015. Temperature sensitivity as an explanation of the latitudinal pattern of green‐up date trend in Northern Hemisphere vegetation during 1982–2008. International Journal of Climatology, 35(12), pp.3707-3712.

Shen, M., Tang, Y., Chen, J., Yang, X., Wang, C., Cui, X., Yang, Y., Han, L., Li, L., Du, J. and Zhang, G., 2014. Earlier-season vegetation has greater temperature sensitivity of spring phenology in Northern Hemisphere. PLoS One, 9(2), p.e88178.

Smith, N.G., Malyshev, S.L., Shevliakova, E., Kattge, J. and Dukes, J.S., 2016. Foliar temperature acclimation reduces simulated carbon sensitivity to climate. Nature Climate Change, 6(4), p.407.

Soja, A.J., Tchebakova, N.M., French, N.H., Flannigan, M.D., Shugart, H.H., Stocks, B.J., Sukhinin, A.I., Parfenova, E.I., Chapin III, F.S. and Stackhouse Jr, P.W., 2007. Climate-induced boreal forest change: predictions versus current observations. Global and Planetary Change, 56(3-4), pp.274-296.

Solomon, S., Qin, D., Manning, M., Averyt, K. and Marquis, M. eds., 2007. Climate change 2007-the physical science basis: Working group I contribution to the fourth assessment report of the IPCC (Vol. 4). Cambridge University Press.

Sprengel, C., 1828. Von den Substanzen der Ackerkrume und des Untergrundes (About the substances in the plow layer and the subsoil). Journal für Technische und Ökonomische Chemie, 2, pp.423–474, and 3, pp.42–99, pp.313–352, pp.397–421.

Statistics Canada, 2019. Total farm area and cropland area, Canada, 1921 to 2016. Accessed May 1, 2019 < https://www150.statcan.gc.ca/n1/daily-quotidien/170510/cg-a002-eng.htm >.

Stocks, B.J., Mason, J.A., Todd, J.B., Bosch, E.M., Wotton, B.M., Amiro, B.D., Flannigan, M.D., Hirsch, K.G., Logan, K.A., Martell, D.L. and Skinner, W.R., 2002. Large forest fires in Canada, 1959–1997. Journal of Geophysical Research: Atmospheres, 107(D1), pp.FFR-5.

Sturm, M., Racine, C. and Tape, K., 2001. Climate change: increasing shrub abundance in the Arctic. Nature, 411(6837), p.546.

Sulla-Menashe, D., Woodcock, C.E. and Friedl, M.A., 2018. Canadian boreal forest greening and browning trends: an analysis of biogeographic patterns and the relative roles of disturbance versus climate drivers. Environmental Research Letters, 13(1), p.014007.

Tape, K.E.N., Sturm, M. and Racine, C., 2006. The evidence for shrub expansion in Northern Alaska and the Pan‐Arctic. Global Change Biology, 12(4), pp.686-702.

Taylor, K.E., Stouffer, R.J. and Meehl, G.A., 2012. An overview of CMIP5 and the experiment design. Bulletin of the American Meteorological Society, 93(4), pp.485-498.

Thomson, A.M., Calvin, K.V., Smith, S.J., Kyle, G.P., Volke, A., Patel, P., Delgado-Arias, S., Bond-Lamberty, B., Wise, M.A., Clarke, L.E. and Edmonds, J.A., 2011. RCP4. 5: a pathway for stabilization of radiative forcing by 2100. Climatic Change, 109(1-2), p.77.

Thoning, K.W., Tans, P.P. and Komhyr, W.D., 1989. Atmospheric carbon dioxide at Mauna Loa Observatory: 2. Analysis of the NOAA GMCC data, 1974–1985. Journal of Geophysical Research: Atmospheres, 94(D6), pp.8549-8565.

Thornton, M.M., P.E. Thornton, Y. Wei, R.S. Vose, and A.G. Boyer. 2018. Daymet: Station-Level Inputs and Model Predicted Values for North America, Version 3. ORNL DAAC, Oak Ridge, Tennessee, USA. https://doi.org/10.3334/ORNLDAAC/1391

Tian, F., Fensholt, R., Verbesselt, J., Grogan, K., Horion, S. and Wang, Y., 2015. Evaluating temporal consistency of long-term global NDVI datasets for trend analysis. Remote Sensing of Environment, 163, pp.326-340.

Tømmervik, H., Bjerke, J.W., Park, T., Hanssen, F. and Myneni, R.B., Legacies of Historical Exploitation of Natural Resources Are More Important Than Summer Warming for Recent Biomass Increases in a Boreal–Arctic Transition Region. Ecosystems, pp.1-18.

Tømmervik, H., Høgda, K.A. and Solheim, I., 2003. Monitoring vegetation changes in Pasvik (Norway) and Pechenga in Kola Peninsula (Russia) using multitemporal Landsat MSS/TM data. Remote Sensing of Environment, 85(3), pp.370-388.

Toutoubalina, O.V. and Rees, W.G., 1999. Remote sensing of industrial impact on Arctic vegetation around Noril'sk, northern Siberia: preliminary results. International Journal of Remote Sensing, 20(15-16), pp.2979-2990.

Trenberth, K.E. and Fasullo, J.T., 2013. An apparent hiatus in global warming? Earth's Future, 1(1), pp.19-32.

Tucker, C.J., 1979. Red and photographic infrared linear combinations for monitoring vegetation. Remote Sensing of Environment, 8(2), pp.127-150.

United States Forest Service (USFS), 2019. Timber Harvests (Feature Layer). Accessed May 1, 2019 <https://enterprisecontent-usfs.opendata.arcgis.com/datasets/2228fa1c8ce94350984871e39acfeeaf_8>.

Vautard, R., Yiou, P. and Ghil, M., 1992. Singular-spectrum analysis: A toolkit for short, noisy chaotic signals. Physica D: Nonlinear Phenomena, 58(1-4), pp.95-126.

Veraverbeke, S., Rogers, B.M., Goulden, M.L., Jandt, R.R., Miller, C.E., Wiggins, E.B. and Randerson, J.T., 2017. Lightning as a major driver of recent large fire years in North American boreal forests. Nature Climate Change, 7(7), p.529.

Verbesselt, J., Hyndman, R., Newnham, G. and Culvenor, D., 2010. Detecting trend and seasonal changes in satellite image time series. Remote Sensing of Environment, 114(1), pp.106-115.

Verma, M., Friedl, M.A., Richardson, A.D., Kiely, G., Cescatti, A., Law, B.E., Wohlfahrt, G., Gielen, B., Roupsard, O., Moors, E.J. and Toscano, P., 2014. Remote sensing of annual terrestrial gross primary productivity from MODIS: An assessment using the FLUXNET La Thuile data set. Biogeosciences, 11, pp.2185–2200.

Vogelsang, T.J., 1998. Trend function hypothesis testing in the presence of serial correlation. Econometrica, 66(1), pp.123-148.

von Liebig, J.F., Playfair, L.P.B. and Webster, J.W., 1841. Organic chemistry in its applications to agriculture and physiology. J. Owen.

Walker, D.A., Raynolds, M.K., Daniëls, F.J., Einarsson, E., Elvebakk, A., Gould, W.A., Katenin, A.E., Kholod, S.S., Markon, C.J., Melnikov, E.S. and Moskalenko, N.G., 2005. The circumpolar Arctic vegetation map. Journal of Vegetation Science, 16(3), pp.267-282.

Walther, G.R., 2010. Community and ecosystem responses to recent climate change. Philosophical Transactions of the Royal Society B: Biological Sciences, 365(1549), pp.2019-2024.

Walther, G.R., Post, E., Convey, P., Menzel, A., Parmesan, C., Beebee, T.J., Fromentin, J.M., Hoegh-Guldberg, O. and Bairlein, F., 2002. Ecological responses to recent climate change. Nature, 416(6879), p.389.

Wang, J., Rich, P.M., Price, K.P. and Kettle, W.D., 2004. Relations between NDVI and tree productivity in the central Great Plains. International Journal of Remote Sensing, 25(16), pp.3127-3138.

Wang, X., Piao, S., Xu, X., Ciais, P., MacBean, N., Myneni, R.B. and Li, L., 2015. Has the advancing onset of spring vegetation green ‐ up slowed down or changed abruptly over the last three decades? Global Ecology and Biogeography, 24(6), pp.621-631.

Welp, L.R., Patra, P.K., Rödenbeck, C., Nemani, R., Bi, J., Piper, S.C. and Keeling, R.F., 2016. Increasing summer net CO 2 uptake in high northern ecosystems inferred from atmospheric inversions and comparisons to remote-sensing NDVI. Atmospheric Chemistry and Physics, 16(14), pp.9047-9066.

White, J.C., Wulder, M.A., Hermosilla, T., Coops, N.C. and Hobart, G.W., 2017. A nationwide annual characterization of 25 years of forest disturbance and recovery for Canada using Landsat time series. Remote Sensing of Environment, 194, pp.303-321.

White, M.A., de Beurs, K.M., Didan, K., Inouye, D.W., Richardson, A.D., Jensen, O.P., O'KEEFE, J.O.H.N., Zhang, G., Nemani, R.R., van Leeuwen, W.J. and Brown, J.F., 2009. Intercomparison, interpretation, and assessment of spring phenology in North America estimated from remote sensing for 1982–2006. Global Change Biology, 15(10), pp.2335-2359.

White, M.A., Thornton, P.E. and Running, S.W., 1997. A continental phenology model for monitoring vegetation responses to interannual climatic variability. Global Biogeochemical Cycles, 11(2), pp.217-234.

Xia, J., Niu, S., Ciais, P., Janssens, I.A., Chen, J., Ammann, C., Arain, A., Blanken, P.D., Cescatti, A., Bonal, D. and Buchmann, N., 2015. Joint control of terrestrial gross primary productivity by plant phenology and physiology. Proceedings of the National Academy of Sciences of the United States of America, 112(9), pp.2788-2793.

Xu, L., Myneni, R.B., Chapin Iii, F.S., Callaghan, T.V., Pinzon, J.E., Tucker, C.J., Zhu, Z., Bi, J., Ciais, P., Tømmervik, H. and Euskirchen, E.S., 2013. Temperature and vegetation seasonality diminishment over northern lands. Nature Climate Change, 3(6), p.581.

Yamori, W., Hikosaka, K. and Way, D.A., 2014. Temperature response of photosynthesis in C 3, C 4, and CAM plants: temperature acclimation and temperature adaptation. Photosynthesis Research, 119(1-2), pp.101-117.

Yan, K., Park, T., Yan, G., Chen, C., Yang, B., Liu, Z., Nemani, R., Knyazikhin, Y. and Myneni, R., 2016a. Evaluation of MODIS LAI/FPAR product collection 6. Part 1: Consistency and improvements. Remote Sensing, 8(5), p.359.

Yan, K., Park, T., Yan, G., Liu, Z., Yang, B., Chen, C., Nemani, R., Knyazikhin, Y. and Myneni, R., 2016b. Evaluation of MODIS LAI/FPAR product collection 6. Part 2: Validation and intercomparison. Remote Sensing, 8(6), p.460.

Yang, X., Tang, J., Mustard, J.F., Lee, J.E., Rossini, M., Joiner, J., Munger, J.W., Kornfeld, A. and Richardson, A.D., 2015. Solar‐induced chlorophyll fluorescence that correlates with canopy photosynthesis on diurnal and seasonal scales in a temperate deciduous forest. Geophysical Research Letters, 42(8), pp.2977-2987.

Zellweger, F., De Frenne, P., Lenoir, J., Rocchini, D. and Coomes, D., 2019. Advances in microclimate ecology arising from remote sensing. Trends in Ecology & Evolution, 34(4), pp.327–341.

Zhang, X., Friedl, M.A., Schaaf, C.B., Strahler, A.H., Hodges, J.C., Gao, F., Reed, B.C. and Huete, A., 2003. Monitoring vegetation phenology using MODIS. Remote Sensing of Environment, 84(3), pp.471-475.

Zhang, Y., Guanter, L., Berry, J.A., Joiner, J., van der Tol, C., Huete, A., Gitelson, A., Voigt, M. and Köhler, P., 2014. Estimation of vegetation photosynthetic capacity from space ‐ based measurements of chlorophyll fluorescence for terrestrial biosphere models. Global Change Biology, 20(12), pp.3727-3742.

Zhao, F. and Zeng, N., 2014. Continued increase in atmospheric CO 2 seasonal amplitude in the 21st century projected by the CMIP5 Earth system models. Earth System Dynamics, 5(2), pp.423-439.

Zhao, J., Zhang, H., Zhang, Z., Guo, X., Li, X. and Chen, C., 2015. Spatial and temporal changes in vegetation phenology at middle and high latitudes of the Northern Hemisphere over the past three decades. Remote Sensing, 7(8), pp.10973-10995.

Zhao, M., Heinsch, F.A., Nemani, R.R. and Running, S.W., 2005. Improvements of the MODIS terrestrial gross and net primary production global data set. Remote Sensing of Environment, 95(2), pp.164-176.

Zhou, S., Zhang, Y., Ciais, P., Xiao, X., Luo, Y., Caylor, K.K., Huang, Y. and Wang, G., 2017. Dominant role of plant physiology in trend and variability of gross primary productivity in North America. Scientific Reports, 7, p.41366.

Zhu, Z., Bi, J., Pan, Y., Ganguly, S., Anav, A., Xu, L., Samanta, A., Piao, S., Nemani, R. and Myneni, R., 2013. Global data sets of vegetation leaf area index (LAI) 3g and fraction of photosynthetically active radiation (FPAR) 3g derived from global inventory modeling and mapping studies (GIMMS) normalized difference vegetation index (NDVI3g) for the period 1981 to 2011. Remote Sensing, 5(2), pp.927-948.

Zhu, Z., Piao, S., Myneni, R.B., Huang, M., Zeng, Z., Canadell, J.G., Ciais, P., Sitch, S., Friedlingstein, P., Arneth, A. and Cao, C., 2016. Greening of the Earth and its drivers. Nature Climate Change, 6(8), p.791.

Zhu, Z., Wulder, M.A., Roy, D.P., Woodcock, C.E., Hansen, M.C., Radeloff, V.C., Healey, S.P., Schaaf, C., Hostert, P., Strobl, P. and Pekel, J.F., 2019. Benefits of the free and open Landsat data policy. Remote Sensing of Environment, 224, pp.382-385.

CURRICULUM VITAE

[redacted]

[redacted]

[redacted]

[redacted]

[redacted]

[redacted]

[redacted]

[redacted]

[redacted]

[redacted]